UC/CLC CAMPUS EARTHQUAKE PROGRAM

Strong Earthquake Motion Estimates for the UCSB Campus, and Related Response of the Engineering I Building.

R. Archuleta, UCSB
F. Bonilla, UCSB
M. Doroudian, UCLA
A. Elgamal, UCSD
F. Heuze, LLNL
M. Hoehler, LLNL
T. Lai, UCSD
D. Lavallée, UCSB
P-C. Liu, UCSB
A. Martin, UCSB
M. Riemer, UCB
J. Steidl, UCSB
M. Vucetic, UCLA
Z. Yang, UCSD

August, 2000

University of California San Diego

SDSU

UCRL-ID-138641

DISCLAIMER

Work performed under the auspices of the U. S. Department of Energy by the University of California Lawrence Livermore National Laboratory under Contract W-7405-Eng-48.

PREFACE

This report was prepared under the UC/CLC Campus Earthquake Program. The project was initiated as part of the Campus-Laboratory Collaboration (CLC) Program created by the University of California Office of the President (UCOP).

The UC/CLC Campus Earthquake Program (CEP) started in March 1996, and has involved a partnership between seven campuses of the University of California - Berkeley, Davis, Los Angeles, Riverside, San Diego, Santa Barbara, Santa Cruz - and the Lawrence Livermore National Laboratory (LLNL). It is designed to estimate the effects of large earthquakes on three of those campuses. Each campus has selected a critical site to demonstrate the methods and procedures used by the CEP. The following sites have been selected: the Rivera Library at U.C. Riverside, the Thornton Hospital at U.C. San Diego, and the Engineering I building at U.C. Santa Barbara.

The project focuses on the estimation of strong ground motions at each critical site. These estimates are obtained by using an integrated geological, seismological, geophysical, and geotechnical approach, bringing together the unique capabilities of the campus and laboratory personnel. This project is also designed to maximize student participation. Many of the site-specific results are also applicable to risk evaluation of other sites on the respective campuses. In the future, we plan to extend the integrated studies of strong ground motion effects to other interested U.C. campuses, which are potentially at risk from large earthquakes.

To put things in perspective, the aim of the CEP is to provide University campuses with site-specific assessments of their strong earthquake motion exposure, in addition to estimates they obtain from consultants according to the state-of-the-practice, i.e. Building Codes (UBC 97, IBC 2000), and Probabilistic Seismic Hazard Analysis (PSHA). The Building Codes are highly simplified tools, while the more sophisticated PSHA is still somewhat generic in its approach because it usually draws from many earthquakes not necessarily related to the faults threatening the site under study. Eventually, both the results from the state-of-the-practice and from the CEP should be analyzed, to arrive at decisions concerning the design-basis assumptions for buildings on U.C. campuses.

This report describes how the strong ground motion estimates were obtained at U.C. Santa Barbara, where a new seismic station was installed in 1997, and how the Engineering I building would respond to those motions. The Principal Investigator at Santa Barbara is Professor Ralph Archuleta.

This UC/CLC project is funded from several additional sources, which leverage the core support provided by the Office of the President and which are gratefully acknowledged. These include the University Relations Program at LLNL, directed by Dr. Claire Max, and the offices of the appropriate Vice-Chancellors on the various campuses. At U.C. Santa Barbara, the Vice-Chancellor for Administrative Services is David Sheldon.

The Director of the UC/CLC Campus Earthquake Program is Dr. Francois Heuze from LLNL.

TABLE OF CONTENTS

Page

EXECUTIVE SUMMARY

This is the second report on the UC/CLC Campus Earthquake Program (CEP), concerning the estimation of exposure of the U.C. Santa Barbara campus to strong earthquake motions (Phase 2 study). The first report (Phase 1), dated December 1997, covered the following topics:

- seismotectonic study of the Santa Barbara region
- definition of causative faults threatening the UCSB campus
- geophysical and geotechnical characterization of the Engineering I site
- installation of the new CEP seismic station
- and, initial acquisition of earthquake data on campus.

The main results of Phase 1 are summarized in the current report.

This document describes the studies which resulted in site-specific strong motion estimates for the Engineering I site, and discusses the potential impact of these motions on the building. The main elements of Phase 2 are:

- determining that a M 6.8 earthquake on the North Channel-Pitas Point (NCPP) fault is the largest threat to the campus. Its recurrence interval is estimated to be in the range of 350 to 525 years.
- recording earthquakes from that fault on March 23, 1998 (M 3.2) and May 14, 1999 (M 3.2) at the new UCSB seismic station.
- using these recordings as empirical Green's functions (EGF) in scenario earthquake simulations which provided strong motion estimates (seismic syntheses) at a depth of 74 m under the Engineering I site; 240 such simulations were performed, each with the same seismic moment, but giving a broad range of motions that were analyzed for their mean and standard deviation.
- laboratory testing, at U.C. Berkeley and U.C. Los Angeles, of soil samples obtained from drilling at the UCSB station site, to determine their response to earthquake-type loading.
- performing nonlinear soil dynamic calculations, using the soil properties determined in-situ and in the laboratory, to calculate the surface strong motions resulting from the seismic syntheses at depth.
- comparing these CEP-generated strong motion estimates to acceleration spectra based on the application of state-of-the-practice methods - the IBC 2000 code, the UBC 97 code, and Probabilistic Seismic Hazard Analysis (PSHA). This comparison will be used to formulate design-basis spectra for future buildings and retrofits at UCSB.
- comparing the response of the Engineering I building to the CEP ground motion estimates and to the design-basis earthquake (DBE) motions used for its retrofit.

Because of the new, site-specific approach which the CEP studies represent, an extensive effort of validation is documented on several fronts:

- validation of the EGF methodology used in the seismic syntheses of strong motions at depth
- validation of the soil profile used for the Engineering I site
- validation of the 1-D vertical seismic wave propagation assumption for the UCSB site
- validation of the nonlinear soil models used to obtain strong motions at the surface

The ever-growing database of strong earthquake records clearly demonstrates the potential for great variability of ground motions from site to site in a given earthquake. These variations are only reflected in a coarse way in the state-of-the-practice Probabilistic Seismic Hazard Analyses, which are rather generic. Nor are these variations described by the simplified design spectra of the Building codes (UBC 97, IBC 2000). These shortcomings provide a strong justification for augmenting the state-of-the-practice estimates with site-specific studies such as done by the Campus Earthquake Program.

At UCSB, the Phase 2 studies lead to the following important conclusions:

- the current (1999) design–basis earthquake (DBE) motions for the campus (10% in 50 years probability of occurrence, or 475-yr return period) are generally consistent with the mean of the CEP surface motion estimates. This means that 50% of the M 6.8 expected earthquakes on the NCPP fault would create ground motions exceeding the current DBE.
- the acceleration spectrum of the 5% in 50-yr probabilistic earthquake (950-yr return period) is generally consistent with the 84^{th} percentile of the CEP-estimated motions. This spectrum is very close to the new IBC 2000 spectrum for UCSB and is generally comparable to the UBC 97 spectrum. Only one in six M 6.8 earthquakes on the North Channel-Pitas Point fault would be expected to exceed this level of motion.
- as to the Engineering I building retrofit, for which a 1994 DBE was used, the 50^{th} percentile CEP motions are about twice the retrofit design motions, and the 84^{th} percentile CEP motions are about 4 times the retrofit design motions. The CEP motions result in roof-to-base relative column displacements which are 2 to 5 times higher than those calculated with the1994 DBE.

LIST OF FIGURES

LIST OF TABLES

1.0 INTRODUCTION

1.1 The Campus Earthquake Program (CEP)

The approach of the CEP is to combine the substantial expertise that exists within the U.C. system in geology, seismology, geophysics, and geotechnical engineering, to estimate the earthquake strong motion exposure of U.C. facilities. These estimates draw upon recent advances in hazard assessment, seismic wave propagation modeling in rocks and soils, and dynamic soil testing. The U.C. campuses initially participating in the application of our integrated methodology are Riverside, San Diego, and Santa Barbara. The procedure starts with the identification of possible earthquake sources in the region and the determination of the most critical fault(s) related to earthquake exposure of the campus. Combined geological, seismological, geophysical, and geotechnical studies are then conducted to characterize each campus with specific focus on the location of particular target buildings of special interest to the campus administrators. Deep boreholes are drilled and geophysically logged, next to the target structure, to provide in-situ measurements of subsurface material properties and to install uphole and downhole 3-component seismic sensors capable of recording both weak and strong motions. The boreholes provide access below the soil layers, to deeper materials that have relatively high seismic shear-wave velocities. Analyses of conjugate downhole and uphole records provide a basis for optimizing the representation of the low-strain response of the sites. Earthquake rupture scenarios of identified causative faults are combined with the earthquake records and with nonlinear soil models to provide site-specific estimates of surface strong motions at the selected target locations. The CEP estimates are shared with the U.C. consultants, so that they can be used in defining the design-basis earthquake for campus buildings.

Thus, for each campus targeted by the CEP project, the strong motion studies consist of two phases: Phase 1 – initial source and site characterization, drilling, geophysical logging, installation of the seismic station, and initial seismic monitoring, and Phase 2 – extended seismic monitoring, dynamic soil testing, calculation of estimated site-specific earthquake strong motions at depth and at the surface, and, where applicable, calculation of the response of selected buildings to the CEP-estimated strong motions.

1.2 Previous CEP Studies Completed at U.C. Santa Barbara

The Phase 1 studies were completed in 1997, and are reported in detail in Archuleta et al, 1997. The main results are summarized below.

An extensive seismotectonic study of the Santa Barbara region was completed. Part of it had been performed under a previous earthquake hazard study supported by the Minerals Management Service, in collaboration with the Lawrence Livermore National Laboratory (LLNL). A regional fault map of the Santa Barbara area is shown in Figure 1.1 and a summary of the causative faults

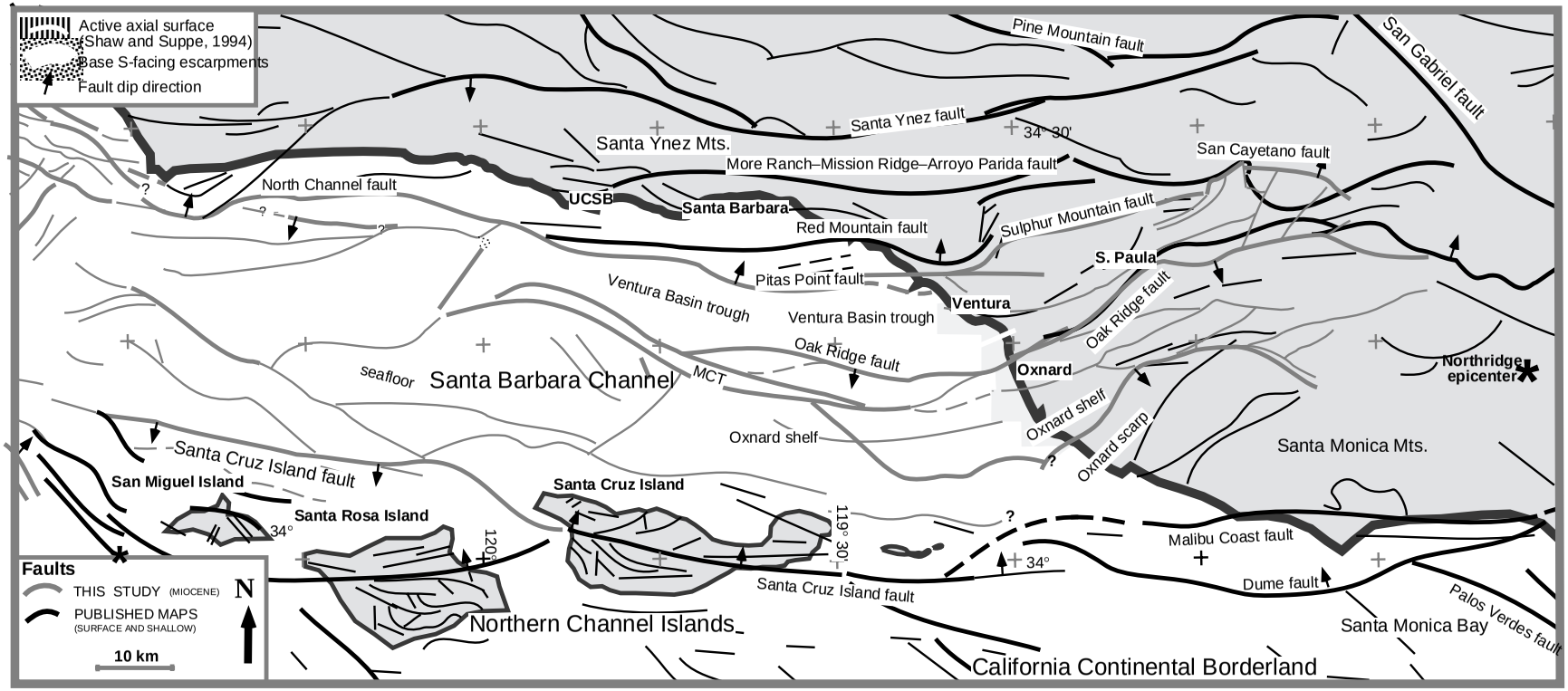

Figure 1.1 Regional fault map of the Santa Barbara area (after Sorlien et al, 1995)

which create a seismic hazard for UCSB is shown in Table 1.1. The most severe seismic exposure is thought to be due to the North Channel-Pitas Point (NCPP) fault, at a distance of only 5 km from the campus and with a maximum credible earthquake of magnitude 6.8 to 7.2. This fault was the focus of the current studies. The strong motion estimates presented here are for a M 6.8 earthquake on the NCPP.

The seismic, geophysical and geotechnical site characterization included:

- temporary, surface deployment of seismometers at three locations on campus (Engineering I, Old Gym, West campus).
- P and S-wave seismic refraction surveys at several campus locations.
- five cone-penetration tests (CPT) to depths up to 45 m, at sites surrounding the Engineering I building. These included S-wave velocity and pore-pressure dissipation measurements.
- P and S-wave suspension logging of the 75-m deep hole at the location of the new seismic station.

These studies established that the UCSB campus has a shallow, 5-m or so, soil cover underlain by the very thick (several hundred meters) Sisquoc formation, which is a weak siltstone, or a highly overconsolidated silt. Its seismic velocity profile is shown in Figure 1.2. The velocity increase with depth is uniform and has a low gradient.

The water table was shown at a depth of about 12 m. The in-situ fluid conductivity of the Sisquoc formation, determined from piezocone pore-pressure dissipation measurements during CPT testing, was calculated at about 10^{-11} m/s. This is a very low permeability material.

Two significant earthquakes recorded during the temporary surface deployment also indicated some variability of surface response between the three locations, with the Engineering I site showing a peak acceleration greater by about 25% than at the other sites. This is most likely due to some variability in the properties of the soil column in the top 30 meters or so. It highlights the requirement for obtaining site-specific earthquake response information.

In 1977, the new UCSB seismic station was installed. It is shown in Figure 1.3. The station has four three-component accelerometers, two at the surface and two in contiguous boreholes at a depth of 74 m. The two surface instruments are respectively a Wilcoxon accelerometer, capable of recording from micro-g's to 0.5 g, and a Kinemetrics force-balance accelerometer (FBA) that can record up to 2 g's. The downhole instruments are the borehole versions of the surface sensors. The Wilcoxon data are digitized by a 24-bit Quanterra recorder and monitored in real time by the USGS/Caltech Southern California Seismic Network. Earthquakes are digitally recorded both locally onto a disk drive at UCSB and at the Southern California Earthquake Center (SCEC) data center, where the data are available for retrieval to all researchers via the Internet. The FBA data (both downhole and surface) are digitized and recorded by a Kinemetrics K2 recorder at UCSB. The station became operational in July 1997.

Table 1.1: Faults of the Santa Barbara region and their earthquake threat to UCSB.

Abbreviated Fault Name	Primary Style of Faulting*	UCSB Distance (km)	Maximum Credible Magnitude	Peak Site Accelerat. (g)	Estimated Slip Rate (mm/yr)	Estimated Recurrence Interval (yr)
Arroyo Parida –More Ranch – Mission Ridge	LS	1	6.7-7.0	0.70+	0.4-2.0	750-3000
Big Pine	LS	35	7.2	0.20	0.8-2.0	1000-2700
Casmalia – Orcutt – Little Pine	Rv?	20	6.5-6.8	0.25	0.2-0.4	2900
Channel Islands–Santa Monica	O-Rv?	20?	7.2-7.5	0.40+	1.2-3.0	600-1400
West Garlock	LS	95	7.2-7.5	0.15	7.0-11.0	530
Hosgri	O-Rv-RS	70	7.1-7.5	0.15	1.0-5.0	650-2000
Los Alamos	Rv	15	6.8-7.0	0.30	0.7-1.0	1500
Malibu Coast – Pt.Dume	LS	70	7.0-7.5	0.15	1.0-3.0	700-3000?
Mesa – Rincon – Lavigia	O-Rv-LS	10	6.5	0.30+	0.3-0.5?	1000-2000?
North Channel – Pitas Point	O-L-Rv	5	6.8-7.2	0.75+	1.0-3.0	300-1500
Offshore Oak Ridge	O-L-Rv	20	6.9-7.2	0.40+	1.6-3.0	400-1200
Onshore Oak Ridge	O-L-Rv	50	7.2-7.5	0.25	3.5-6.0	300-600
Ozena – South Cuyama	O-Rv?	50	6.8	0.15	?	?
Pine Mountain	LS?	50	7.0	0.20	1.5-3.5	500-1500
Pleito	Rv?	70	7.0-7.2	0.10	1.4-2.0	750-1470
Red Mountain	O-Rv	20	6.8-7.2	0.20–0.30+	0.9-3.5	510-870
San Andreas	RS	70	7.5-8.0	0.15-0.25	35	150-350
San Cayetano	O-Rv	63	6.8-7.3	0.17	3.6-5.6	200-600
Santa Cruz-Santa Catalina Ridge – San Clemente Island	RS	70	6.5-7.0	0.10	1.0-5.0	350-2000
Santa Cruz Is – Santa Rosa Is – Anacapa Island	LS	43	6.8-7.3	0.30	1.0-1.7	530-1200
San Gabriel	RS	90	7.0	0.10	1.0-5.0	1250
Santa Susana	O-Rv	100	6.8-7.3	0.10	4.3-7.0	630
Santa Ynez	O-R-LS	10-12	7.0-7.5	0.40-0.60	0.4-2.0	670-3200
Simi – Santa Rosa	O-Rv?	70	6.7-7.0	0.10	0.5-1.5	950
White Wolf	O-L-Rv	90	7.2-7.5	0.15	3.0-8.5	300-850

* LS – Left Slip; RS – Right Slip; O-L – Oblique-Left; O-R – Oblique-Right; Rv – Reverse.

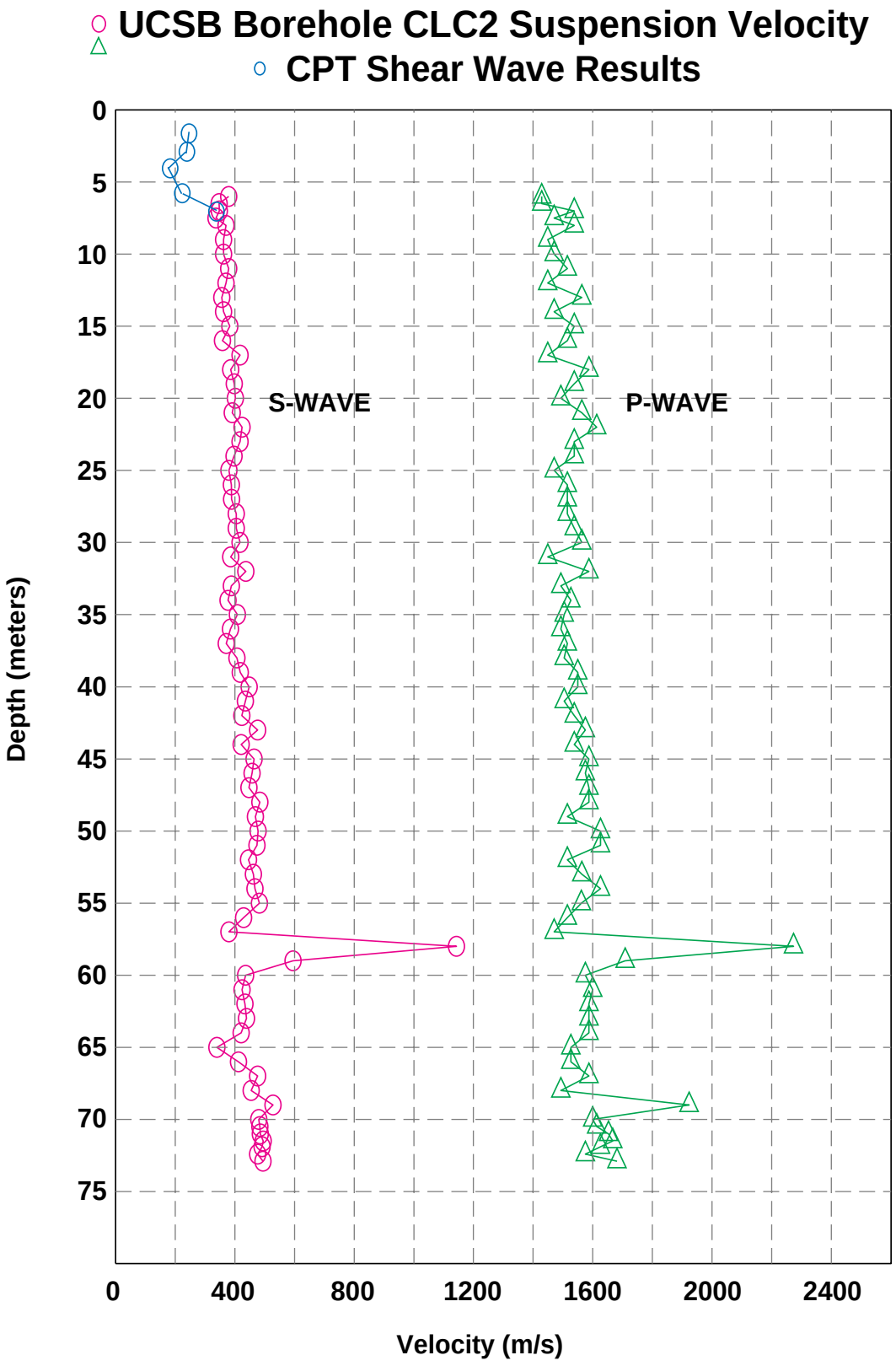

Figure 1.2: Seismic velocity profile of the Engineering I site at UCSB.

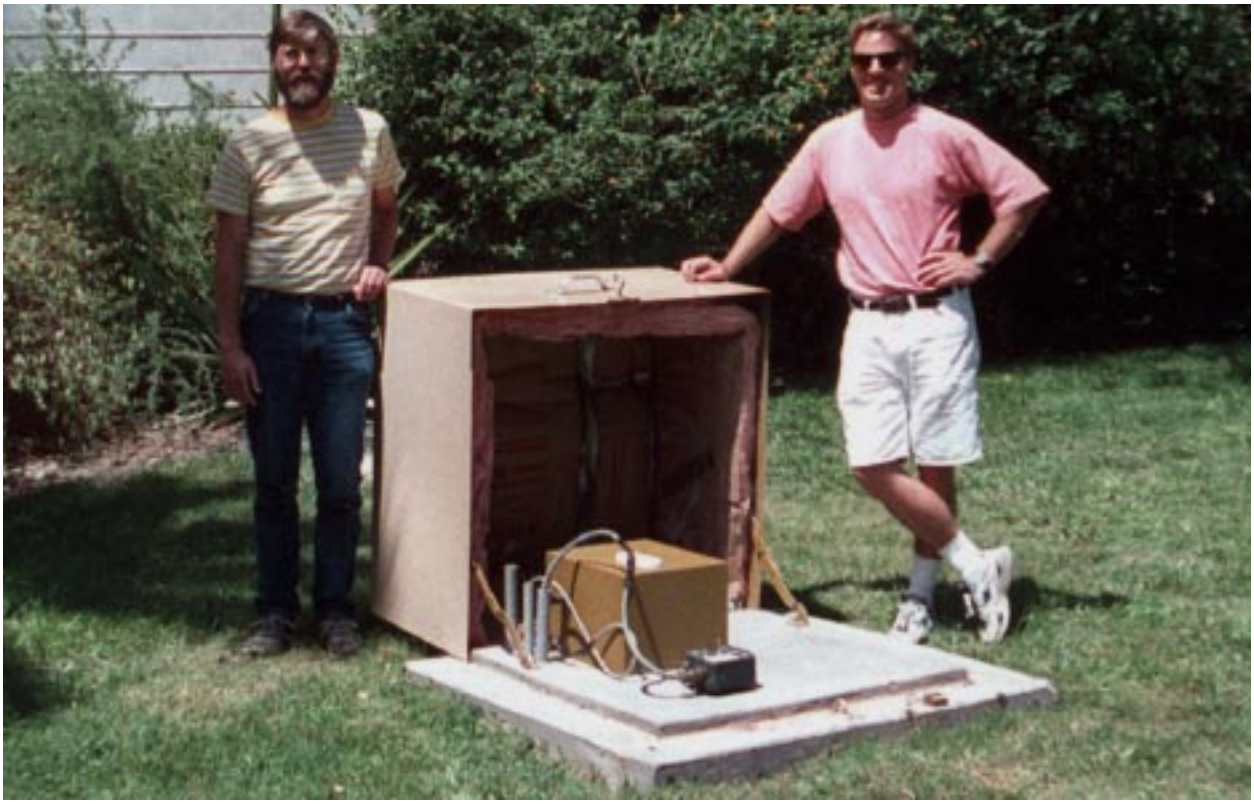

Figure 1.3 The new seismic station at U.C. Santa Barbara, August 1997.

2.0 NEW SEISMOLOGICAL STUDIES

2.1 New Earthquake Records

The dates, locations, and magnitudes of numerous earthquakes for which high quality records were obtained at the new UCSB station between July 1997 and March 2000 are summarized in Table 2.1. Two of them are of particular interest, because they originated on the NCPP Fault: the M 3.2 event of March 23, 1998, and the M 3.2 event of May 14, 1999. Their records are shown in Figures 2.1 and 2.2. These earthquakes provide direct information on the propagation of seismic waves between the main causative fault for UCSB and the campus itself. Other entries show that distant events were recorded, as well, including the Hector Mine earthquake (M 7.1 at 327 km).

Table 2.1 Earthquakes recorded at the new UCSB seismic station - July, 1997 to March, 2000.

Date	Time (hr:min:sec)	Lat. (North)	Long. (West)	Magn.	Distance (km)	Remark
07/26/1997	03:14:56	33.390	-116.350	4.9	345.3	
08/21/1997	01:29:05	34.180	-118.520	3.3	127.2	
09/14/1997	08:31:21	34.370	-119.030	3.3	77.1	
11/15/1997	06:00:20	37.280	-117.830	4.7	365.6	
03/06/1998	05:47:40	36.070	-117.640	5.2	272.2	
03/07/1998	00:36:47	36.080	-117.620	5.0	274.3	
03/11/1998	12:18:52	34.040	-117.250	4.5	245.1	
03/23/1998	18:56:15	34.480	-119.460	3.2	37.9	NCPP Fault.
08/16/1998	13:34:40	34.120	-116.930	4.8	272.8	
08/20/1998	23:49:58	34.370	-117.650	4.4	204.1	
10/27/1998	01:08:41	34.320	-116.840	4.9	278.8	
12/11/1998	08:15:01	34.400	-120.700	3.7	76.7	
12/11/1998	16:37:27	34.740	-120.590	3.3	74.5	
05/14/1999	19:38:36	34.340	-119.600	3.2	26.7	NCPP Fault
05/15/1999	13:22:10	37.530	-118.830	4.5	356.2	
07/22/1999	09:57:24	34.400	-118.600	4.0	116.6	
08/15/1999	04:47:33	34.510	-119.760	3.2	13.1	Sta.Ynez Fault
10/16/1999	09:46:44	34.594	-116.271	7.1	327.0	Hector Mine
02/21/2000	13:49:43	34.965	-120-727	3.8	97.1	
03/19/2000	13:23:55	34.403	-119.925	2.3	5.9	

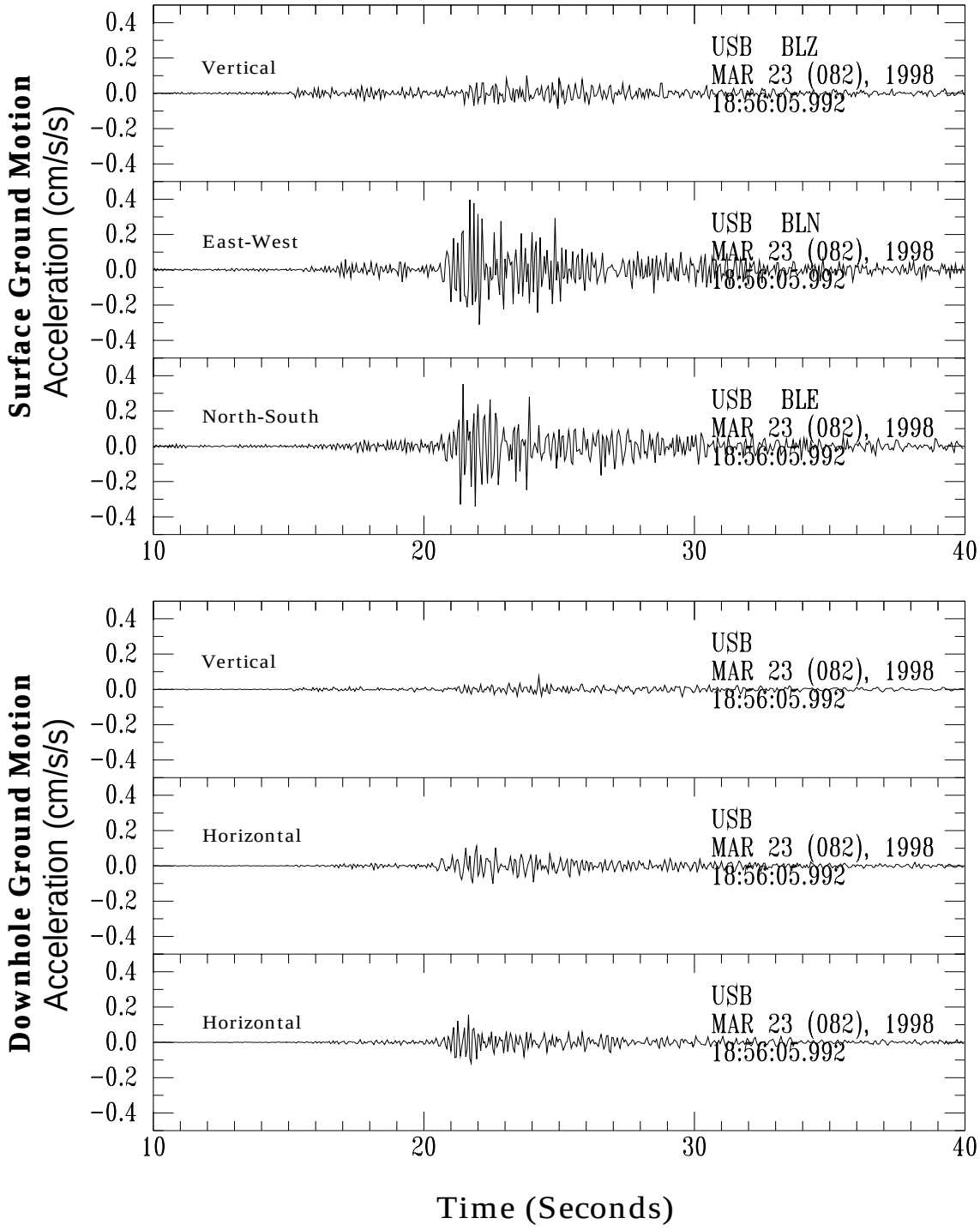

Figure 2.1 : UCSB Records of the M 3.2 Earthquake of March 23, 1998, on the NCPP Fault

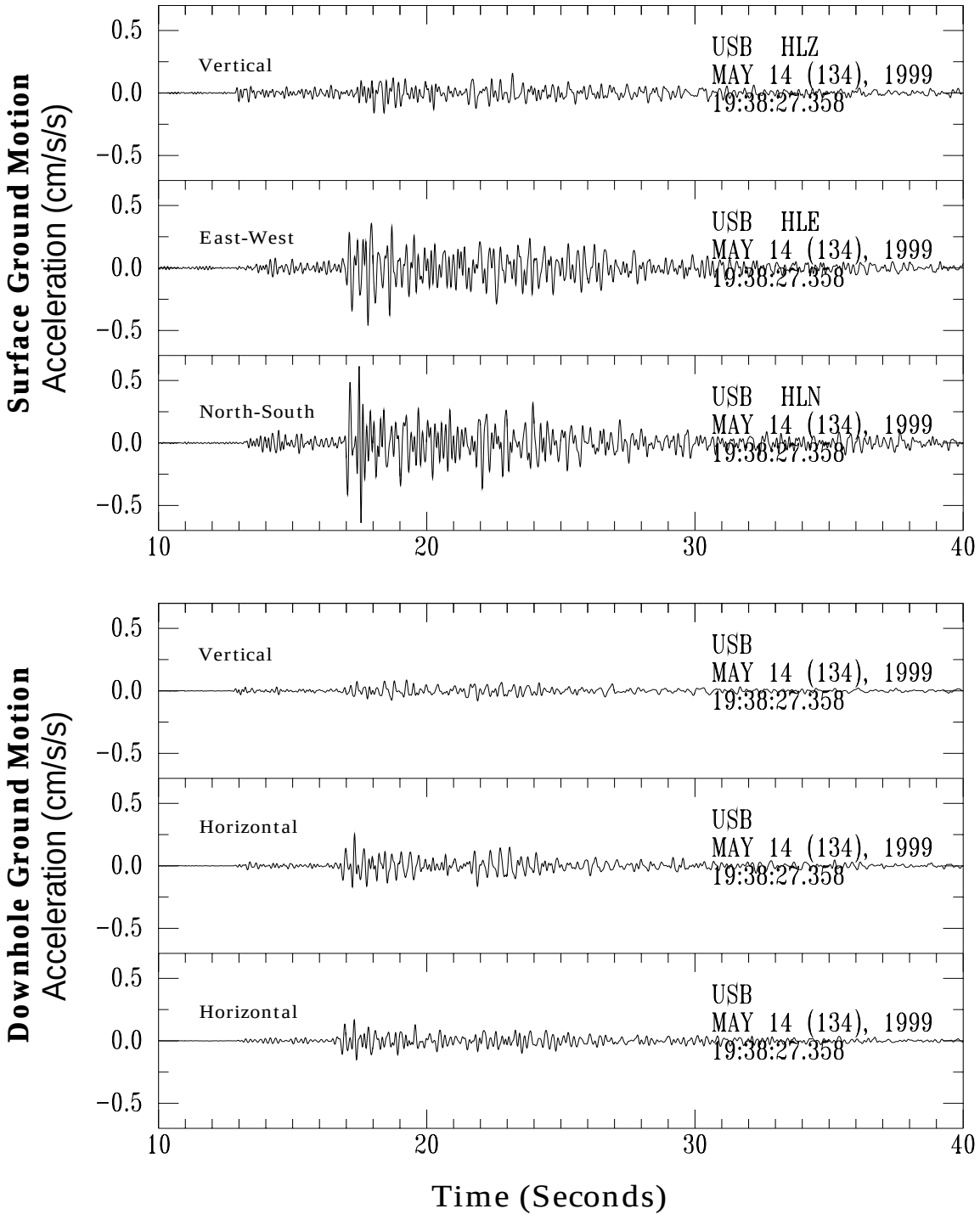

Figure 2.2 : UCSB Records of the M 3.2 Earthquake of May 14, 1999, on the NCPP Fault

2.2 Downhole Strong Motion Syntheses

2.2.1 Method

The basic principle used in the simulations is the representation theorem (e.g., see Aki and Richards, 1980). This theorem states that the ground motion observed at a location is the spatial integral over the fault plane of the temporal convolution of the source time-function with a Green's function. The source time-function may vary from point to point on the fault as can the Green's function. This is the basic method used in kinematic modeling of seismic sources. The key ingredients in this method are the specifications for the source time-function and for the Green's function.

Let us consider the Green's function. The Green's function is the response of the medium recorded by an observer due to an impulsive force applied at a point in the medium. In our case the natural location is a point on the fault plane. Green's functions can be computed numerically provided that the material properties of the medium can be specified for the entire region of interest. Of course, as one goes to higher frequencies (shorter wavelengths), knowledge of the material properties becomes more uncertain. Also, the expense of computing high-frequency Green's functions in a three-dimensional medium scales with the fourth power of the frequency. To circumvent the uncertainty in the description of the medium and the expense of computing high-frequency 3-D Green's functions, we have used an empirical Green's function (EGF) method that originated with Hartzell (1978). In the EGF method, small earthquakes recorded at the site of interest are used as if they were point sources. The primary advantage of this method is that if the source is on the fault of interest, the ray paths that are sampled by the small earthquake include the 3-D heterogeneity of the earth between the source and the observer. Thus the effects of propagation are naturally accounted for.

The empirical Green's function (EGF) method has been used extensively for deterministically synthesizing strong ground motion, as well as in inversions for parameters of the source rupture process (Hartzell, 1978; Wu, 1978; Hutchings, 1991; Tumarkin and Archuleta, 1994; Hutchings et al., 1996; Pavic et al., 2000). The primary assumption of the EGF method is that locations of small earthquakes are near the fault of the expected large event. Consequently, a small earthquake recording represents the impulse response of the path between the source and receiver. The complexity of the earthquake rupture is convolved with the Green's function to produce broadband strong ground motions. To date it has been impossible to model deterministically the detailed source process and wave propagation in such a way as to reproduce acceleration waveforms that match in both phase and amplitude for large earthquakes. However, we can avoid some of these difficulties in the estimation of strong ground motion by randomizing some source parameters and by using small earthquake recordings as empirical Green's functions (Hartzell, 1978; Wu, 1978).

The source description itself presents difficulties. The fault area has to be populated in some way with parameters that describe the kinematics of the source. There are different ways to subdivide the fault plane. In our method we grid the fault into a large number (10,000) of equal-sized subfaults. For each subfault we represent the source with three basic parameters: a stress parameter that corresponds to Brune's (1970) effective stress, a corner frequency, and a rupture time. The seismic moment is proportional to the stress parameter divided by the corner frequency cubed. The sum of all subfault moments is equal to the seismic moment of the large event. The corner frequency is inversely related to the rise time—the time it takes for the slip to reach its static value. The rupture time is the time after nucleation at which a point on the fault initiates slipping. The rupture time enforces causality of slip on the fault plane. These three parameters can be easily related to the parameters of the Haskell (1966) kinematic source description that has been the basis for numerous inversions and forward modeling efforts. The difficulty is in selecting the appropriate combination of the parameters to ensure that these parameters reflect the faulting that occurs during actual earthquakes.

Besides the seismic moment, corner frequency, and location of small event, we must specify the following input parameters for the simulated large event:

- seismic moment and corner frequency (only seismic moment if constant stress drop scaling is assumed)
- geometry of the main fault (strike, dip, length, and width) and location of the hypocenter.

Strong ground motion from the large event can be simulated by first adjusting the scaling and timing of small event records and then summing them appropriately. The Fourier amplitude at a given observer and at a given frequency for the large event $U_l(f)$ is the summation of seismograms radiated from each subfault:

$$U_l(f) = \sum_{j=1}^{N} \frac{\tilde{\sigma}_j \sqrt{A_l/N}}{M_s f_{cs}^2} \frac{R_s}{R_j} \frac{\left(f_{cs} + \mathbf{i}f\right)^2}{\left(f_{cj} + \mathbf{i}f\right)^2} U_s(f) \exp\left(-\mathbf{i}2\pi f\left(t_{sj} + t_{rj}\right)\right) \exp\left(\frac{\pi f\left(R_s - R_j\right)}{\overline{Q}\,\overline{V}_s}\right) \qquad (1)$$

Here $U_s(f)$, M_s, and f_{cs} are the Fourier amplitude at frequency *f*, seismic moment, and corner frequency of a small event, respectively. R_s/R_j is the geometrical spreading correction. $\overline{Q}$ and $\overline{V}_s$ are average values of quality factor and S-wave velocity along the path between the source and receiver. N is the number of subfaults. A_l is the area of large fault. $\tilde{\sigma}_j$ and f_{cj} are the stress parameter, that proportions to stress drop $\Delta\sigma$, and the corner frequency of the subfaults, respectively. For each subfault the seismogram is delayed by the S-wave travel time from the subfault to the receiver (t_{sj}) and the time for the rupture to propagate from the hypocenter to the subfault (t_{rj}). The source parameters t_{rj}, f_{cj}, and $\tilde{\sigma}_j$ of the subfaults are described as random variables that are constrained by the overall source properties of the large event.

The rupture time is determined by dividing the distance between the center of the subfault and the hypocenter by the rupture velocity. We assume the rupture velocity of the fault to be uniformly distributed on the interval of (0.7β, 1.0β), where β is the S-wave velocity of the material in which the fault is embedded. This assumption results in an average rupture velocity of 0.85β, which is a reasonable value.

For simplicity, the stress parameter of each subevent ($\tilde{\sigma}$) is described by the Gamma distribution. The probability density function is of the form

$$p(\tilde{\sigma}) = \gamma^2 \tilde{\sigma} \exp(-\gamma \tilde{\sigma}), \tag{2}$$

where $\gamma = 2\sqrt{1.5A_l}/M_0 f_l^2$, M_0 and f_l are the seismic moment and corner frequency of the large event, respectively. The expression of γ is derived from the high-frequency acceleration spectrum and using an ω^{-2} source model (Aki, 1967; Brune, 1970).

Through numerical tests to match Brune's ω^{-2} source model, we find that the Beta distribution,

$$p(f_c) = \frac{12}{(f_{c\max} - f_{c\min})^4}(f_c - f_{c\min})(f_{c\max} - f_c)^2, \tag{3}$$

is an appropriate probability distribution for corner frequencies (f_c) of subfaults. We assume the $f_{c\min}$ equal to f_{cl}. The $f_{c\max}$ is chosen such that the total moment of the summed subevents is the same as the moment of the large event.

The subelement stress parameter and the corner frequency are randomly selected from the distributions described by Eqs. 2 and 3, respectively. While the range of values for these parameters is documented for real earthquakes, in our models we have assumed that: 1) there is no spatial correlation for the parameters, 2) the parameters are independent of each other, and 3) the radiation pattern for all waves is isotropic. These assumptions can affect the resulting ground motion. For example, including spatial correlation could produce more coherent pulses with time-scales on the order of the correlated distance divided by the rupture velocity. The correlation length itself is a parameter that is unknown for real earthquakes. Besides the spatial correlation, there will always remain a question about the independence of the variables. One can force, a priori, a relationship between variables such as stress drop and corner frequency, but there has been no study to prescribe such a relationship.

2.2.2 Validation

The basic issue of validation is the degree to which a method produces realistic estimates of the ground motion. The measure of ground motion one uses can vary significantly. For example, one could compare computed peak values of ground motion, such as peak acceleration or peak velocity, with those obtained from a specific earthquake. Other comparisons might be between the complete

time-histories in phase and amplitude or perhaps between response spectra at different periods. Each measure can be evaluated on an earthquake-by-earthquake basis.

A critical measure for our method is whether the simulated spectrum approximates the Fourier amplitude spectrum of large earthquakes (Aki, 1968, Brune, 1970) because we have assumed (based on numerous studies) that a large earthquake has a Fourier amplitude displacement spectrum which has a characteristic shape, often referred to as ω^{-2} spectrum. In Figure 2.3 we compare the results of our simulation with Brune's ω^{-2} spectrum. For the entire frequency range the kinematic source spectrum agrees with Brune's ω^{-2} spectrum. We performed several tests using a different number of subevents: the kinematic modeling results are almost independent of the number of subevents when that number is greater than 3000.

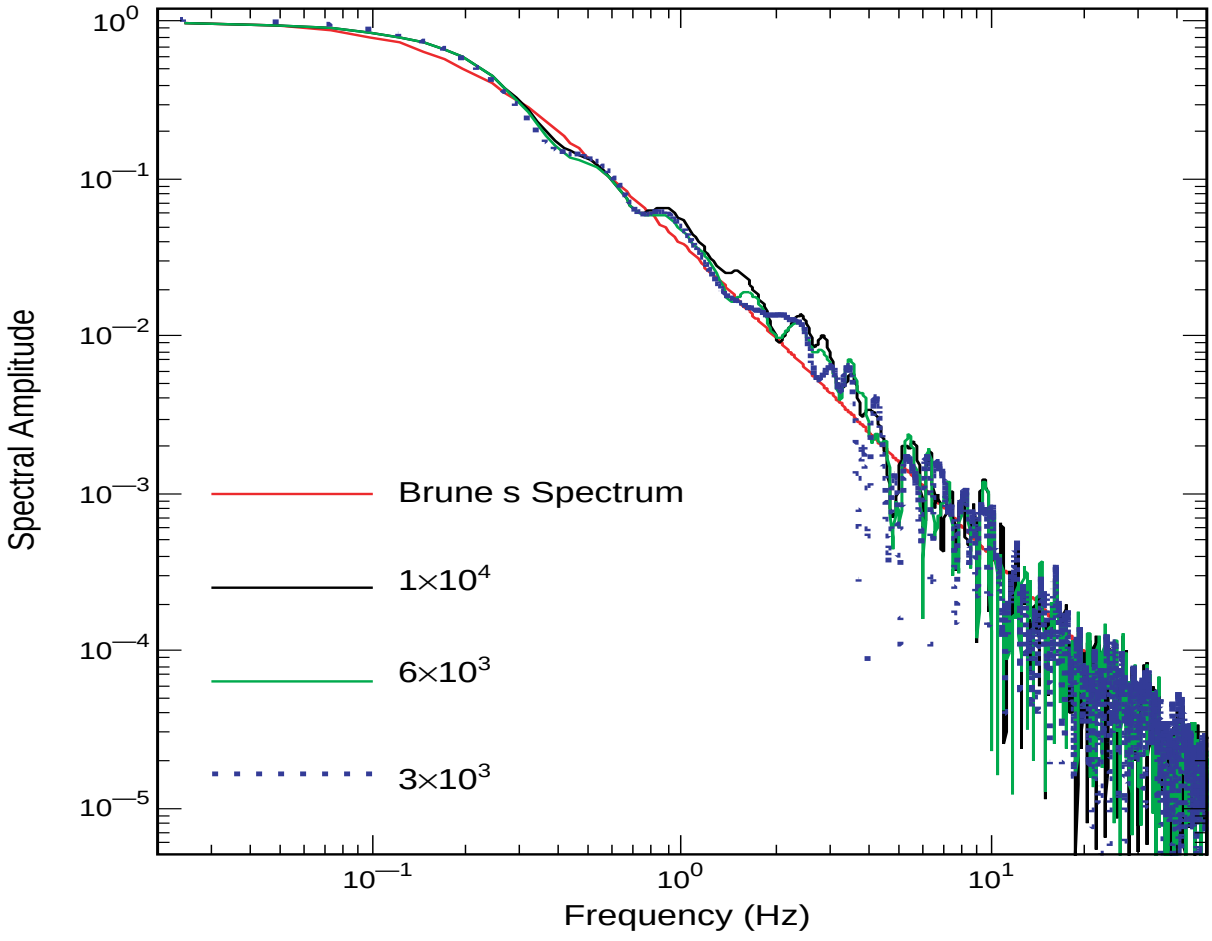

Figure 2.3 Comparison of Brune's spectrum with stochastic simulations. The corner frequency is 0.5 Hz. We separately used 3,000, 6,000, and 10,000 subevents to simulate the Brune's spectrum.

Another measure is the basic shape and level of ground motion, as compared to that predicted by probabilistic seismic hazard analysis. The probabilistic method represents an average of ground motions from a suite of different earthquakes for the same distance and magnitude as that simulated by the stochastic method. As shown later in this report, the shape and level of the synthetic response spectra agree with the probabilistic ground motions over a broad frequency range.

As a further assessment, we illustrate how an ensemble of synthetic ground motions based on the method described above can be compared with data, by using response spectra from the 1994 Northridge earthquake. We take the fault plane and hypocenter, as known. We use two well-recorded aftershocks as EGF's. For each EGF we compute 150 synthetic (linear) time-histories of acceleration from which we calculate the mean response spectrum and its standard deviation. Examples of the response spectra at three stations: Canoga Park (CPC), Santa Susana (SSA) and Moorpark (MPK) are shown in Figures 2.4, 2.5, and 2.6, respectively. The closest distance to the fault is 15.7 km, 18.1 and 26.4 km for Canoga Park, Santa Susana, and Moorpark, respectively. Canoga Park and Moorpark are alluvial sites; Santa Susana is a sandstone rock site. All three components of motion are shown. The solid line is the spectrum of the Northridge record, and the dashed lines represent the ± one standard deviation (sigma) of our estimates. Overall, the range of ground motion in the synthetics reflects the general shape of the response spectra from the Northridge earthquake.

We estimate the modeling error using the computed ground motion for the Northridge earthquake. Our model is a stochastic one that involves a convolution of an EGF with a stochastic source description. The source model parameters are the seismic moment of the mainshock, the corner frequency of the mainshock, the average rupture velocity, the fault geometry, and the hypocenter. The EGF is also part of the model in that it represents the wave propagation from source to receiver. Thus uncertainties in the model include the EGF. The output of the model, e.g., average response spectrum, average peak acceleration, average peak particle velocity, are obtained only after 150 stochastic source models have been simulated. For Northridge we fixed the source parameters and used two different EGF's. To compute the modeling standard deviation we compare the observed and computed average response spectra at seven stations. The standard deviation is computed for the period range of 0.05–2.0 s. The natural log of the standard deviation is 0.4. This modeling error is consistent with modeling standard deviation (natural log) of 0.5 found by Hartzell et al. (1996, Figure 9B) but less than the average standard deviation–about 0.8 natural log units–determined from six different methods for the 1988 Saguenay earthquake (Abrahamson and Becker, 1999).

There are differences between simulations using the two different aftershocks as EGFs, as will also be evident in the synthetics generated for UCSB. These differences reflect modeling uncertainty due to the selection of the EGF. Dan et al. (1990) found using 17 EGF's to simulate a M 6.7 event

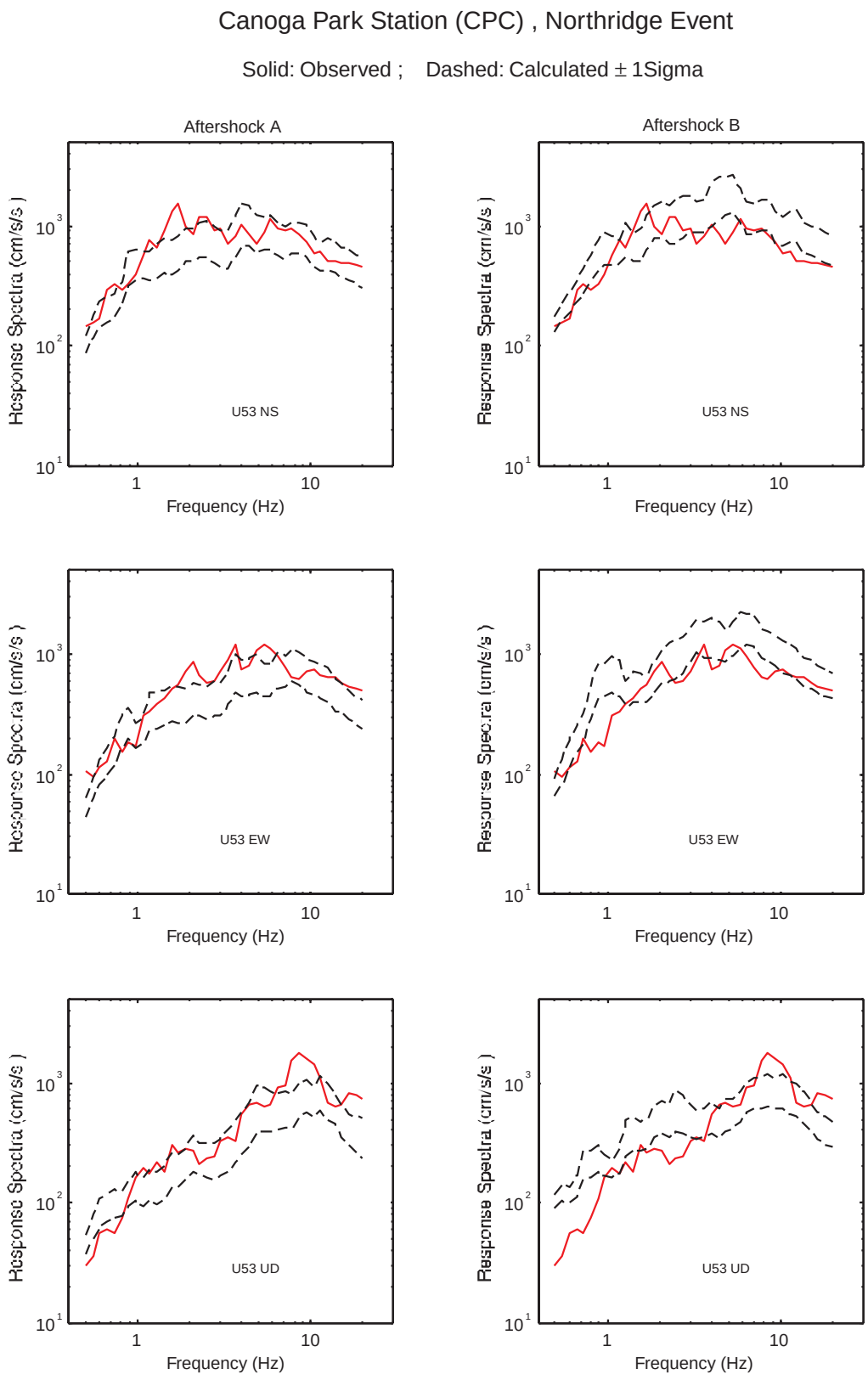

Figure 2.4 Comparison of observed and calculated spectra for Northridge records at CPC station.

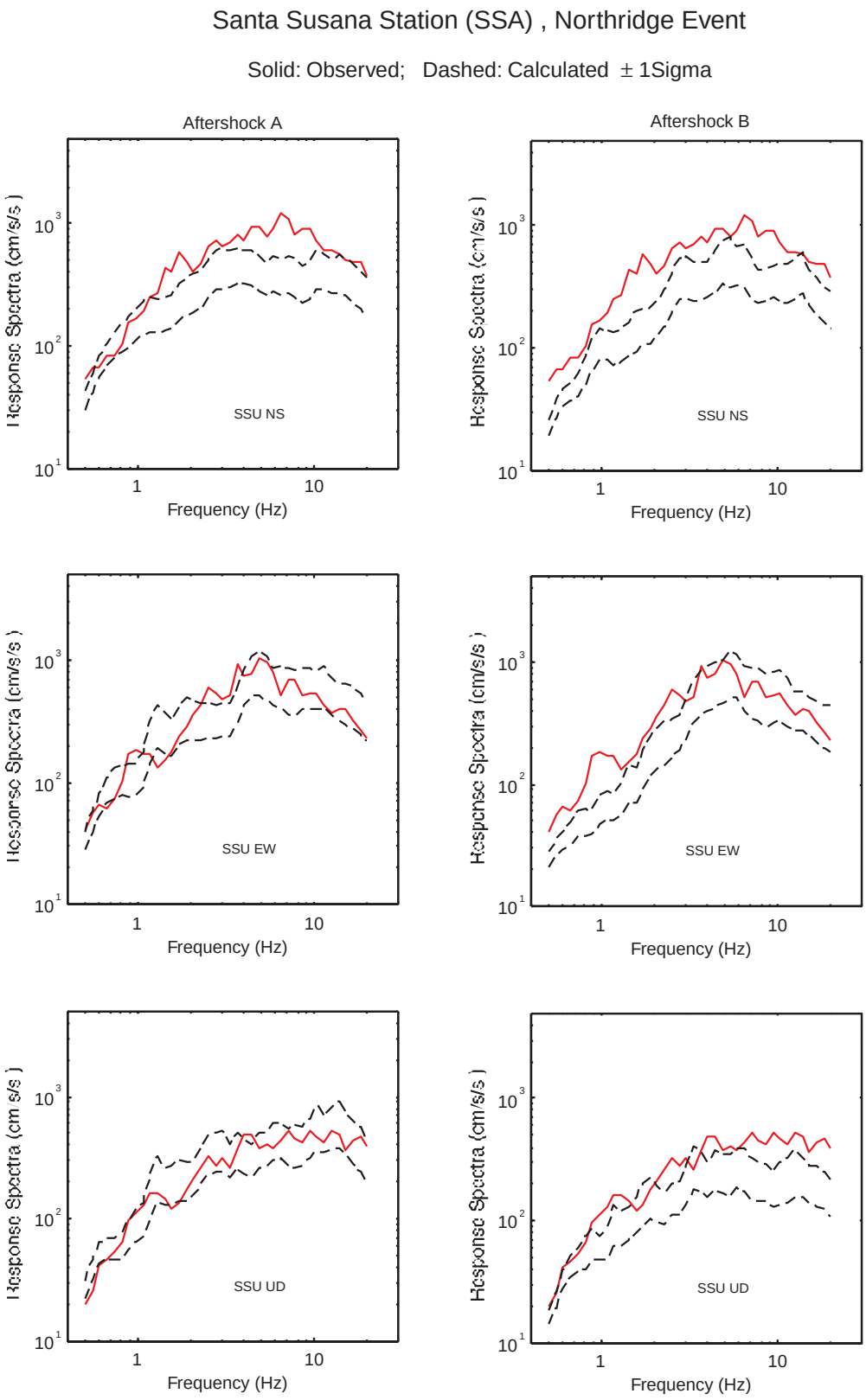

Figure 2.5 Comparison of observed and calculated spectra for Northridge records at SSA station.

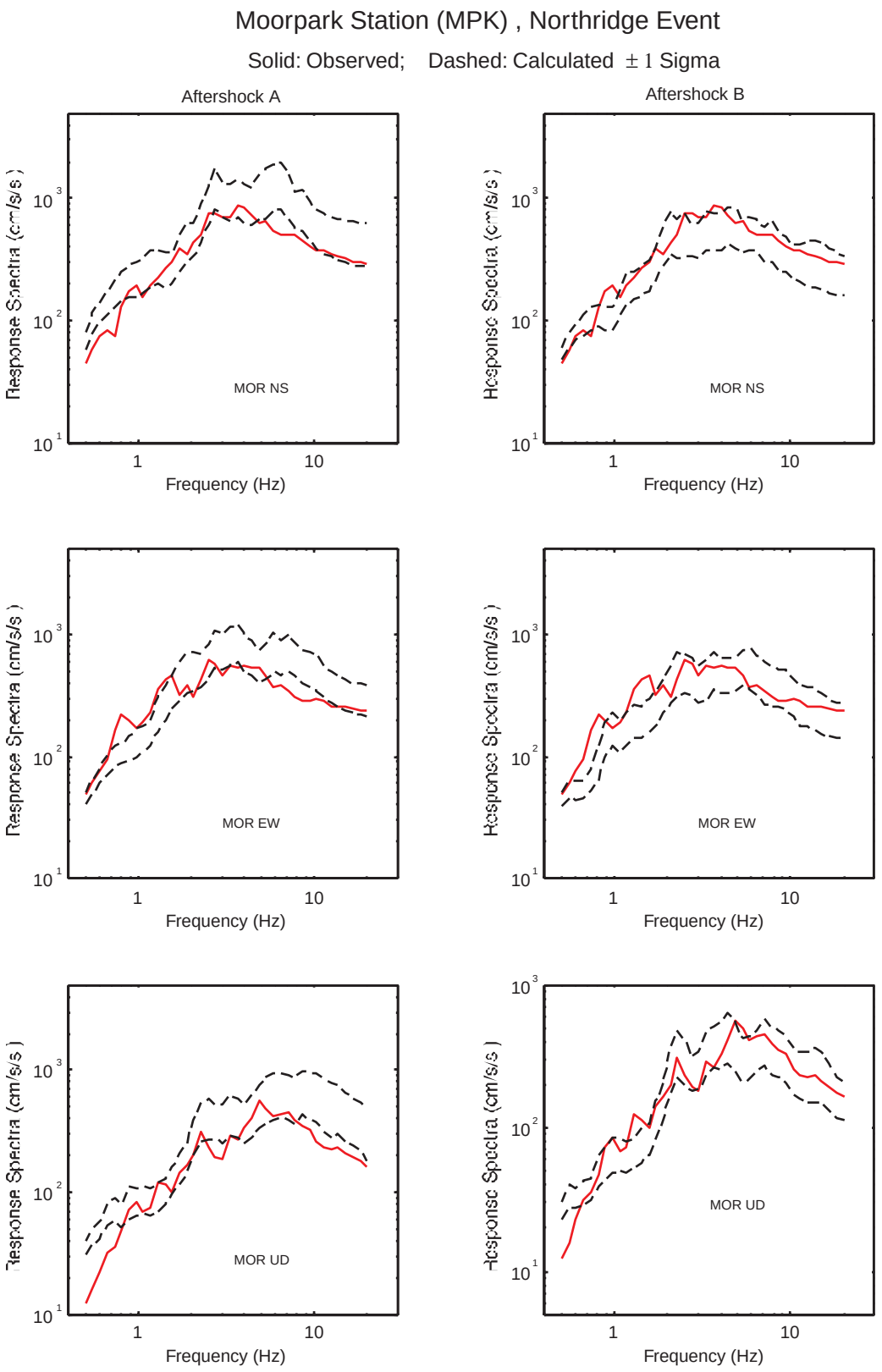

Figure 2.6 Comparison of observed and calculated spectra for Northridge records at MPK station.

(JMA magnitude) that the standard deviation was about 45%. They also found that combining all 17 EGF's into a single computation reduced the coefficient of variation to about 15% but systematically underpredicted the peak acceleration, peak velocity and spectral intensity by 12%, 11% and 19%, respectively. Jarpe and Kasameyer (1996) used EGF's to simulate ground motion at different stations for the Loma Prieta earthquake. Each of the stations had a different numbers of EGF's available to be used in the synthesis. They found no correlation between the standard error and the number of EGF's used to simulate the ground motion.

2.2.3 Fault Rupture Scenarios for the North Channel-Pitas Point Fault

U.C. Santa Barbara is located within one of the more seismically active regions of California. Thus it can expect to experience moderate to large, and perhaps even great, earthquakes within the lifetime of many existing and proposed campus buildings. The primary seismic hazard to UCSB, however, originates from a series of local active faults. Among these faults, the North Channel—Pitas Point (NCPP) fault is believed to be the main controlling structure for producing strong-ground motion at UCSB, because of its size, proximity, and inferred slip rate and because it likely extends directly beneath the campus (Archuleta, et al., 1997). The NCPP fault is imaged in 2-D and 3-D seismic surveys as a blind thrust that terminates about 1.5 km below the seafloor and dips 20^0 -40^0 to the north. This fault is easily capable of generating moderate to large earthquakes (in the magnitude M6 to M7 range) that would produce large-displacement, high-acceleration ground motions at UCSB. The CEP scenario earthquake is assumed to be located on the NCPP fault and to be about of magnitude M_W 6.8.

We use a fault model with a strike of 274^0 and a dip of 45^0 to the north (Hornafius, et al., 1995). The fault plane measures 35 km in length and extends from a depth of 5 km to 15 km, for a down-dipping width of 14 km, and has the same rupture area as the Northridge earthquake (Hartzell et al., 1996). The two shallowest corners of the fault plane are at 34.3419^0N, 119.500^0W and 34.3692^0N, 119.879^0W. The fault parameters and geometry relative to UCSB are shown in Figure 2.7.

We assume that the fault rupture initiates at some point on the fault (the hypocenter) and proceeds outward along the fault surface. Because the position of the hypocenter for any earthquake can not be reliably predicted, a range of hypocenter locations is used. Considering that the NCPP fault is a blind thrust fault, we choose 6 deeper hypocenters separately as shown in Figure 2.8.

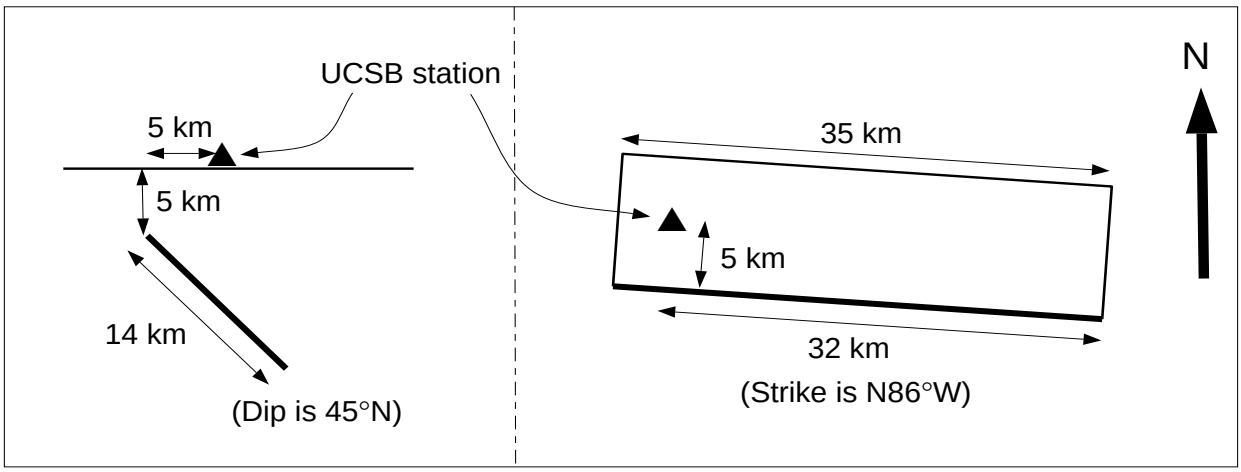

Figure 2.7 Model of the North Channel-Pitas Point fault relative to UCSB (cross-section on left, and plan view on right). The fault surface is denoted by the heavy line.

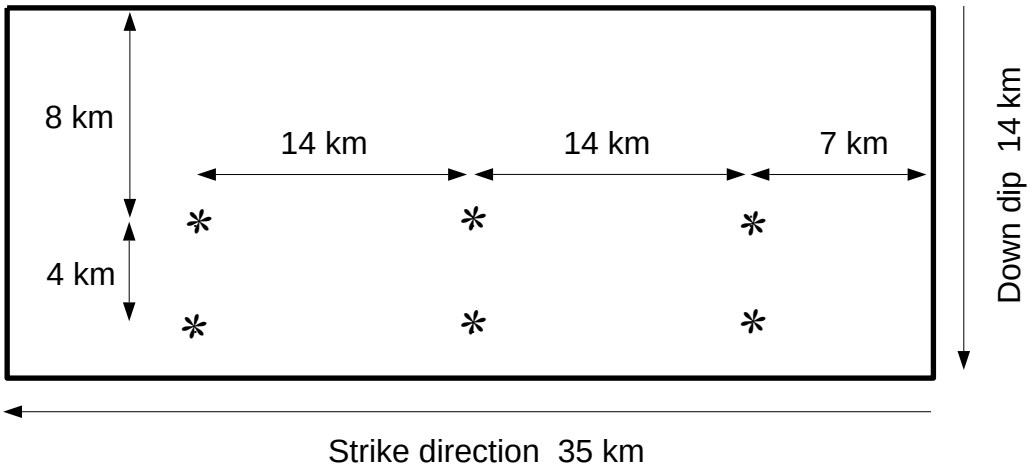

Figure 2.8 Location of 6 assumed hypocenters (star symbols) on the fault surface.

2.2.4 Recurrence Interval for the North Channel-Pitas Point Deterministic Event

The recurrence interval (RI) for a NCPP event was originally given as 300 to 1,500 years in the UCSB Phase 1 report (Archuleta et al., 1997), as shown in Table 1.1. This estimate has been updated, as follows. For the M 6.8 magnitude the moment is 1.78 10^{26} dyne-cm; the fault area is 35x14 km; the shear modulus is 3.43 10^{11} dyne/cm^2. Hence the average slip is 105 cm. Based on estimated slip rates of 2mm/year (Petersen at al, 1996) to 3mm/year (Kamerling and Sorlien, 1999) the RI is estimated to be in the range of 350 to 525 years.

2.2.5 Stochastic Syntheses of Strong Motions

The fault plane of the scenario earthquake is divided into 10,000 square subfaults such that the time difference between arrivals from the adjacent subfaults is less than the periods of interest. The corner frequency (f_c) of the scenario earthquake is estimated in the range of 0.1 Hz to 0.2 Hz, with an average value of 0.15 Hz. The seismic moment (M_0) of a M_W 6.8 earthquake is 1.78×10^{26} dyne-cm. The fault is embedded in a material with a S-wave velocity of 3.5 km/s.

The UCSB/CEP borehole seismic station, at 34.4130^0N, 119.8427^0W, recorded the ground motions of two small earthquakes (March 23, 1998 and May 14, 1999) which occured near the NCPP fault and have the same reported magnitude of 3.2. The 1998 event locates at 34.45^0N, 119.49^0W with a depth of 18.1 km, and the 1999 event locates at 34.35^0N, 119.62^0W with a depth of 13.1 km. The recordings of the 1998 and 1999 events were sampled at 20 and 100 samples per second (s/s), respectively. However the surface recordings of the 1999 event (100 s/s data) show good signal-to-noise only for frequencies below 10 Hz which is the same as the Nyquist frequency of the 1998 data. The recordings of both events are separately used as empirical Green's functions in our ground-motion estimation. The empirical Green's functions are band-pass filtered (Butterworth, four poles) with the corner frequencies at 0.5 and 10 Hz, to remove the low- and high-frequency noise in these recordings.

Based on Brune's ω^{-2} source model, we have calculated the seismic moment of both small earthquakes directly from the long-period levels of the S-wave displacement spectra, using an average radiation pattern of 0.6. The seismic moment is 3.7×10^{20} dyne-cm for the March 23, 1998 event, and 5.2×10^{20} dyne-cm for the May 14, 1999 event. The corner frequencies of the two small events are also estimated from the spectra of recordings. They are 7 Hz (1998 event) and 6 Hz (1999 event), respectively. To check the appropriateness of these values, we computed the surface ground motion at UCSB using a point double-couple source and a layered medium. The computed and recorded ground motion agreed within 20% in amplitude, phase, and Fourier amplitude spectrum.

We performed two series of syntheses: based on the 1998 EGF, and based on the 1999 EGF. In each series we calculated 20 scenarios for each hypocenter location, for a total of 120 syntheses per series and a total of 240 three-component time-histories for a M 6.8 event on the NCPP. Because we used the surface records of the 1998 and 1999 events, due to their higher quality, the resulting seismic syntheses were for surface motions.

These time-histories were then linearly deconvolved to a depth of -74m, based on the well-characterized soil profile of the UCSB station site. This deconvolution provided the downhole incident motions. The acceleration spectra of these downhole incident motions are shown in Figures

2.9 to 2.11, which include the mean and the + and – 1 sigma results. The estimated mean and standard deviations for the peak acceleration of downhole incident time-histories are listed in Table 2.2. For these time-histories we determined a standard deviation (natural log units) of 0.5 for the response spectra averaged over the passband 0.5–10 Hz. When the nonlinear response of soils is included (Chapter 3), this parametric uncertainty reduces from 0.5 to 0.45 for the surface response spectra. The total uncertainty—modeling plus parameterization—of the response spectra is the square root of the sum of the variance due to parameterization (0.2025) plus the variance due to modeling (0.16). The total standard deviation is 0.60 (natural log units) averaged over 0.5–10 Hz; the mean plus one standard deviation response spectrum is 83% larger than the mean.

Table 2-2. Statistics of downhole synthesized incident peak accelerations (g)

	Based on the March 23, 1998 event			Based on the May 14, 1999 event		
Component	EW	NS	UP	EW	NS	UP
Mean Value	0.1937	0.2140	0.0862	0.1817	0.1893	0.0765
Standard Deviation	0.0862	0.1043	0.0396	0.0819	0.0921	0.0336

As for the statistics of the set of time-histories, two particular time-histories are found in the 120 synthetic incident waves such that their response spectra best fit the overall mean and mean plus one standard deviation. We use these two response-spectrum-compatible time-histories as representative of the downhole statistical results (Figure 2.12 and 2.13).

To provide the estimated surface strong motions, the two sets of 120 incident time-histories each are propagated to the surface, up the soil column. These calculations are made with nonlinear dynamic soil models (section 3.3).

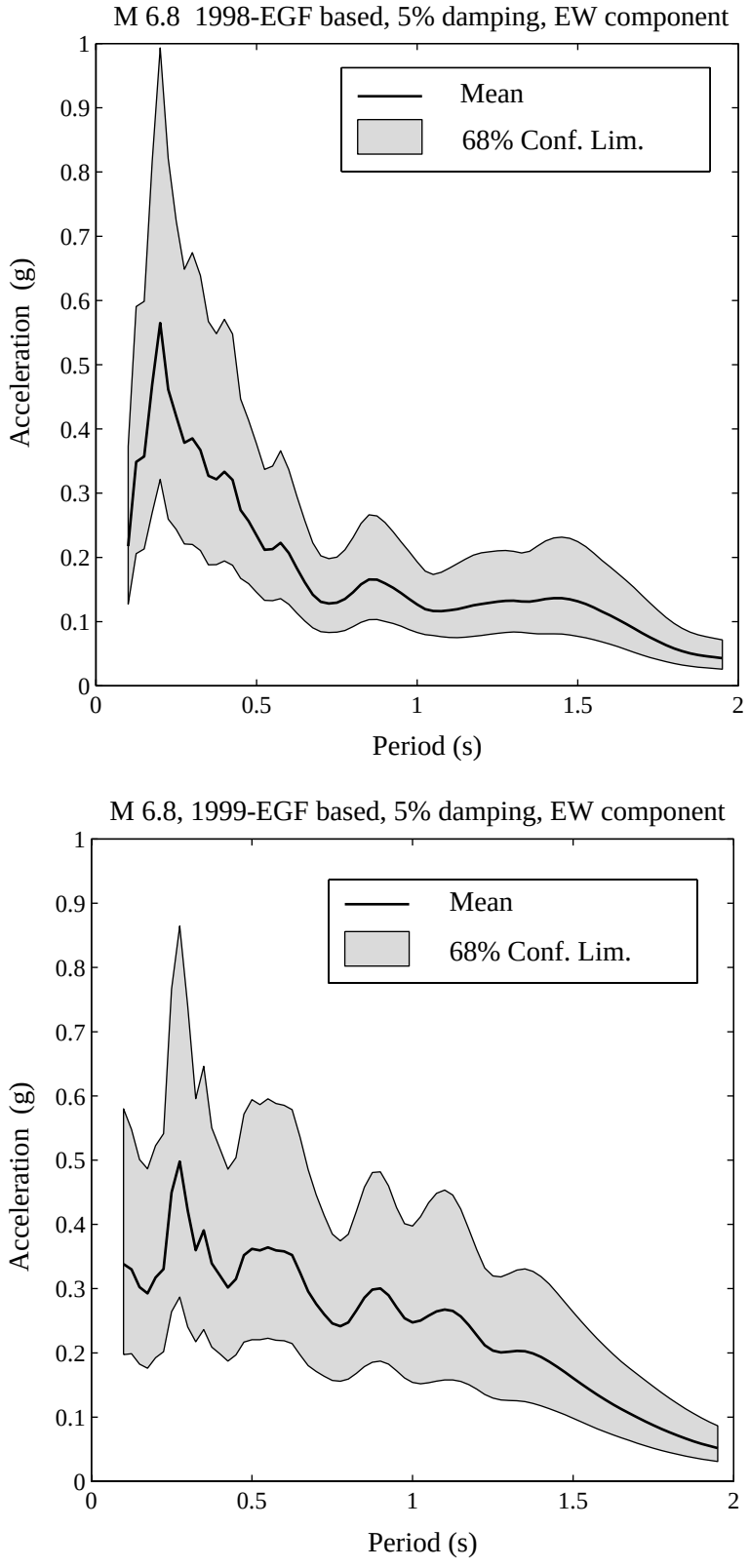

Figure 2.9 Acceleration spectra of downhole incident motion, EW component (98 and 99-based)

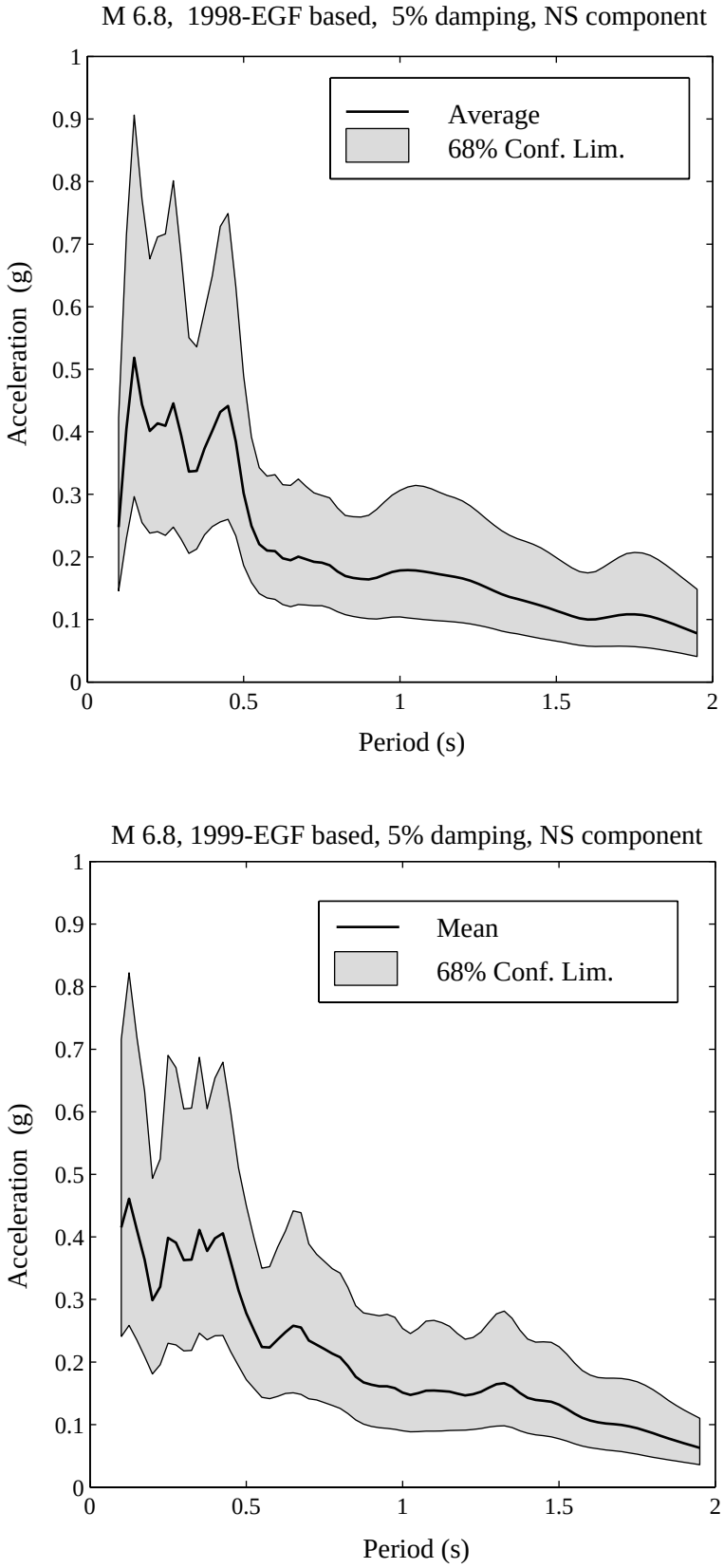

Figure 2.10 Acceleration spectra of downhole incident motion, NS component (98 and 99-based)

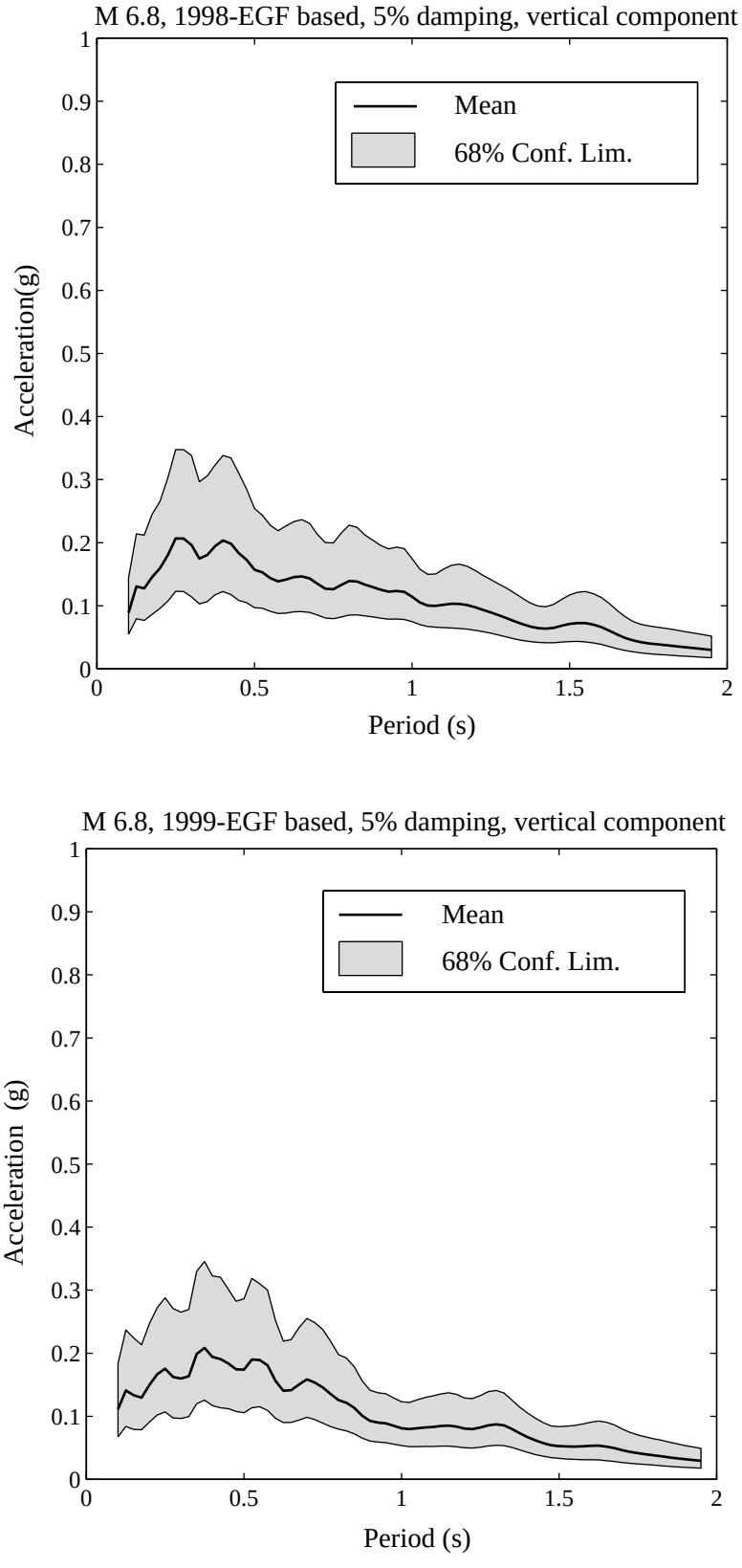

Figure 2.11 Acceleration spectra of downhole incident motion, UP component (98 and 99-based)

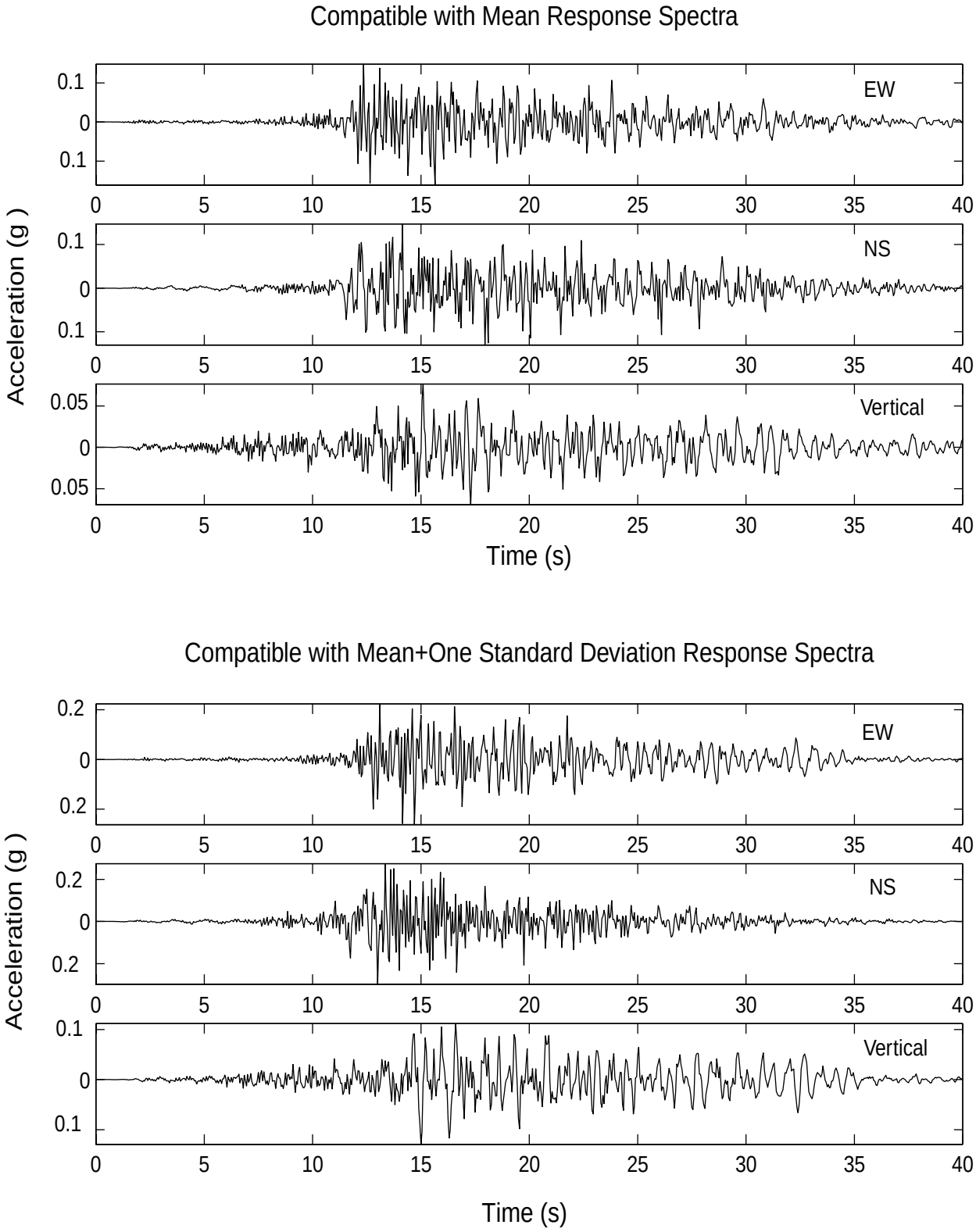

Figure 2.12 Representative downhole incident time-histories, 1998-EGF based.

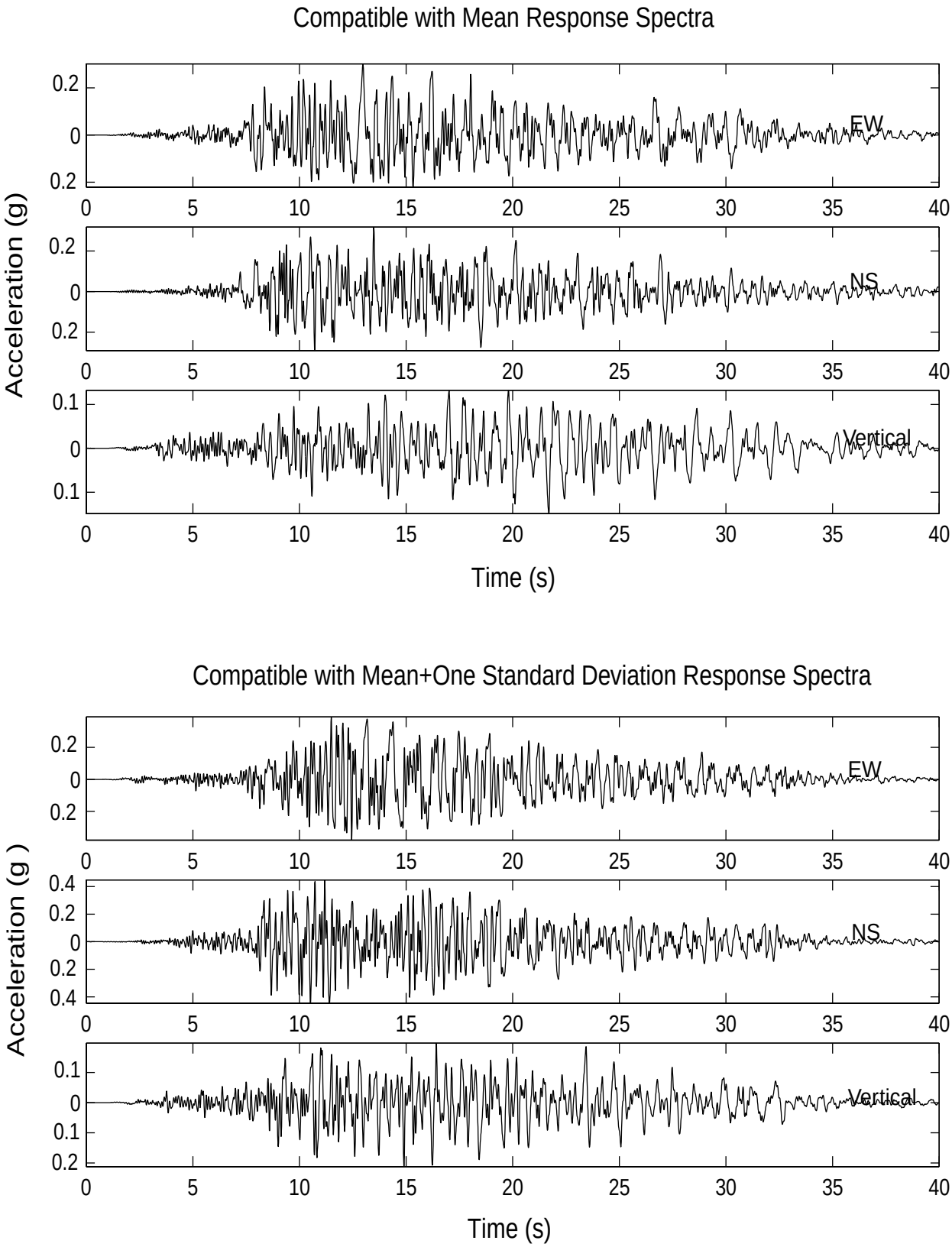

Figure 2.13 Representative downhole incident time-histories, 1999-EGF based.

3.0 SOIL DYNAMICS STUDIES

3.1 Laboratory Tests on UCSB Soils

Soil samples were recovered by Shelby tubes and Pitcher samplers at the location of the seismic station (Figure 3.1). In order to complement the in-situ characterization tests and to obtain properties required for soil dynamics calculations, laboratory tests were performed on the samples. Soil classification and cyclic simple shear tests were conducted at the University of California at Los Angeles (UCLA), and monotonic triaxial tests were done at the University of California at Berkeley (UCB). The detailed test results are presented in Doroudian and Vucetic (1999), and in Riemer and Abu-Safaqah (1999), respectively. Only a summary is given here.

3.1.1 Basic Soil Properties and Soil Classification

The soils at the UCSB's seismic station fall into two groups. In the first 5 m from the surface they are silty sands (SM symbol in the Unified Soil Classification System). Below that, is the Sisquoc formation, a high-plasticity silt (MH symbol). A summary of sample properties is given in Table 3.1. The Sisquoc formation is heavily overconsolidated. Its overconsolidation ratio was measured on a sample from a depth of 31 m to be OCR=17. This is consistent with the known geologic history of the marine terrace on which UCSB is founded, which was overlain in past geological times by several hundred meters of Sisquoc formation, later uplifted and eroded.

Table 3.1 Basic properties of the soils from the UCSB seismic station site

Sample label	Depth (m/ft)	LL*	PI*	Soil Classification	Dry unit Weight (kN/m^3)	Water Content (w, %)	Void Ratio (e)	Saturation of test samples (S_r, %)
SB-4	1.4/4.6	-	0	SM – non-plastic silty sand	16.6	10.6	0.54	51.2
SB-6	1.9/6.2	-	0	SM – non-plastic silty sand	15.4	17.8	0.65	71.5
SB-12	3.7/12.1	-	0	SM – non-plastic silty sand	13.9	27.3	0.86	84.5
SB-32	9.5/31.2	92	38	MH – plastic silt	9.5	61.9	1.79	93.4
SB-68	20.7/68	83	33	MH – plastic silt	10.9	52.0	1.42	99.0
SB-102	31.0/102	82	31	MH – plastic silt	11.2	47.3	1.35	94.2
SB-212	64.6/212	81	30	MH – plastic silt	11.1	46.1	1.36	91.2

* LL: Liquid Limit PI: Plasticity Index

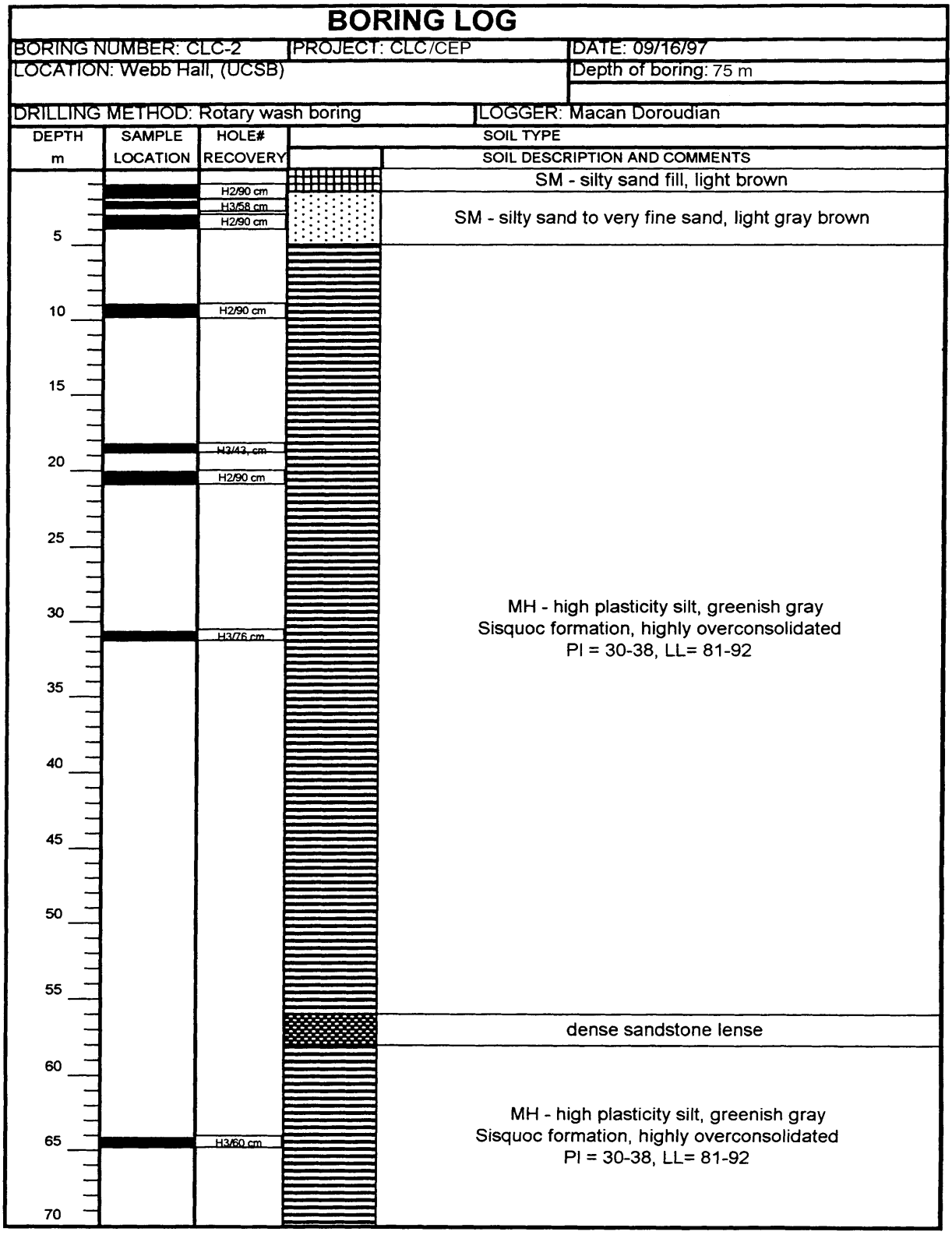

Figure 3.1 Lithologic profile and locations of soil samples at the UCSB seismic station site.

3.1.2 Cyclic Simple Shear Tests

These tests were conducted in the Civil Engineering Department at UCLA. The device used was designed by Doroudian and Vucetic (1995). As shown in Figure 3.2, its most unique feature is that two parallel specimens of the same soil are tested simultaneously. Such a special configuration enables almost complete elimination of problems associated with false deformation, system compliance, and friction. As a result, very small strains can be applied and measured in a controlled manner, as well as the resulting stresses. The cyclic response of the soil samples is recorded in terms of the variation of shear stress vs. shear strain over numerous cycles of loading with increasing strain amplitude. From these records, one can describe the progressive decay of soil shear modulus, G, and the increase in the equivalent viscous damping ratio, λ. The definitions of these quantities are illustrated in Figures 3.3 and 3.4.

Seven samples, recovered from depths between 1.4 and 64.6 m (Table 3.1), were tested in a cyclic strain-controlled mode. The cyclic frequency was lower than 0.25 Hz. The dynamic properties of cohesionless soils, such as those in the upper few meters at UCSB, are practically independent of loading frequency (Hardin, 1965). And tests on cohesive soils, such as the Sisquoc, have shown the effect of frequency to be small so that it can be assumed negligible (Kramer et al, 1992).

The test results are summarized in Figure 3.5; the symbols were defined in Table 3.1. The variation of shear modulus with shear strain was measured over a broad range of strains. Values of the equivalent viscous damping ratio were also obtained for strains up to a least 10^{-4}.

The maximum shear modulus (Gmax) measured in the laboratory can be compared to that obtained from in-situ shear-wave velocity logs. At UCSB, for five depths between 3.6 and 64.6 m, the ratio of laboratory to field values is between 0.29 and 0.74 (Table 3.2). This shows that, even with very careful sampling and handling techniques, there can be substantial differences between the field and laboratory Gmax values, created by the transfer from the ground to the laboratory testing system.

Table 3.2: Ratio of Laboratory Gmax to Field Gmax for UCSB soils

Depth (m)	Laboratory Gmax (MPa)	Field Gmax (Mpa)	Ratio, Laboratory/Field
3.6	38	71	0.54
9.5	63	221	0.29
20.7	103	259	0.40
31.0	133	247	0.54
64.6	178	239	0.74

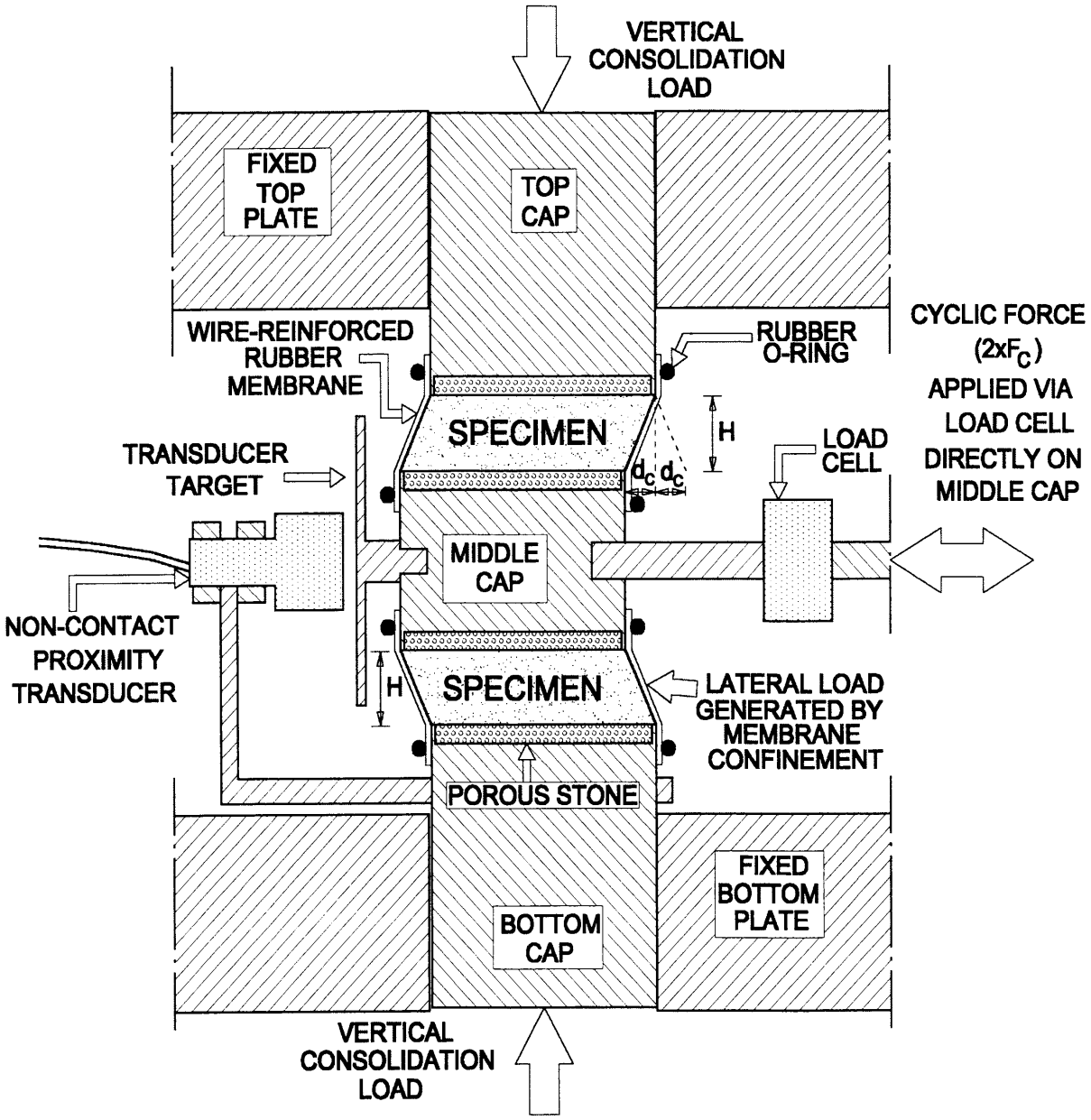

d_C = horizontal cyclic displacement amplitude
F_C = horizontal cyclic shear force
H = height of specimen
A = area of specimen
$\gamma_C = d_C / H$ = horizontal cyclic shear strain amplitude
$\tau_C = F_C / A$ = horizontal cyclic shear stress amplitude

Figure 3.2 Schematic of the UCLA Double Simple-Shear system (Doroudian and Vucetic, 1995).

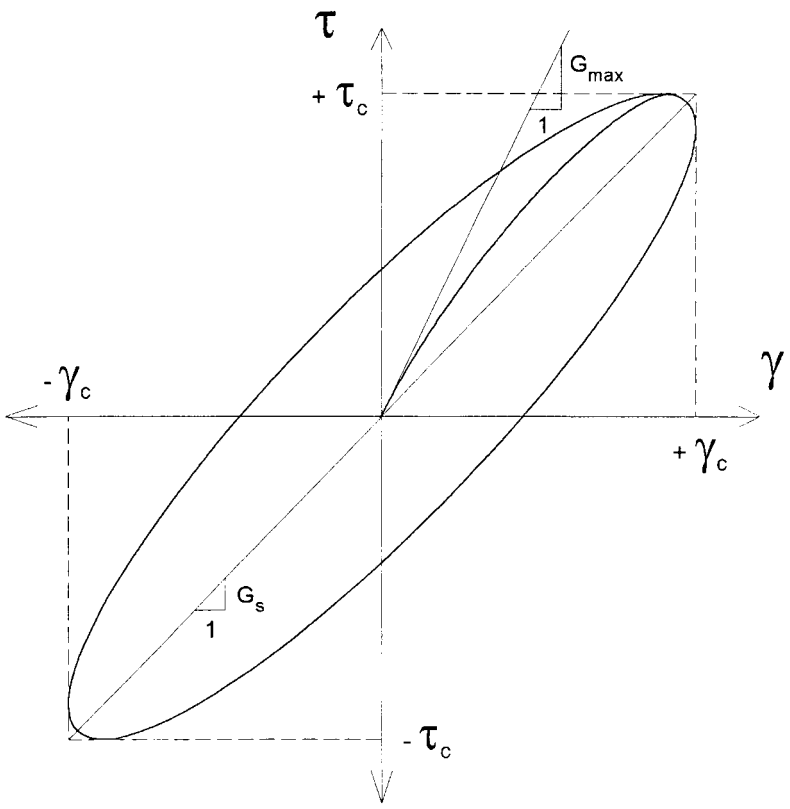

Figure 3.3 Idealized stress-strain loop during cyclic shearing, with parameter definitions.

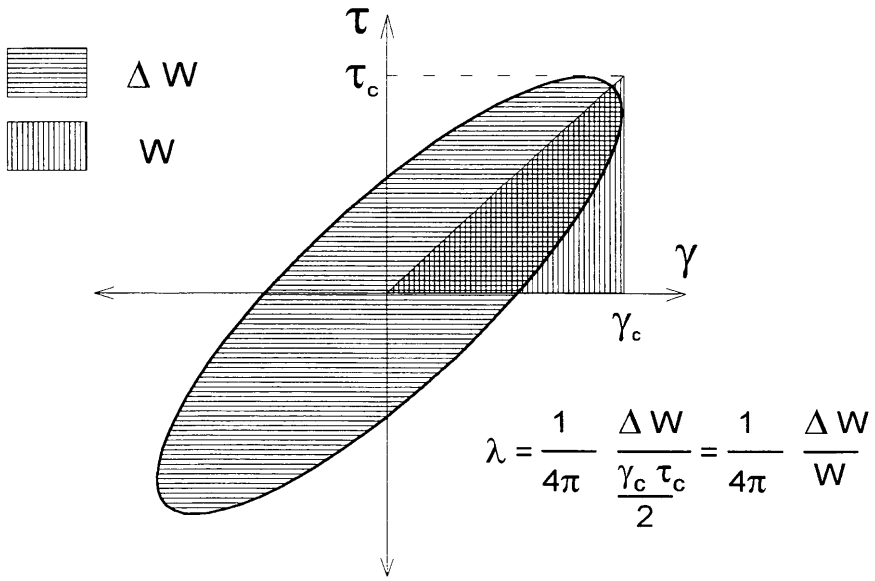

Figure 3.4 Definition of the equivalent viscous damping ratio used in this study.

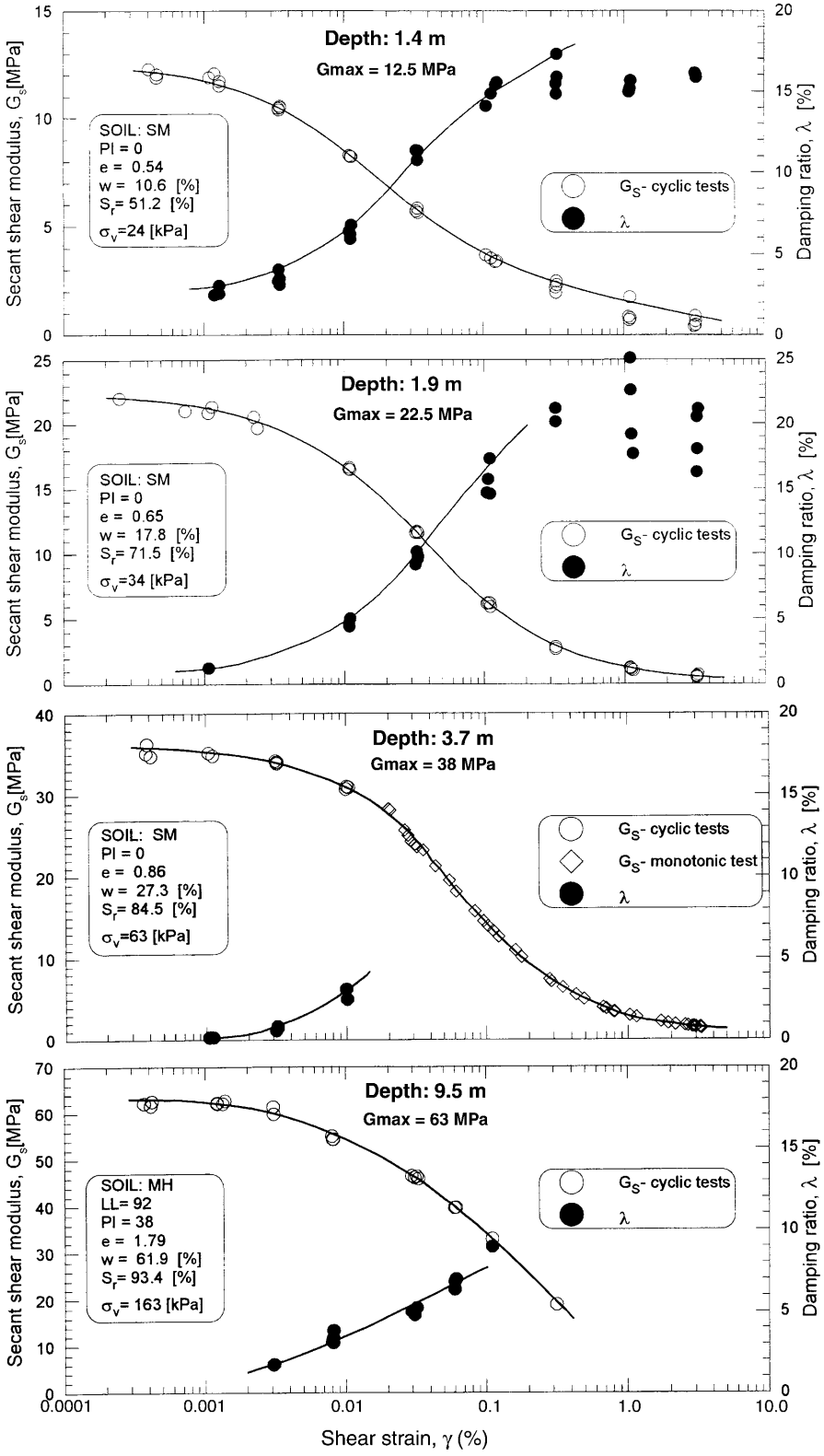

Figure 3.5 Summary of simple shear test results on soils from the UCSB seismic station site.

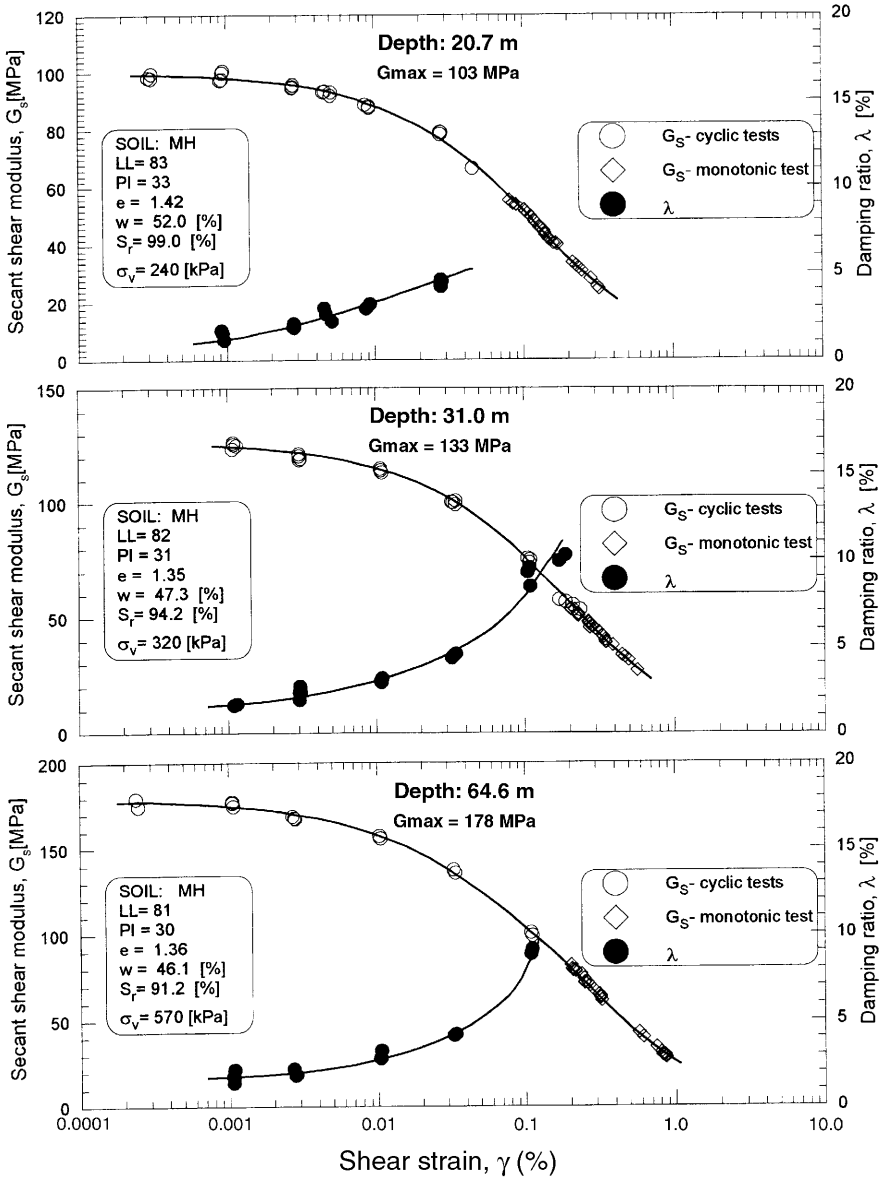

Figure 3.5 (cont.).

For nonlinear soil dynamics computations, the laboratory results at the lowest strain (10^{-6}) are set to the value of Gmax and the rest of the shear-strain shear-modulus curve is normalized to this Gmax value. This is based on the premise that the field values are representative of the properties of the undisturbed material. This procedure, commonly used in geotechnical engineering, has recently been compared by other investigators to several possible laboratory-to-field adjustments and was recommended as the best (Pitilakis and Anastasiadis, 1998).

3.1.3 Monotonic Triaxial Tests

These tests were conducted in the Geotechnical Laboratory of the Department of Civil Engineering at U.C. Berkeley. The samples were first saturated, and then consolidated to the desired effective stress prior to testing (Table 3.3). All the tests were performed in drained conditions, using a strain-control mode. The U.C. Berkeley triaxial testing system is shown in Figure 3.6

The failure envelope for the Sisquoc samples (Figure 3.7) combines the results of five tests on samples from various depths and various degrees of lateral confinement. Four of the five samples provided very consistent results. The sample appearing to be weaker than its counterparts was the deepest one. Its relative weakness may reflect a greater amount of disturbance from handling. The effective cohesion is estimated at 50 kPA and the effective friction angle at 40.5 degrees. All samples behaved dilatatively due to the heavy overconsolidation they had been subjected to during their geological history. This indicated that in an earthquake one would not expect a rise in pore-water pressure in the Sisquoc, and the attendant potential loss of strength due to excessive pore-pressure. Any loss of soil strength would be due to the potentially large shear strains experienced during the event.

Two of the silty sand samples (depths 1.5 and 2.2 m) gave a consistent effective friction angle of 40 degrees. The sample from a depth of 3.7 m showed a higher friction angle, at 48 degrees (Figure 3.8). These materials are cohesionless.

Table 3.3 Initial conditions for the triaxial testing of UCSB samples

Test label	Soil type	Depth (m)	Dry Unit Weight (kN/m^3)	Consolidation Stress (kPa)		Rate (strain/min)
				Horizontal	Vertical.	
SB-1	Sisquoc	9.4	9.91	98	163	0.0004
SB-2	Sisquoc	31.1	11.18	192	320	0.0002
SB-3	Sisquoc	64.3	10.00	342	570	0.0002
SB-4	Fill	3.7	14.86	49	82	0.0002
SB-5	Sisquoc	18.4	9.96	400	200	0.0002
SB-6	Sisquoc	31.1	9.71	326	163	0.0002
SB-7	Fill	2.2	16.0	87	43	0.0004
SB-8	Fill	1.5	15.8	40	20	0.0004

Figure 3.6 The U.C. Berkeley triaxial testing system (courtesy of Dr. M. Riemer).

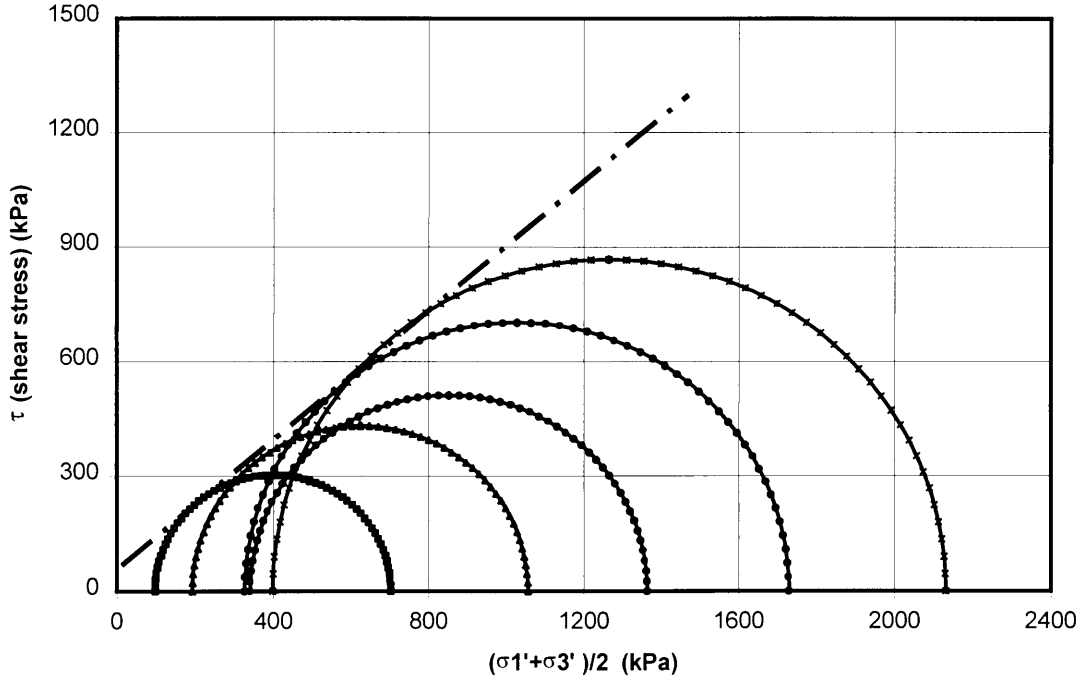

Figure 3.7 Failure envelope for the Sisquoc soil material.

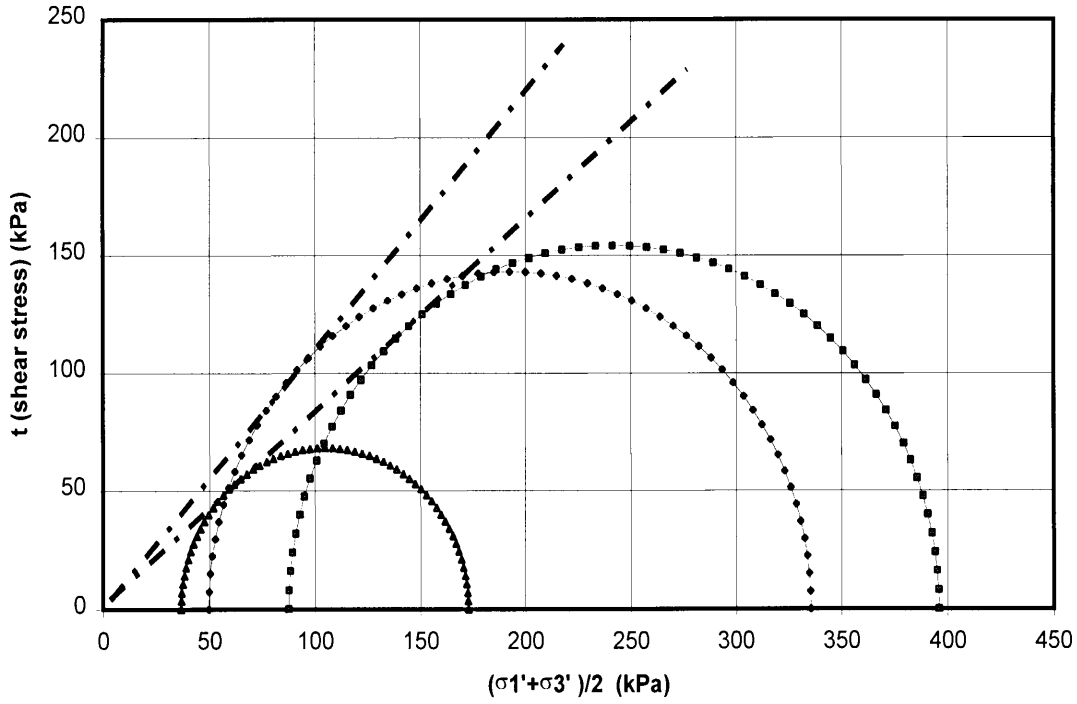

Figure 3.8 Failure envelopes for the top soils of the UCSB seismic station site.

3.2 Soil Dynamics Computational Models

3.2.1 The NOAH Soil Dynamics Computer Model of UCSB

The first computational model of nonlinear soil response to earthquake used for the CEP studies at UCSB is a formulation by Bonilla et al., 1998. This NOAH (NOnlinear Analysis Hysteretic) model includes anelastic and hysteretic behavior and is based on the assumption of one-dimensional vertical propagation of the three components (2 horizontal, 1 vertical) of earthquake motion. This is a common and reasonable assumption when there is no indication of potential effects due to basins or other 3-D geologic structures. The soil profile is represented as a series of horizontal layers. The model assumes continuum mechanics and implements a finite-difference based numerical integration of the 1-D shear wave equation of motion with appropriate boundary and initial conditions:

$$\rho \frac{\partial^2 u}{\partial t^2} = \frac{\partial \tau}{\partial z} \tag{3.1}$$

Here $u(z,t)$ denotes the displacement field perpendicular to the vertical axis at position z and time t; ρ is the unstrained density of the material, and $\tau(z,t)$ is the shear stress.

The stress-strain relationship of the soil is described by a hyperbolic model, given by the following equation (Kondner and Zelasko, 1963):

$$\tau = \frac{G_{\max}\gamma}{1+\left|\frac{G_{\max}}{\tau_{\max}}\gamma\right|} + \eta\frac{\partial \gamma}{\partial t} \tag{3.2}$$

where $\gamma(z,t) = \partial u(z,t)/\partial z$ denotes the shear strain, $G_{\max}$ is the maximum shear modulus at low strain, $\tau_{\max}$ is the maximum stress that the material can support in the initial state, and η is the viscosity factor. The first term on the right hand side of eq. 3.2 corresponds to the anelastic properties, while the second term corresponds to energy dissipation by viscosity. The parameter $\eta = C_1 G_{\max}/C_2\pi$, with $0.01\% \le C_1 \le 1.0\%$ and $1.0 \le C_2 \le 5.0$ Hz. Equations (3.1) and (3.2) hold for both horizontal components of the shear stress. For the vertical stress and the vertical component of the displacement field $w(z,t)$, two similar relationships are used with u replaced by w and the parameter $G_{\max}$ replaced by M in the previous equations. The parameter $M = \rho v_p^2$ is the constrained modulus and v_p is the compressional (P-wave) velocity (see Chen and Saleeb, 1982). In this representation, the values of the other parameters are assumed to be the identical for the three components in a given layer.

Hysteresis models have been discussed extensively in the literature (Pyke, 1979; Vucetic, 1990; McCall, 1994; Muravskii and Frydman, 1998; Yoshida et al., 1998, Xu et al., 1998, etc.). In NOAH,

for each of the three components, the hysteretic behavior is implemented with the generalized Masing rules (Archuleta et al., 1999, 2000). This new formulation of hysteresis is based on the original Masing rules (Masing, 1926, Kramer, 1996). The generalized Masing rules provide a framework for understanding the non-uniform dilation and translation of stress-strain loops for a material subject to non-periodic stresses (or strains). This new hysteresis formulation has several interesting features. It has a functional representation that includes the Cundall-Pyke hypothesis (Pyke, 1979) and Masing's original formulation as special cases. In its most elementary implementation, the generalized Masing rule is even simpler than the Masing and extended Masing rules (Kramer, 1996). The model depends only on one free parameter γ_f named the fiducial point. This parameter controls the size of the loop in the stress-strain space and therefore can be related to the amount of energy dissipated through the nonlinear property of the material. In other words, the generalized Masing rules provide a method to introduce the effect of the damping ratio into nonlinear modeling independently of the other soil parameters (Ishihara, 1996). The relationship between the anelastic damping of a stress-strain loop and the fiducial point for cyclic loadings has been derived in Archuleta et al. (1999).

In the generalized Masing rules, the initial loading is given by the backbone curve $F_{bb}(\gamma)$ (eq. 3.2). For the subsequent loadings and unloadings, the strain-stress relationship is given by the following tranformation:

$$\frac{\tau - \tau^{(i)}}{c_H} = F_{bb}\left(\frac{\gamma - \gamma^{(i)}}{c_H}\right) \tag{3.3}$$

until the path prescribed by eq. (3.3) crosses the backbone curve (eq. 3.2) in the stress-strain space (Figure 3.9). Then the current loadings or unloadings return to the backbone curve until the next turning point where eq (3.3) is applied again and the rules are iterated. The coordinates $(\gamma^{(i)},\tau^{(i)})$ correspond to the i^{th} (and previous) reversal point in the strain-stress space (see Figure 3.9 for an illustration with $i = 1$ and 2). In Masing's original formulation, the hysteresis scale factor c_H is equal to 2.0. In the generalized Masing rules, c_H is a function of physical properties of the material and of γ_f (Archuleta et al., 1999, 2000). In the stress-strain space, γ_f controls the intersection between the path given by eq. (3.3) and the backbone curve.

The generalized Masing rules can be summarized by the following relation:

$$\tau(\gamma) = \begin{cases} F_{bb}(\gamma) & \gamma < \gamma^{(1)}, t < t^{(1)} \\ c_H^{(n)} F_{bb}\left(\dfrac{\gamma - \gamma^{(n)}}{c_H^{(n)}}\right) + \tau^{(n)} & |\gamma| \le |\gamma_f|, t \ge t^{(1)} \\ F_{bb}(Sign\left(\frac{d\gamma}{dt}\right)\gamma) & |\gamma| \ge |\gamma_f|, t \ge t^{(1)} \end{cases} \tag{3.4}$$

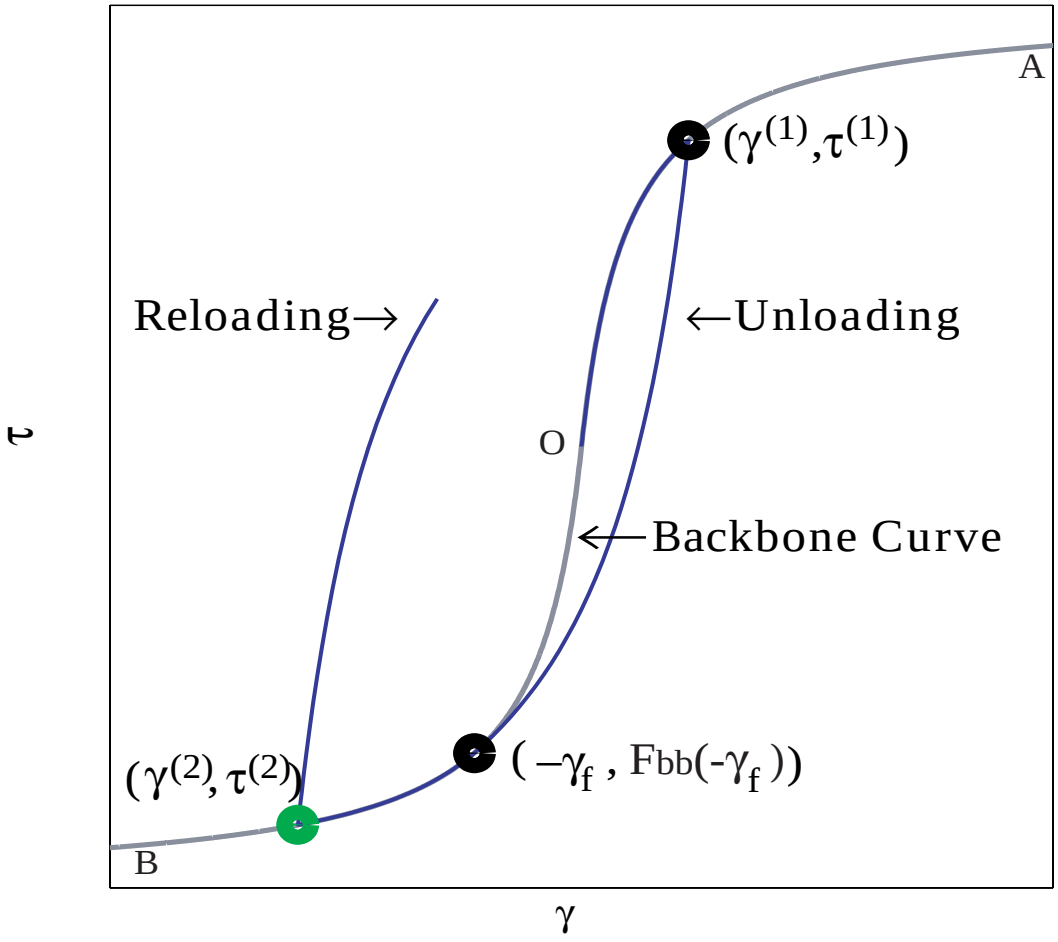

Figure 3.9 Path followed by the stress-strain curve for a soil under noncyclic loading with hysteretic properties controlled by the generalized Masing rules (NOAH model).

where $t^{(1)}$ is the time corresponding to the first turning point and $\tau^{(n)}$ is given by the following relation:

$$\tau^{(n)} = \sum_{i=2}^{n} c_H^{(i-1)} F_{bb}\left(\frac{\gamma^{(i)} - \gamma^{(i-1)}}{c_H^{(i-1)}}\right) + F_{bb}\left(\gamma^{(1)}\right) \tag{3.5}$$

where $\gamma^{(n)}$ corresponds to the turning point at the n^{th} unloading or reloading (the index n is even at reloading and odd when unloading). The time derivative in eq. (3.4) is estimated at any time between the n^{th} and the $(n+1)^{th}$ turning point. The function *Sign* is 1 when its argument is positive, 0 when the argument is 0, and -1 when its argument is negative. The third rule in eq. (3.4)

does not apply for $\gamma_f \to \infty$ and is optional for $\gamma_f = \gamma^{(1)}$. With reference to Figure 3.9, the first rule on the right hand side of eq. (3.4) corresponds to the first loading path. The second rule governs the hysteresis behavior of successive unloading and reloading paths until $|\gamma|$ exceeds $|\gamma_f|$. Note that for an aperiodic signal, successive unloading and reloading paths can occur with the stress-strain path not necessarily crossing the backbone curve. Although each unloading path, or reloading path, follows a track in the stress-strain space directed to the fiducial point $[(-\gamma_f, F_{bb}(-\gamma_f)]$, or $[\gamma_f, F_{bb}(\gamma_f)]$, it may not reach this point if a reversal takes place before getting to the fiducial point. (Each of these reloading/unloading paths are characterized by turning points $|\gamma^{(n)}| < |\gamma_f|$ with $n > 1$.) The term $\tau^{(n)}$, given by eq. (3.4), is determined by the contribution of the previous turning point. When $|\gamma| > |\gamma_f|$, the third rule in eq. (3.4) specifies that the stress-strain path follows the backbone equation. Memory of all previous turning points is erased each time the strain-stress path returns to the backbone curve.

When the backbone curve is given by the hyperbolic model (eq. 3.2), the expression for $c_H^{(n)}$ is given by the following relation:

$$c_H^{(n)} = \frac{\left(F_{bb}(Sign\left(\frac{d\gamma}{dt}\right)|\gamma_f|) - \tau^{(n)}\right)\left|Sign\left(\frac{d\gamma}{dt}\right)|\gamma_f| - \gamma^{(n)}\right|}{\left(Sign\left(\frac{d\gamma}{dt}\right)|\gamma_f| - \gamma^{(n)}\right)\tau_{\max} + \left(\tau^{(n)} - F_{bb}(Sign\left(\frac{d\gamma}{dt}\right)|\gamma_f|)\right)\gamma_{ref}} \qquad (3.6)$$

where the reference strain $\gamma_{ref} = \tau_{\max}/G_{\max}$. Note that, in general, the parameter $c_H^{(n)}$ will have a different value for different unloadings or reloadings. It is convenient to bound the parameter γ_f by the following relationship $|\gamma^{(1)}| \le |\gamma_f| < \infty$, where $\gamma^{(1)}$ corresponds to the first turning point and the upper bound corresponds to the Cundall-Pyke hypothesis (Pyke, 1979). For the CEP ground motion calculations $\gamma_f = \gamma^{(1)}$ with implementation of the third rule in eq. (3.4).

The NOAH code can perform effective stress or total stress analyses. The CEP calculations used the total stress option. Because of the extremely low permeability of the Sisquoc and its dilatant nature in shear, no influence of pore–pressure variation on the ground motion was expected.

3.2.2 Additional Soil Dynamics Computer Models for the UCSB Studies

The field of nonlinear dynamic analysis is much more complex than that of linear analysis. It behooves calculators to make every effort to verify their nonlinear calculations. Since analytical, exact solutions typically do not exist for such purpose, an accepted practice is to compare the

results obtained with different nonlinear models. In order to assess the calculations performed with the NOAH model, the CEP also took advantage of the availability of other soil dynamics models in the U.C. community. Two such codes were exercised on the UCSB ground motion project, as described in paragraph 3.3.2. Both are finite element models which perform three-component 1-D wave propagation through nonlinear soils.

The first one is the SUMDES (Sites Under Multi-Directional Earthquake Shaking) code from U.C. Davis (Li et al, 1992). Its formulation is based on "bounded surface" plasticity. SUMDES can do effective stress analysis. The second one is the CYCLIC code from U.C. San Diego (Elgamal, 1991, 1999a, 1999b). It is an effective stress formulation, as well. Additional information regarding CYCLIC is available on line at http://casagrande.ucsd.edu.

3.2.3 UCSB Soil Profile, and Soil Profile Model Validation

For the purpose of the soil dynamics calculations, the properties of the soil profile at UCSB were derived from the in-situ velocity logs and from the laboratory tests described earlier. The values of some of the properties of the14-layer NOAH model for the UCSB site are shown in Table 3.4.

Table 3.4. Soil profile properties used in the NOAH nonlinear soil model. The water table is located at 4.56 m of depth; ν is the Poisson ratio, and K_0 is the coefficient of earth pressure at rest.

Layer	Depth m	V_s m/sec	ν	ρ kg/m^3	ϕ	K_0
1	1.52	320	0.333	1804	45°	0.5
2	4.56	210	0.333	1804	45°	0.5
3	7.0	361	0.47	1560	40°	1.5
4	16	400	0.46	1682	35°	2.0
5	25	400	0.46	1682	35°	2.0
6	39	458	0.453	1682	35°	2.0
7	55	404	0.461	1682	35°	2.0
8	57	1500	0.114	1800	35°	3.0
9	58	593	0.431	1800	35°	3.0
10	59	431	0.460	1800	37°	3.0
11	64	340	0.474	1800	37°	3.0
12	65	412	0.461	1800	37°	2.0
13	66	465	0.45	1800	37°	2.0
14	68	492	0.452	1800	37°	2.0
Rock	74					

The extensive field and laboratory characterization of the UCSB soils lends confidence in the numerical model of the site. Nevertheless, the availability of actual earthquake records at the surface and at depth below the site provides an opportunity for further checking of that model. This is achieved, for example, by using pairs of up-and-down recordings and determining how well the site model reproduces the downhole record, given the surface motion time-history. The pair of records selected for that verification is from the August 15, 1999 event on the Santa Ynez fault (M 3.2 at 11 km). Figure 3.10 shows the very good agreement between recorded and computed motions, thus further validating the UCSB soil profile model. It also shows that a 1-D vertical wave propagation assumption is appropriate for the UCSB site.

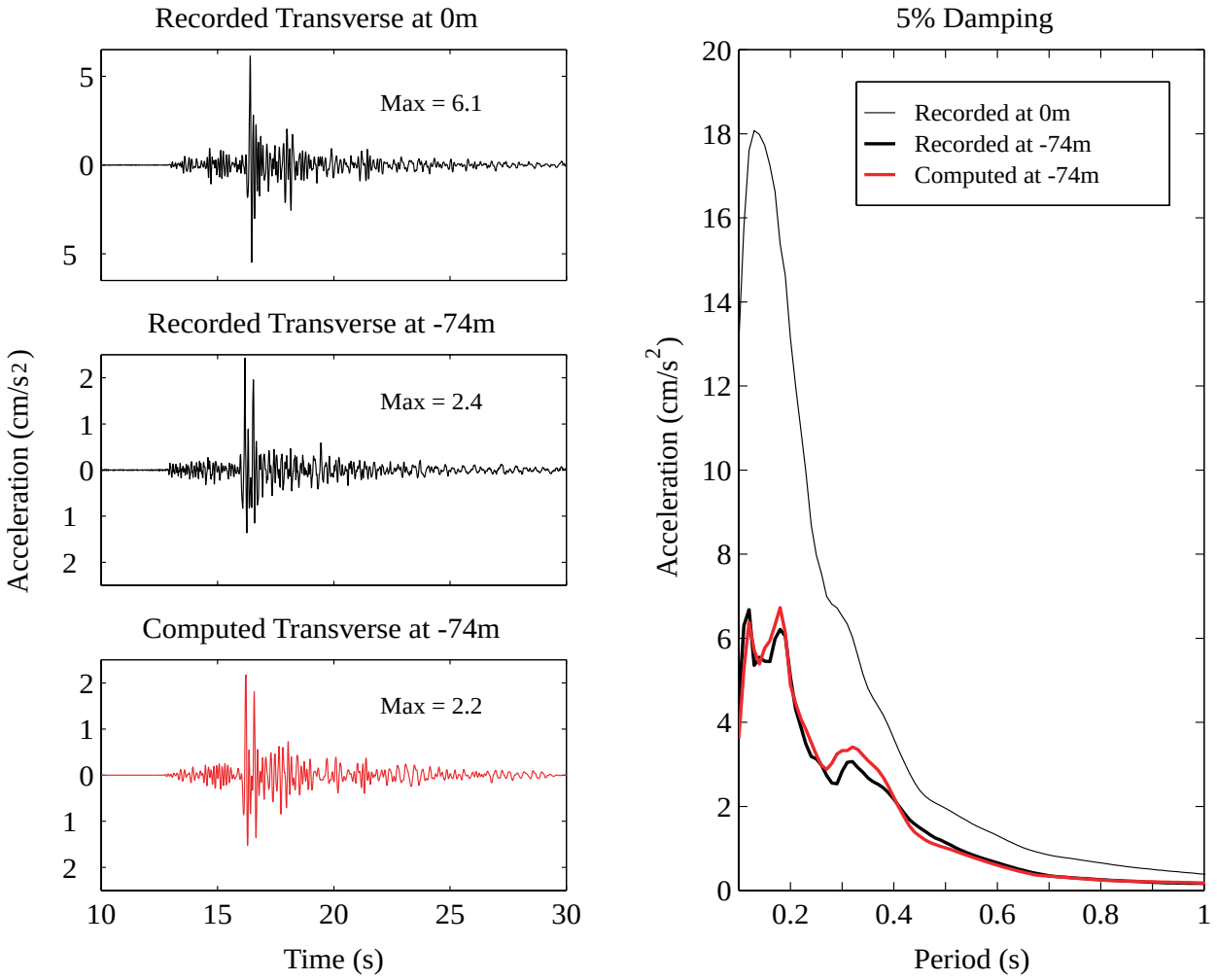

Figure 3.10 Comparison of the computed and recorded accelerograms at 74-m depth for the transverse component. Both the surface and downhole records were rotated to the transverse direction of the event, to maximize the SH component. The computed signal was obtained by a deconvolution of the signal recorded at the surface (the top figure on the left side). On the right side are the corresponding 5% damping response spectra.

3.3 The CEP Surface Strong Motion Estimates for UCSB

3.3.1 Calculations of Surface Strong Motions for UCSB

The downhole incident strong motions obtained as described in Chapter 2 were propagated to the surface using the NOAH model. The results are shown in Figures 3.11 to 3.13 in terms of spectral accelerations versus period. The three spectral lines are respectively the mean and the plus and minus one standard deviation of the scenario population. Surface acceleration time-histories representative of the mean and + 1 standard deviation (+1 sigma) for the 1998-based and 1999-based scenarios are shown in Figures 3.14 and 3.15.

3.3.2 Comparison of Calculations with NOAH and Other Nonlinear Codes

In order to compare calculations from the NOAH, SUMDES, and CYCLIC models, the 1999-based 3-component downhole incident time-histories shown in Figure 2.13 were used as input and propagated up the soil column. In NOAH, the intrinsic attenuation (seismic Q) was taken from the UCLA tests at very low strains; it ranged from 0 to 2.5%, depending upon the layer. In SUMDES and CYCLIC, both finite element codes, the numerical damping was respectively 0.5 % and 0.8%. In all codes the nonlinear hysteretic damping varied with strain, as determined from the UCLA tests.
The comparison of results from the three models, for the three components of motion, are shown in Figures 3.16 to 3.21, both for the time-histories and for the spectral accelerations. The results from the models are quite consistent, thus lending confidence to the surface motion estimates.

.

3.3.3 CEP Surface Motions for UCSB Compared to Northridge Earthquake Records

The strong motion estimates provided by the CEP approach can be evaluated for their relation to reality by looking for actual records obtained at a comparable distance from the epicenter of a similar earthquake in the region. As it turns out, the Northridge earthquake of 1994 was in the same region; its magnitude, M 6.7, was comparable; and there are records from seismometers at distances similar to that of the UCSB campus from a M 6.8 event on the North Channel-Pitas Point fault. Moreover both the NCPP and the fault in the Northridge event have the same type of blind thrust rupture. Figure 3.22 shows records from the NRG and CPC stations, whose closest distance to the fault were respectively 12.9 km and 15.7 km. Both sites were in alluvium with average shear-wave velocities over the top 30 m of 268 and 282 m/s respectively, i.e. slower than UCSB's 383 m/s. The Northridge records were low-passed at 10 Hz, to be compatible with the nonlinear soil calculations. Figure 3.22 calls for the following comments:

- The CPC and NRG East-West records are generally compatible with the mean CEP estimates, and the North-South records are more in line with, and sometimes exceed the + 1 sigma CEP

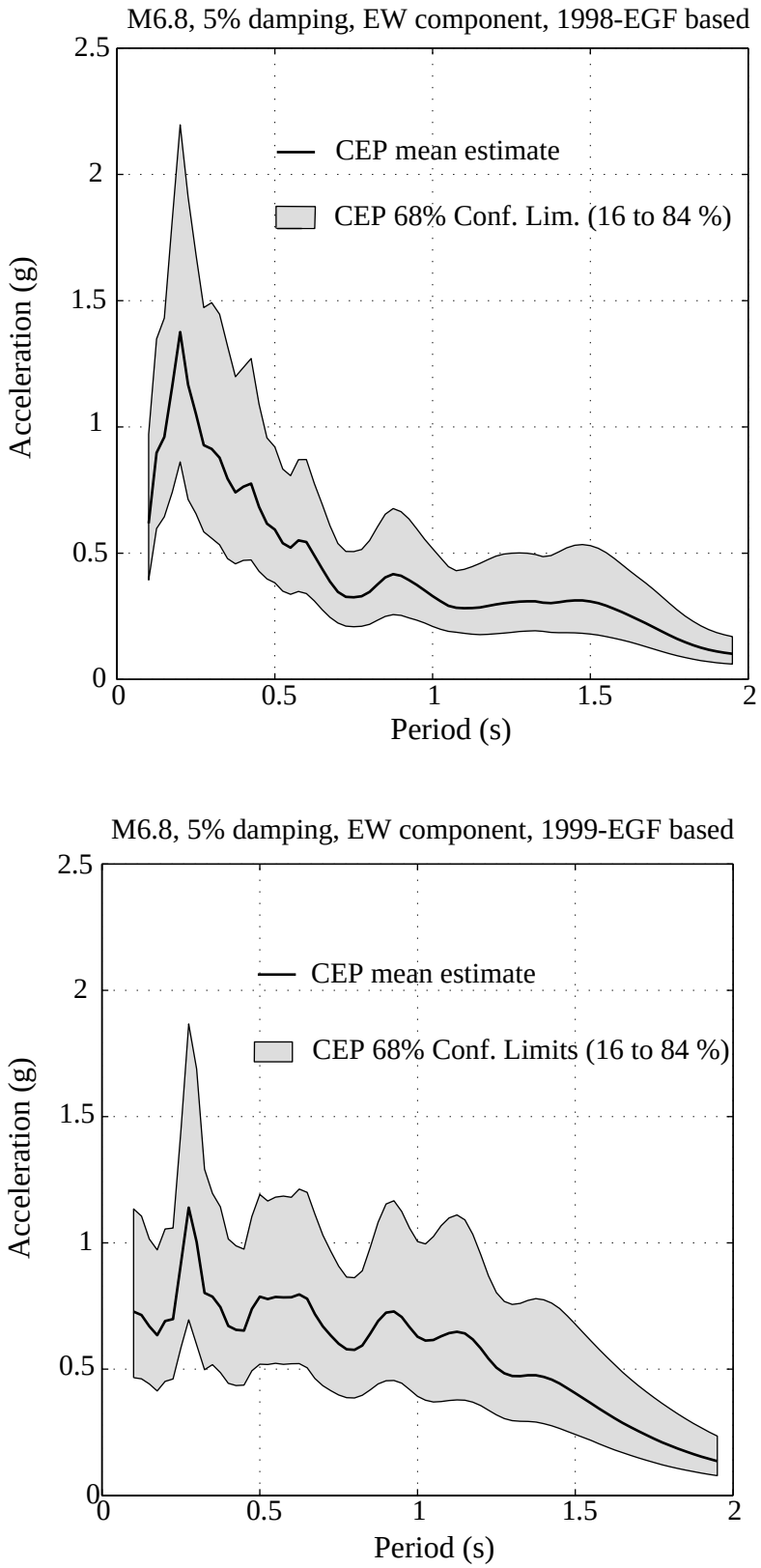

Figure 3.11 UCSB CEP surface motions, EW component 1998- and 1999-based scenarios

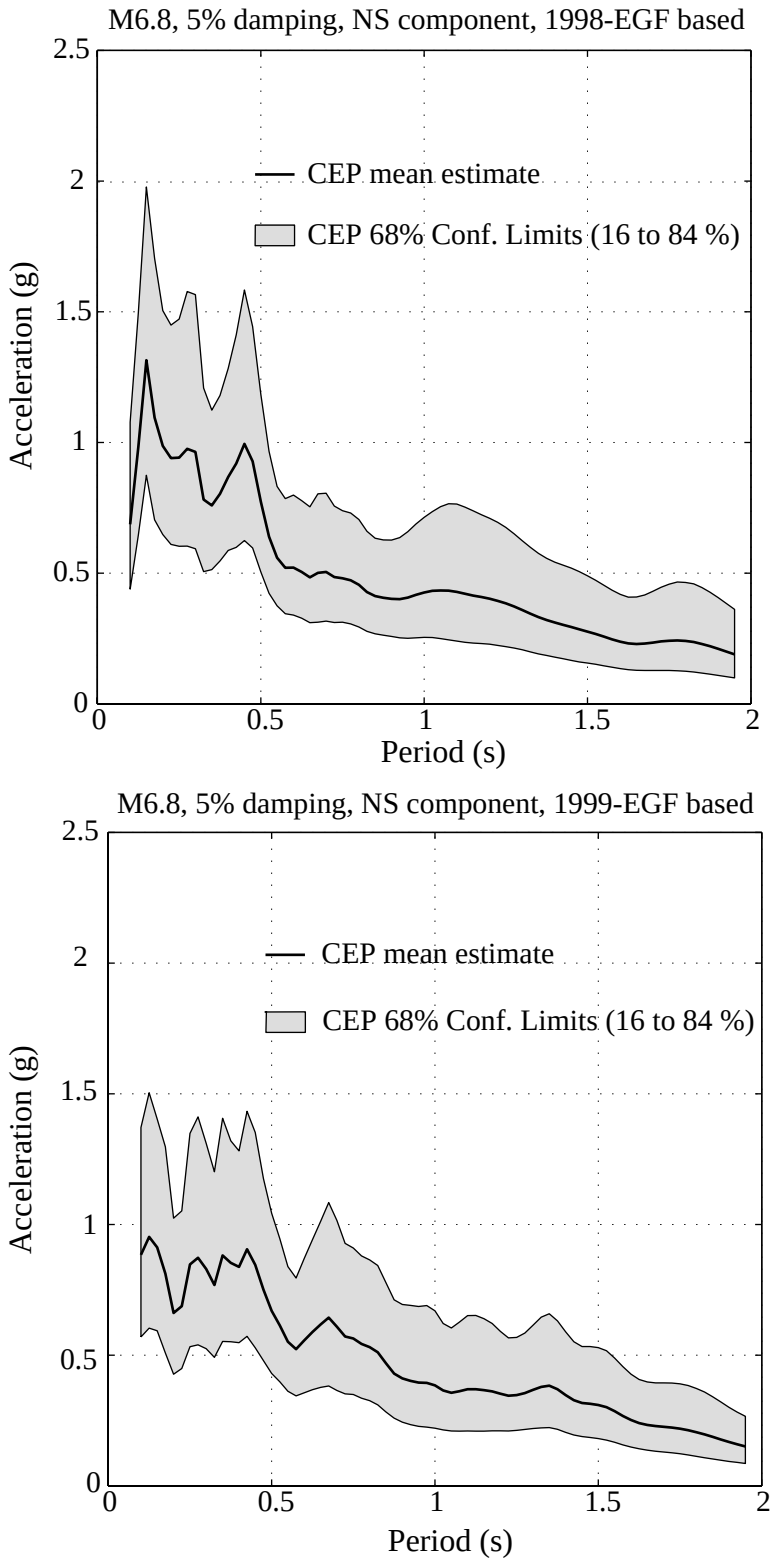

Figure 3.12 UCSB CEP surface motions, NS component, 1998- and 1999-based scenarios,

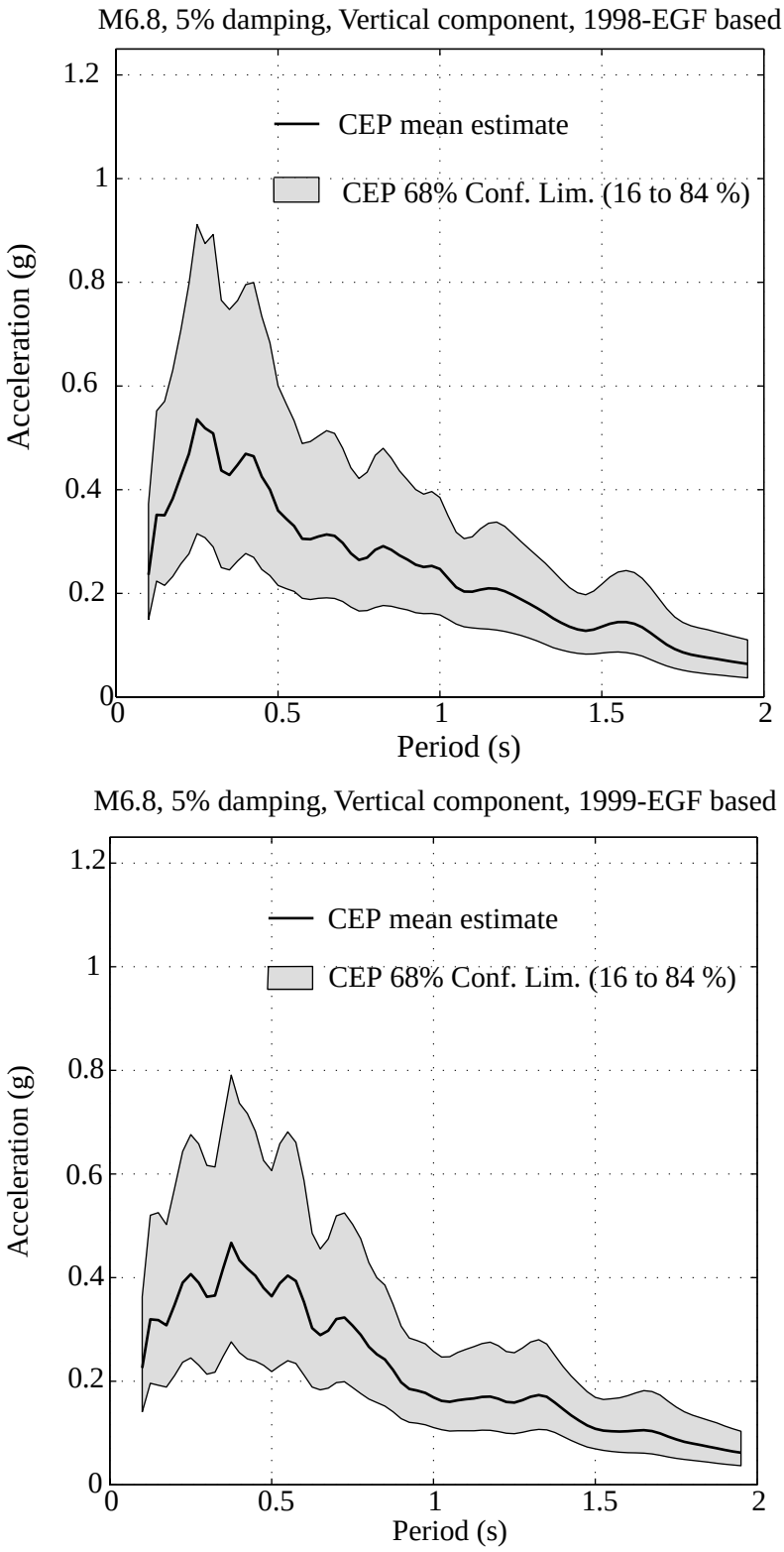

Figure 3.13 UCSB CEP surface motions, vertical component, 1998- and 1999-based scenarios.

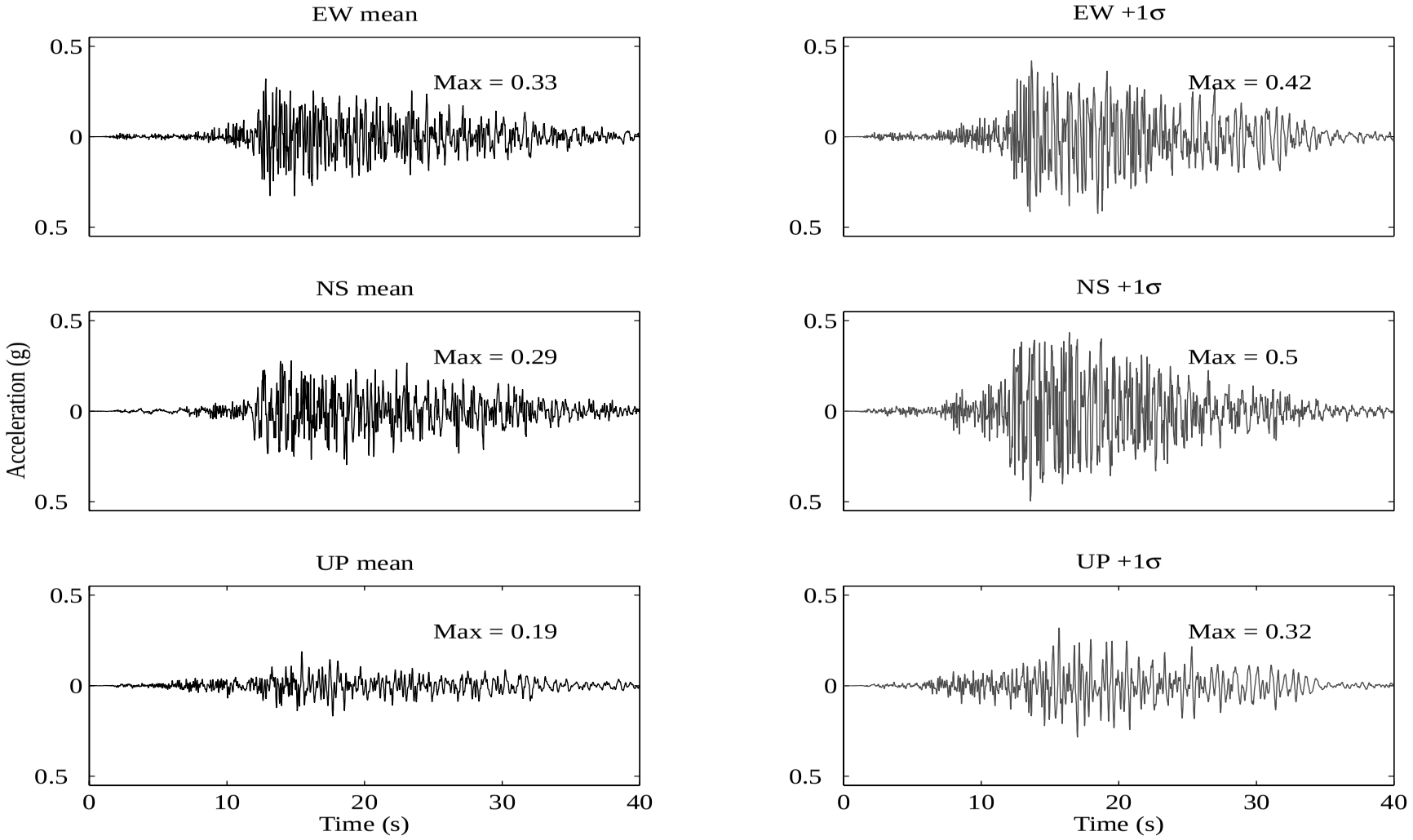

Figure 3.14 Surface acceleration time-histories representative of the mean and + 1 sigma motions, based on the 1998 EGF

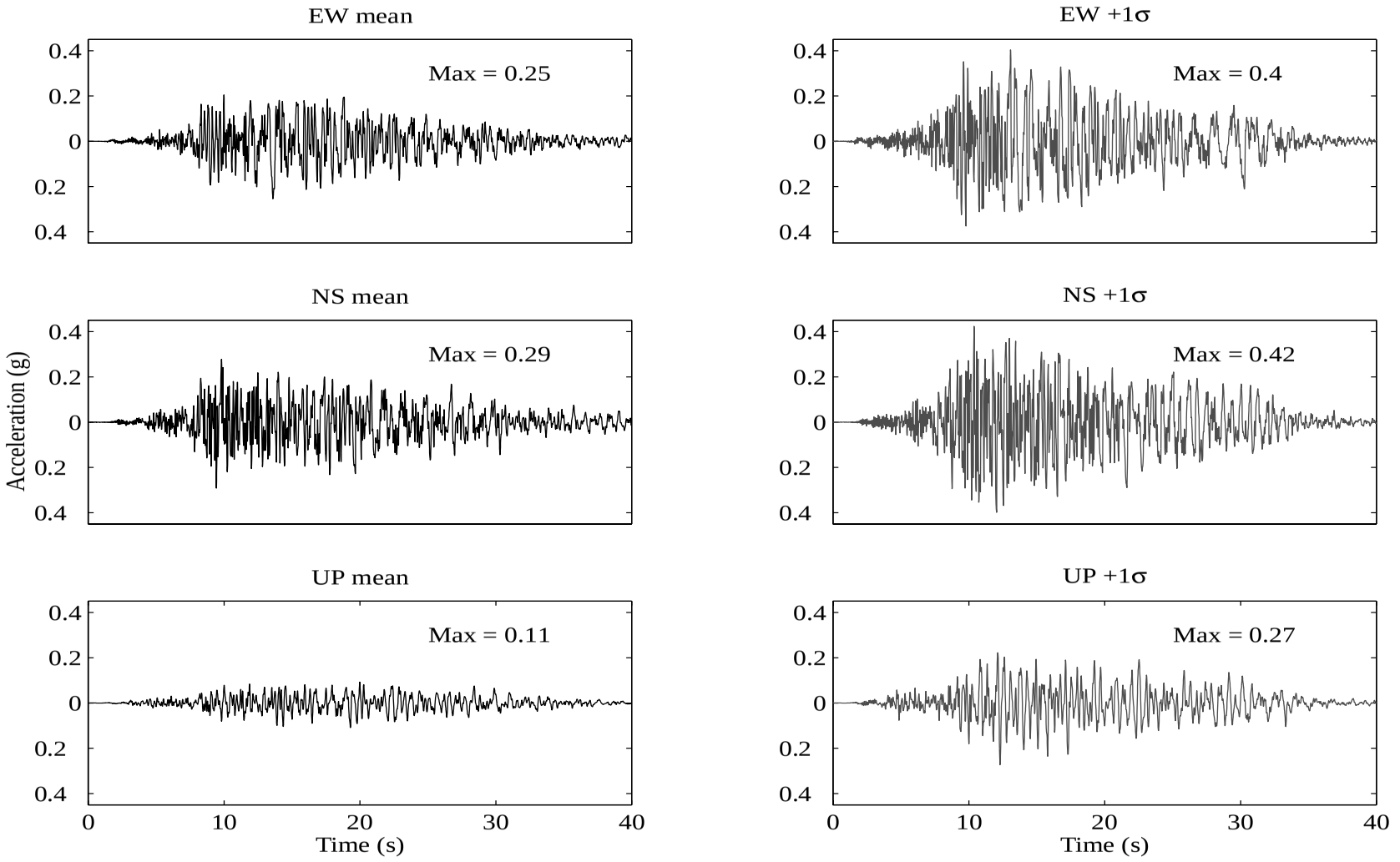

Figure 3.15 Surface acceleration time-histories representative of the mean and + 1 sigma motions, based on the 1999-EGF

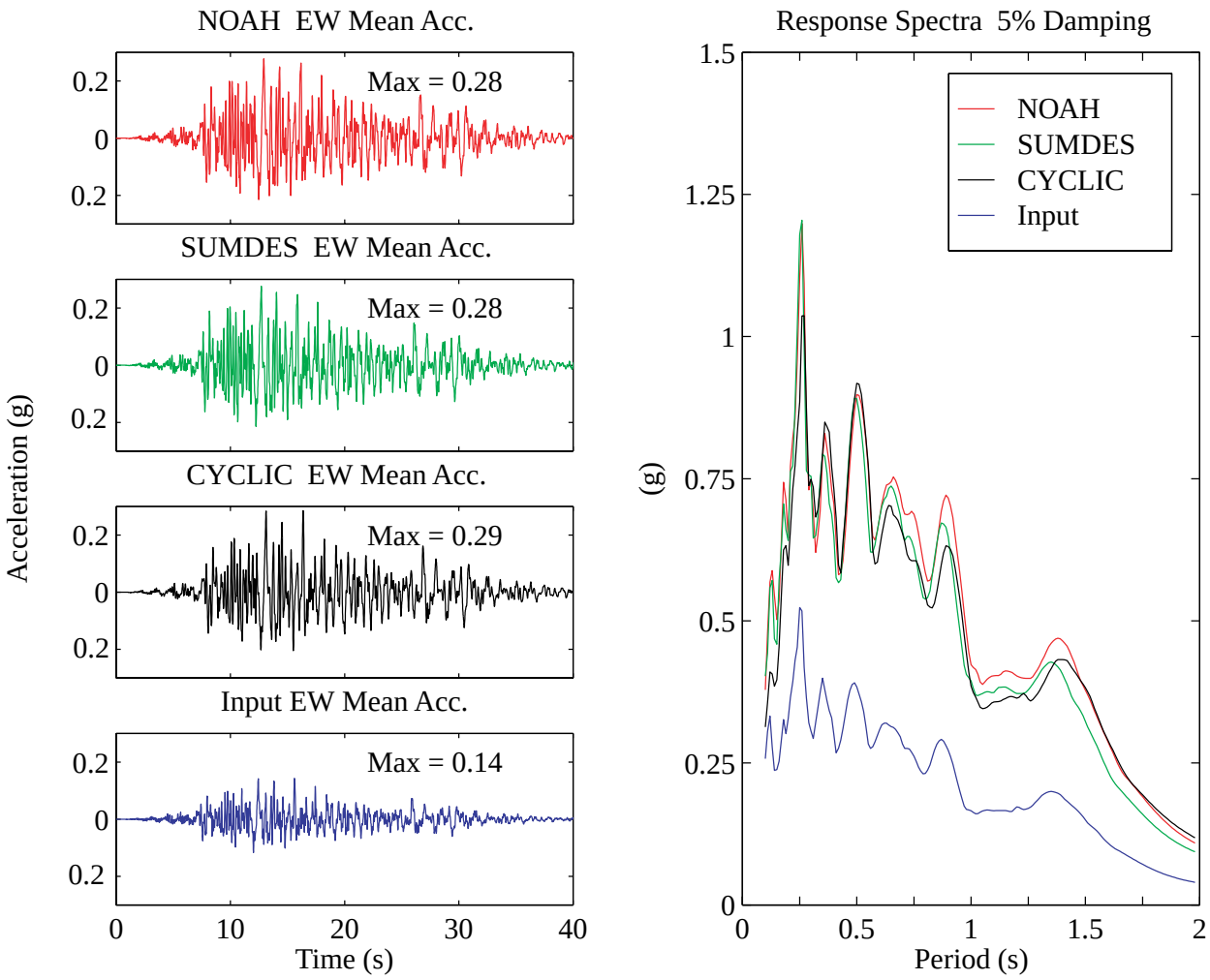

Figure 3.16 Comparison of NOAH, SUMDES, and CYCLIC results, mean, EW component

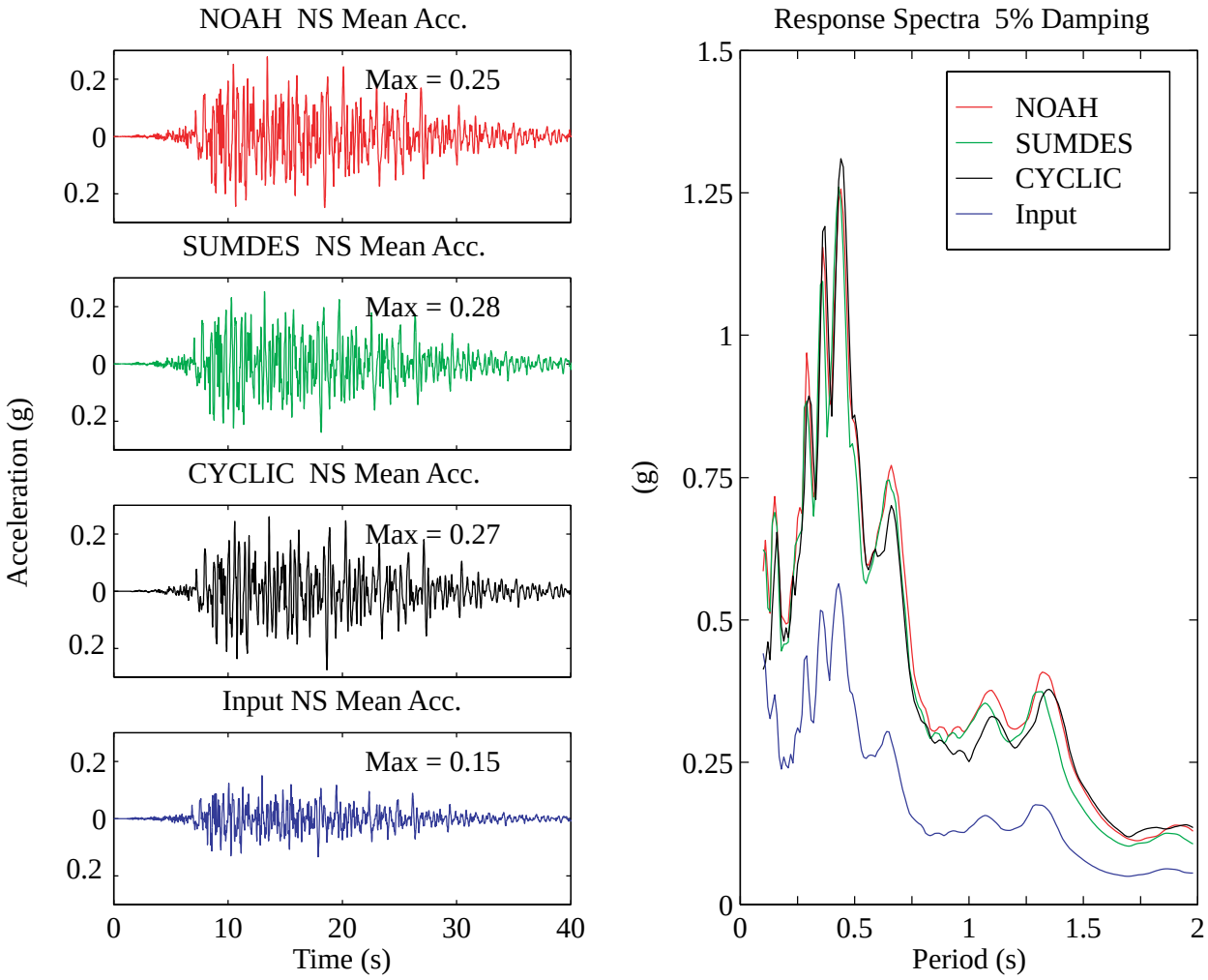

Figure 3.17 Comparison of NOAH, SUMDES, and CYCLIC results, mean, NS component

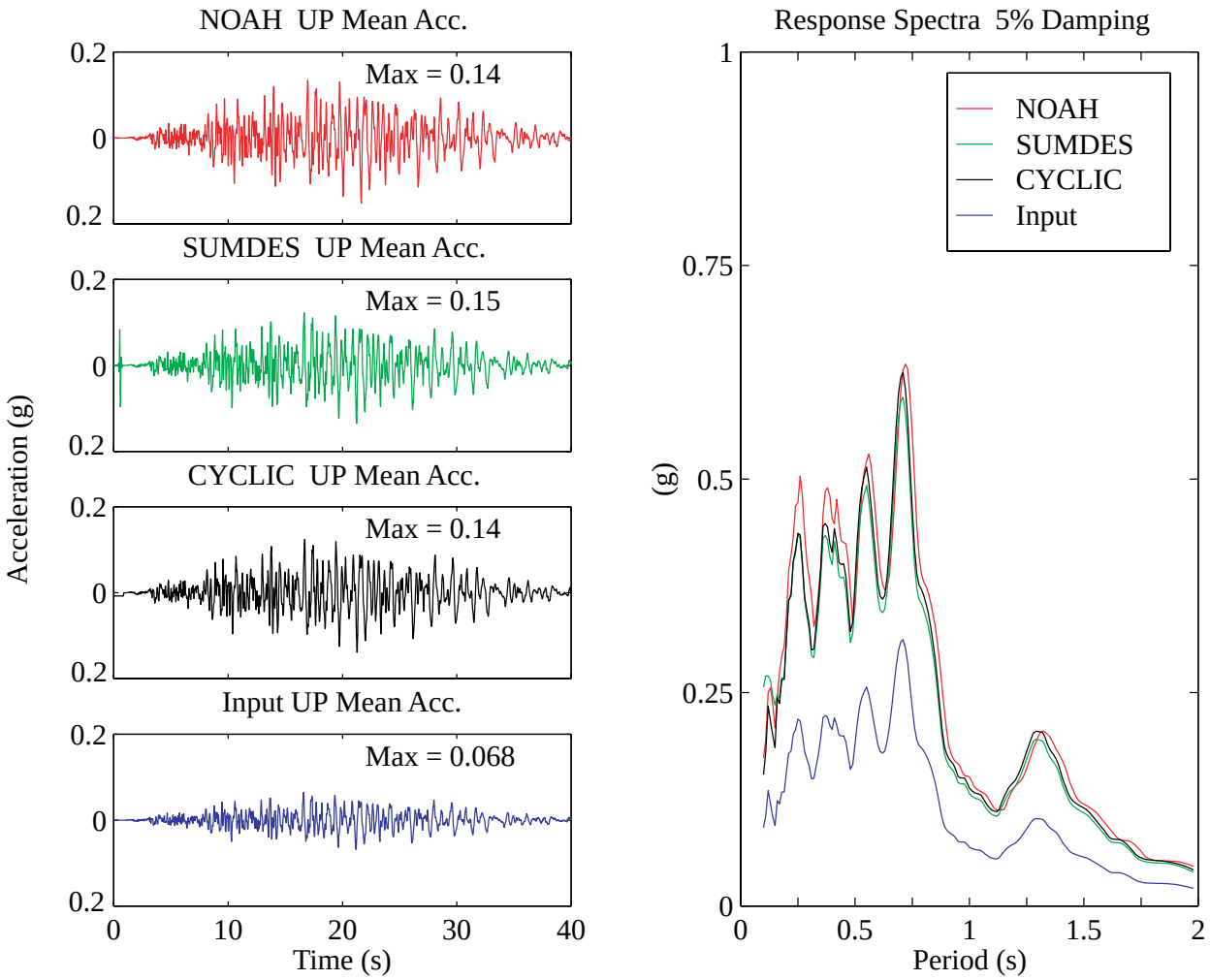

Figure 3.18 Comparison of NOAH, SUMDES, and CYCLIC results, mean, vertical component

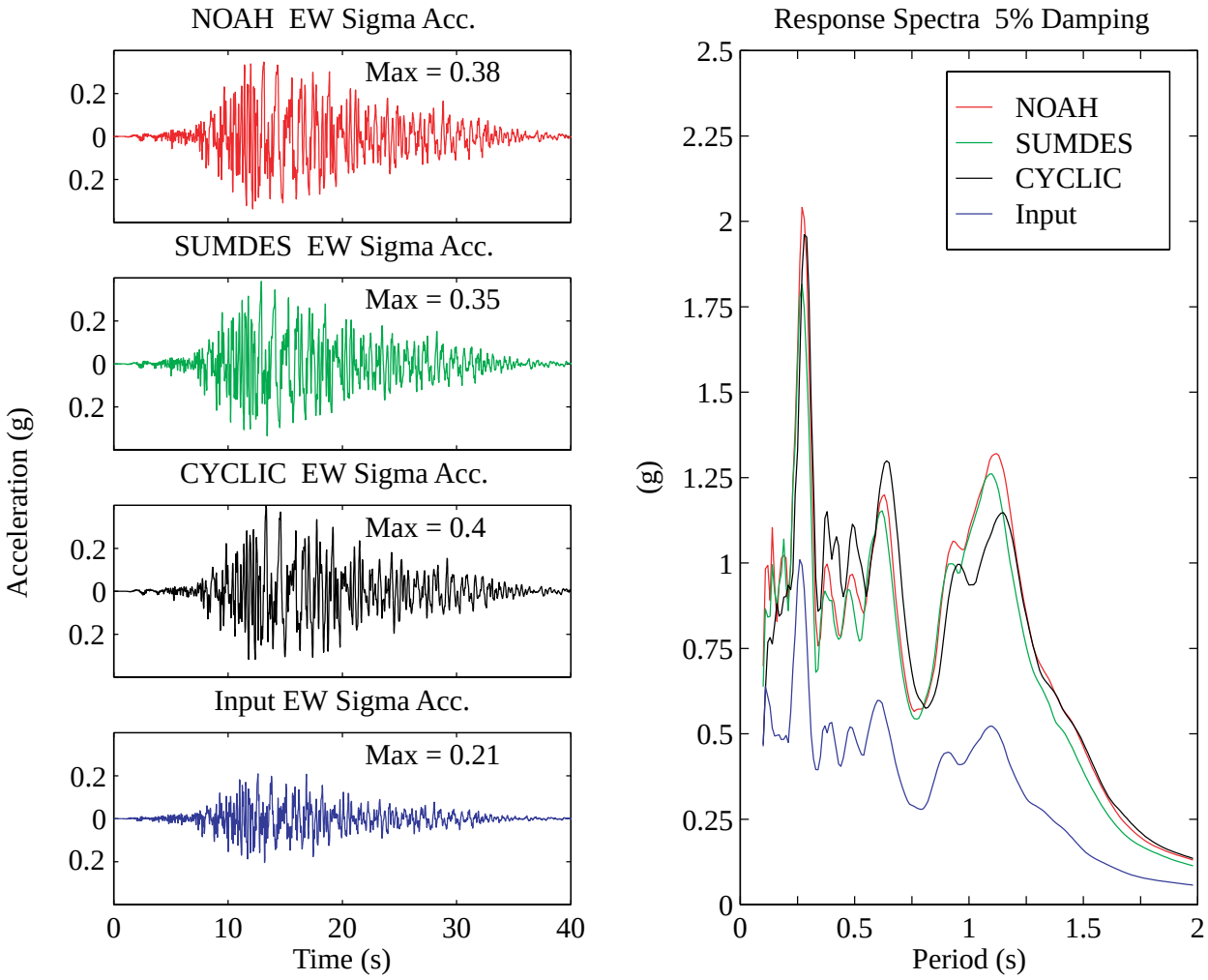

Figure 3.19 Comparison of NOAH, SUMDES, and CYCLIC, + 1 sigma, EW component

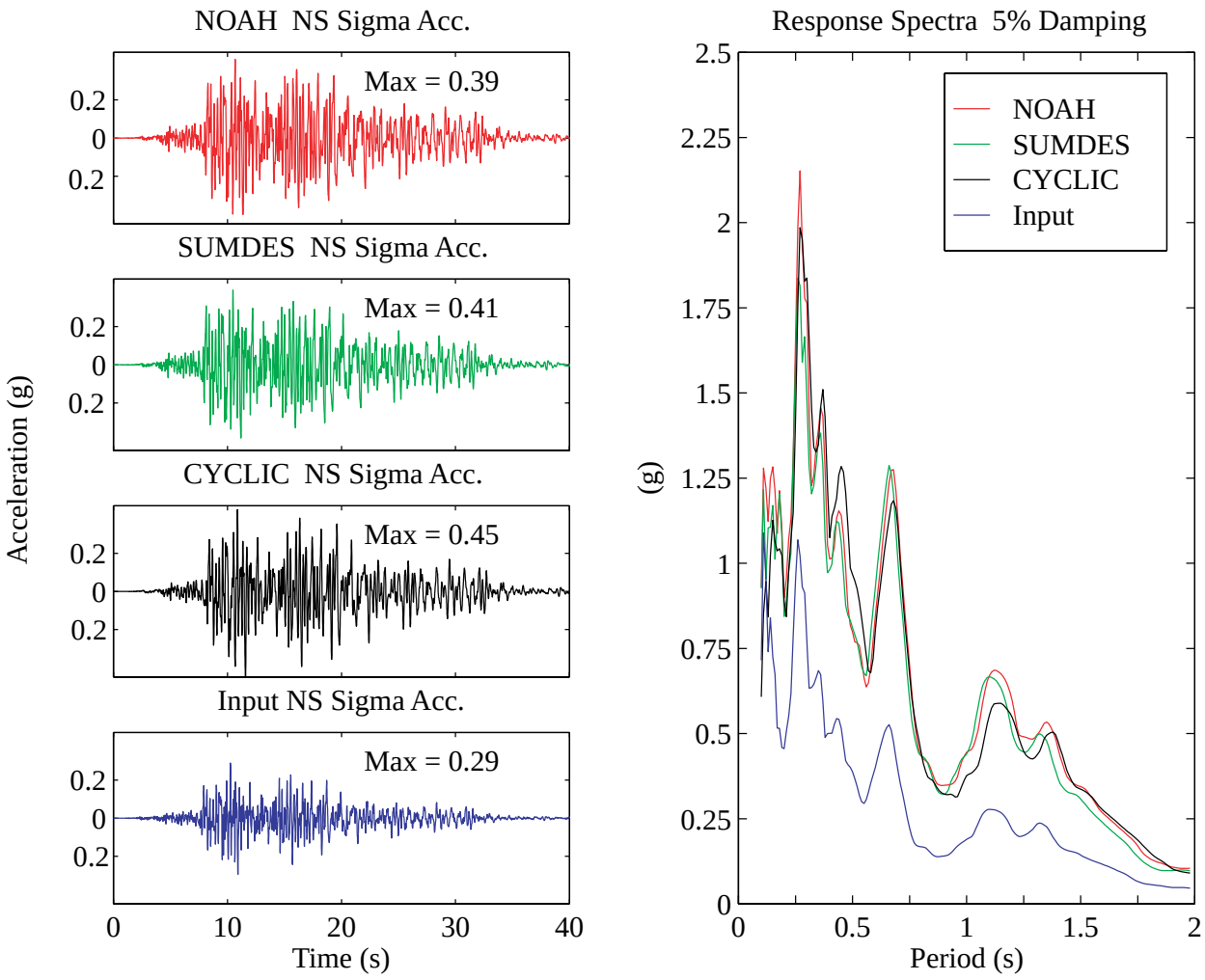

Figure 3.20 Comparison of NOAH, SUMDES, and CYCLIC, + 1 sigma, NS component

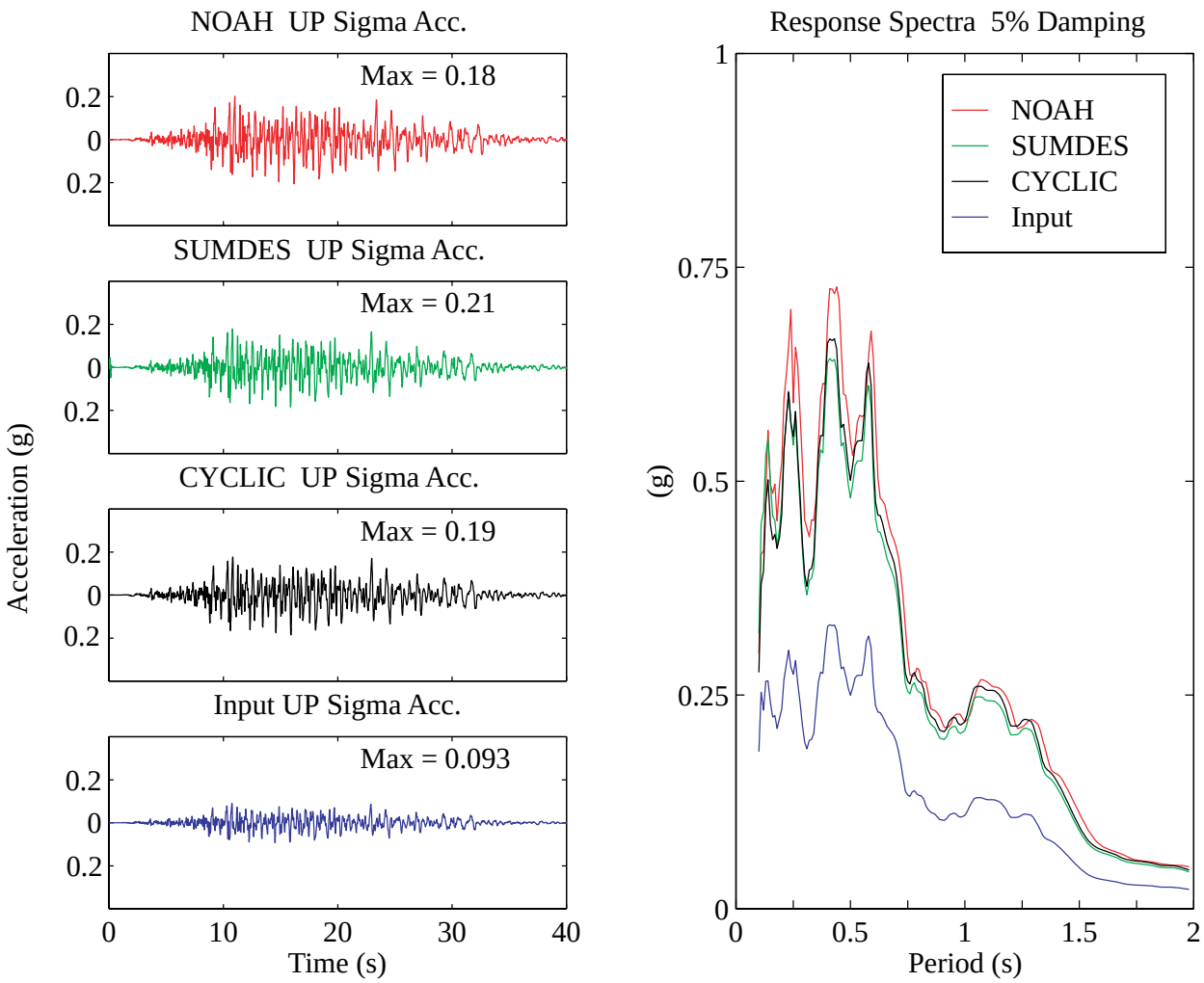

Figure 3.21 Comparison of NOAH, SUMDES, and CYCLIC, + 1 sigma, vertical component

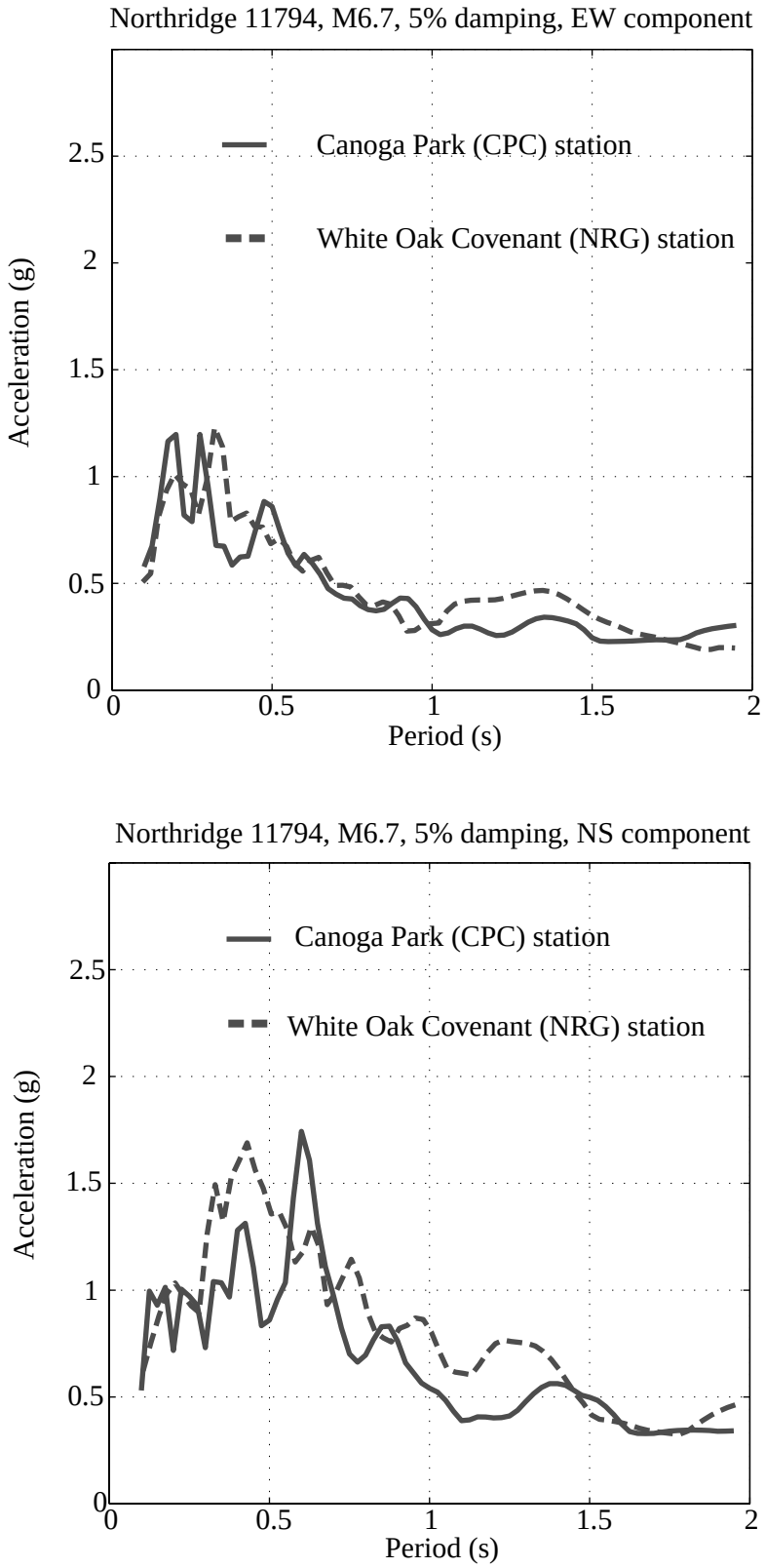

Figure 3.22 Northridge surface records at the NRG and CPC stations for comparison to UCSB estimates. Note the difference between EW and NS and the site effect on acceleration vs. period.

estimates. This draws attention to the need for looking at a broad range of fault rupture scenarios and not limiting one's expectations or design to the assumption of a mean scenario.

- The records show strong differences in amplitude between the EW and NS directions. This clearly emphasizes the fact that state-of-the-practice methods which do not differentiate between horizontal directions may fall short of recognizing the importance of fault rupture kinematics.
- The records highlight the fact that local site response can emphasize some particular frequencies and hence have a more pronounced impact on buildings in a particular height range. This once again reinforces the case for obtaining truly site-specific estimates of strong ground motion.

3.3.4 Nonlinear Behavior of the UCSB soils

The CEP estimates of surface motions use nonlinear soil dynamics models because of the presumed nonlinear response of soils to the strong motions. This assumption is corroborated by the level of shear strains expected in a M 6.8 event on the NCPP fault. Figure 3.23 shows a profile of maximum shear strain in the UCSB soil column, versus depth, for a mean and a + 1 sigma scenario in the NS direction. Based on the modulus degradation curves of section 3.1.2 (Figure 3.5) the shear modulus of the soils in the top 30 m may be reduced by up to 30% in a mean scenario and up to 40% in a + 1 sigma scenario.

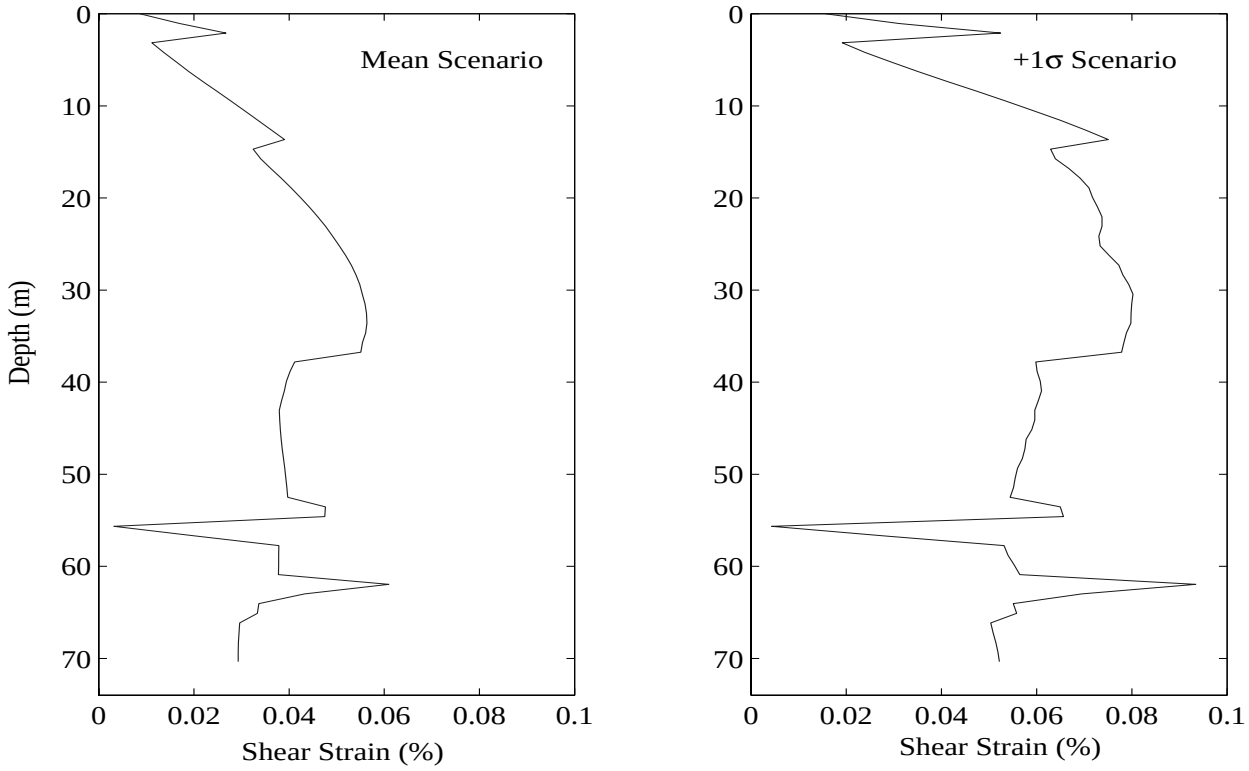

Figure 3.23 Maximum shear strain vs. depth in the NS direction, for the1999-EGF based scenarios

3.4 Overall Comparison of the CEP and State-of-Practice Estimates

Typically, one would obtain ground motion estimates for the UCSB site by using other approaches. One is the 1997 Uniform Building Code (UBC 97) procedure. The outcome is shown in Figure 3.24 for 5% damping and for a Soil C site condition, based on the results of the CEP geophysical logging, and on the relevant causative fault(s) (see International Conference of Building Officials/ICBO, 1997). We also show the General Procedure Response Spectrum based on the 2000 International Building Code (ICBO, 2000).

Another approach is to obtain estimates from Probabilistic Seismic Hazard Analyses (PSHA), such as those based on the research of the California Department of Mines and Geology (Petersen et al, 1996; Blake, 1999). The results are also shown on Figure 3.24 for recurrence probabilities of 10%, 5%, and 2% in 50 years (return periods of 475, 950, and 2375 years respectively). The Design-Basis Earthquake (DBE) used for the retrofit of the Engineering I building is also included in Figure 3.24. It is very clear that this DBE assumption is significantly lower than current state-of-the practice estimates would provide.

In turn, the CEP results of section 3.3.1 are compared to these state-of-practice estimates (Figures 3.25 to 3.27). These overall results provide a new basis for future seismic designs at UCSB.

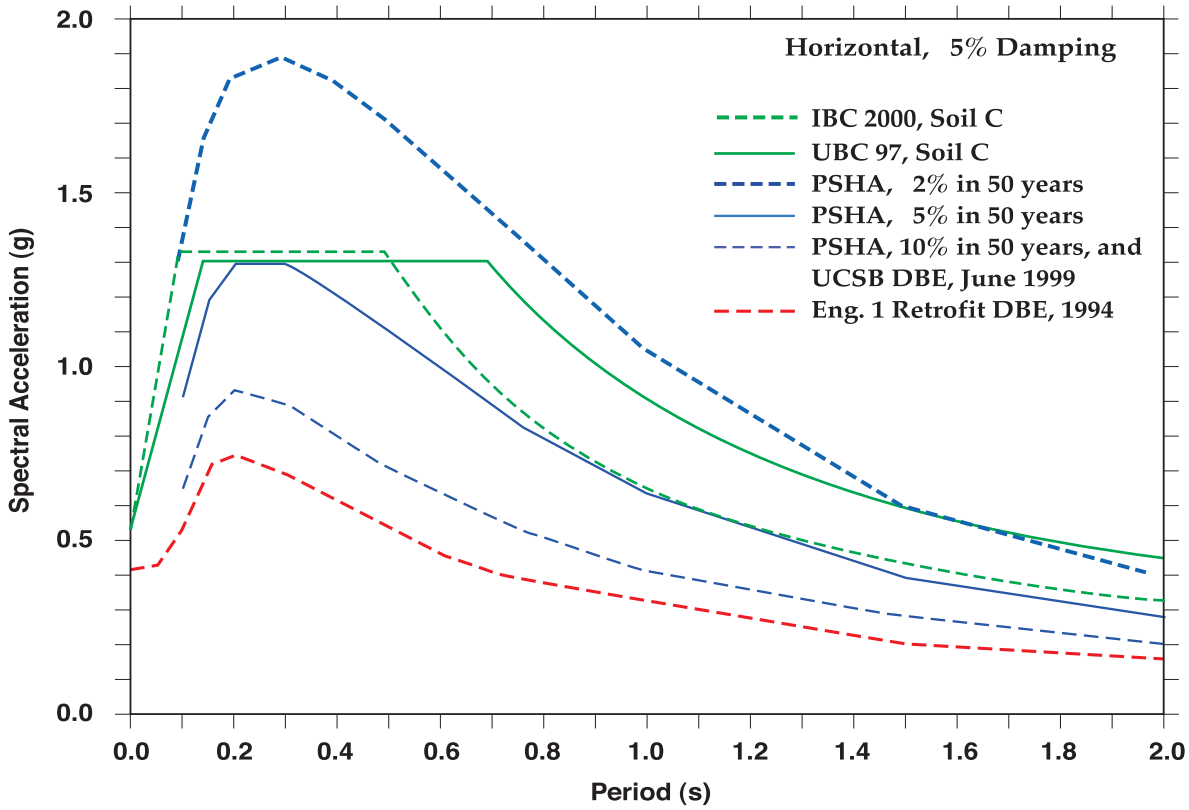

Figure 3.24 Comparison of various state-of-the-practice surface motion estimates for UCSB

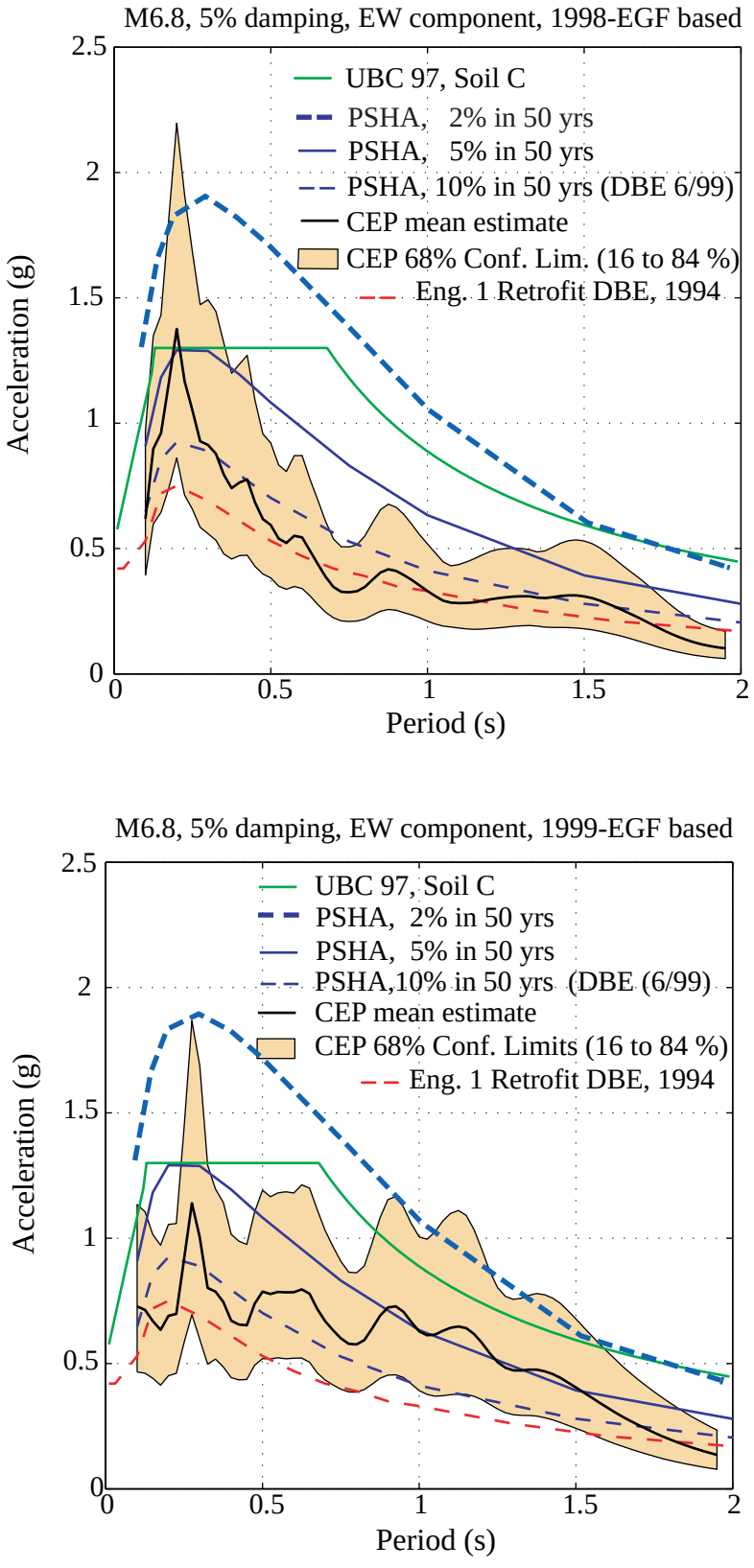

Figure 3.25 Comparison of CEP and state-of-the-practice surface motions, EW component.

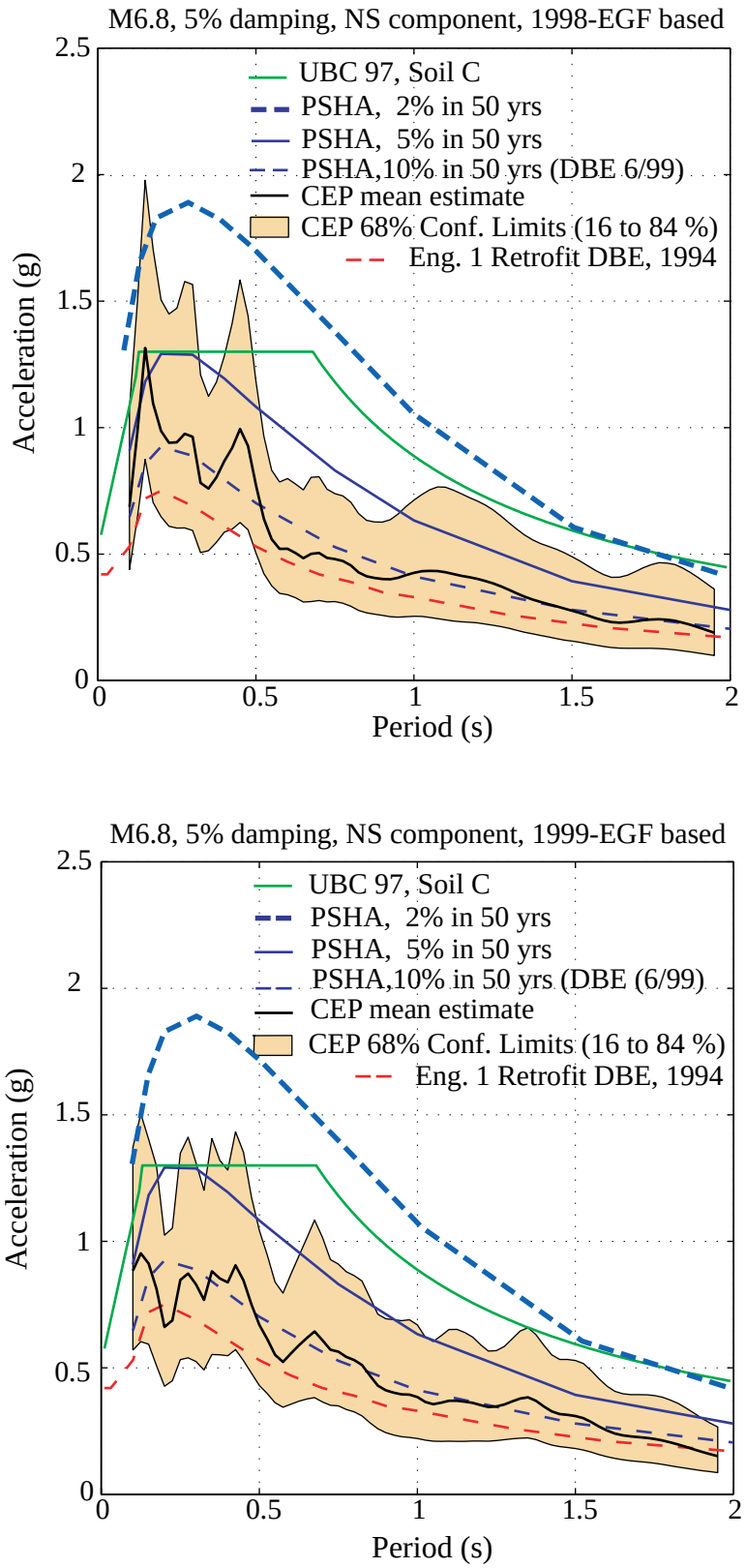

Figure 3.26 Comparison of CEP and state-of-the-practice surface motions, NS component.

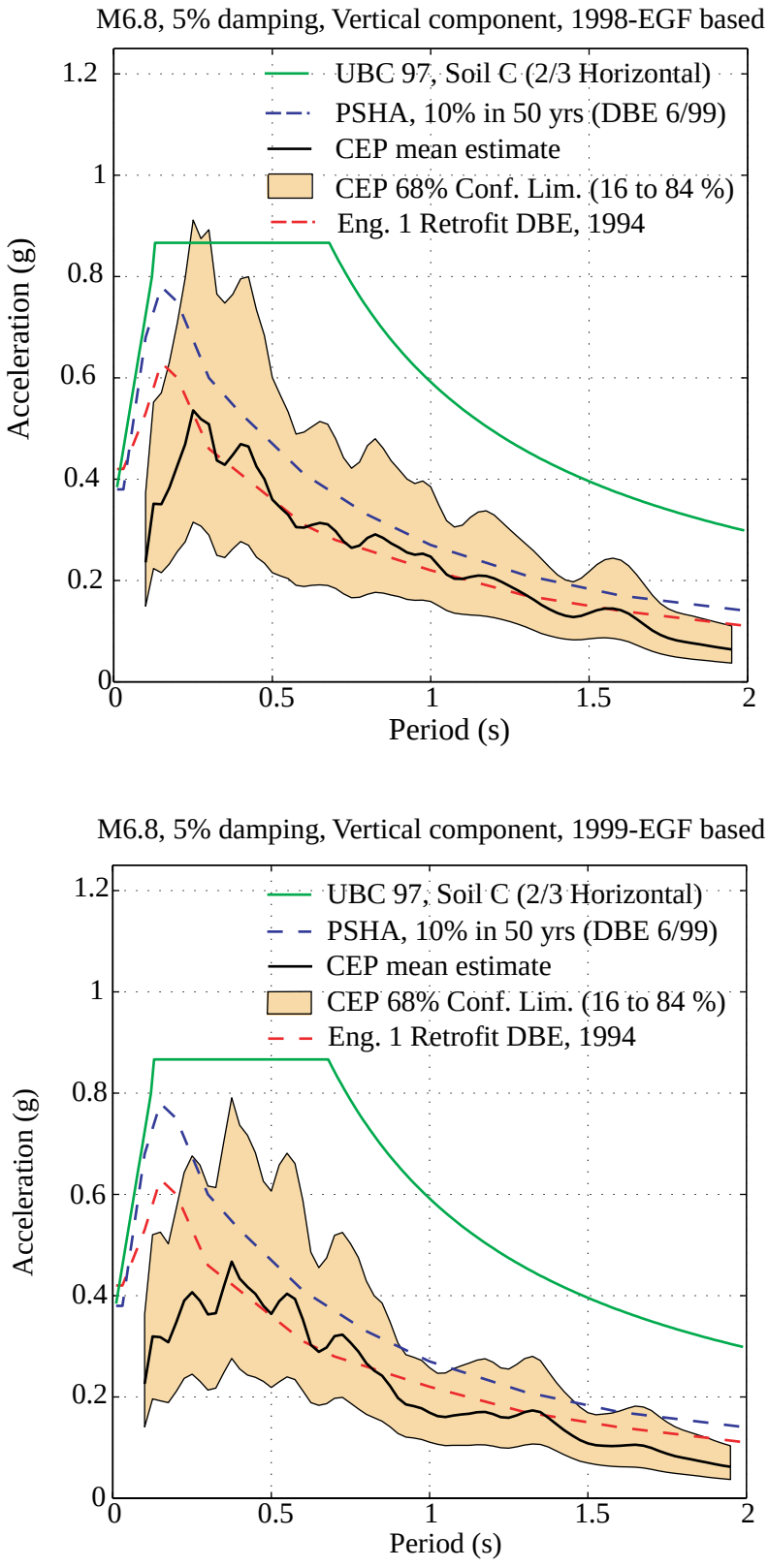

Figure 3.27 Comparison of CEP and state-of-the-practice surface motions, vertical component.

3.5 A Note Concerning the New IBC 2000

The International Building Code 2000 (ICBO, 2000) describes the method for constructing a General Procedure Response Spectrum. For UCSB, this spectrum was shown in Figure 3.24.

The new code also has provisions for Site-Specific Response Spectra, if certain conditions are met. Quoting paragraph 1615.2: "A site-specific study shall account for the regional seismicity and geology; the expected recurrence rates and maximum magnitudes of events on known faults and source zones; the location of the site with respect to these; near-source effects, if any; and the characteristics of subsurface site conditions". For example, these requirements clearly are met by the CEP studies at U.C. Santa Barbara.

The code then addresses the maximum earthquake ground motion to be considered for site-specific approaches. It refers to three spectra:

- the one obtained from a 2%-in-50-years PSHA, which we shall call here spectrum A
- the "Deterministic Limit on Maximum Considered Earthquake", which is constructed based on a specified procedure. We shall call it spectrum B. Spectra A and B were drawn for UCSB and are shown on Figure 3.28.
- and, the "Deterministic Maximum Considered Earthquake", which is a spectrum "calculated as 150% of the median spectral accelerations at all periods resulting from a characteristic earthquake on any known active fault within the region". We will call it spectrum C. As an illustration of what a spectrum C may be for UCSB we have drawn an envelope of the 1998-based EW and NS horizontal spectra and scaled its acceleration by 150%. That is shown on Figure 3.28 as curve C-98. We have done the same for the 1999-based spectra, and show the envelope as C-99.

Then, the IBC states that where spectrum A exceeds spectrum B, the maximum considered spectrum shall be the lesser of A and C, but in no case less than B. In the example of Figure 3.28, this would mean that he maximum ground motion to be considered would be represented by a spectrum which is a composite of A, B, and C.

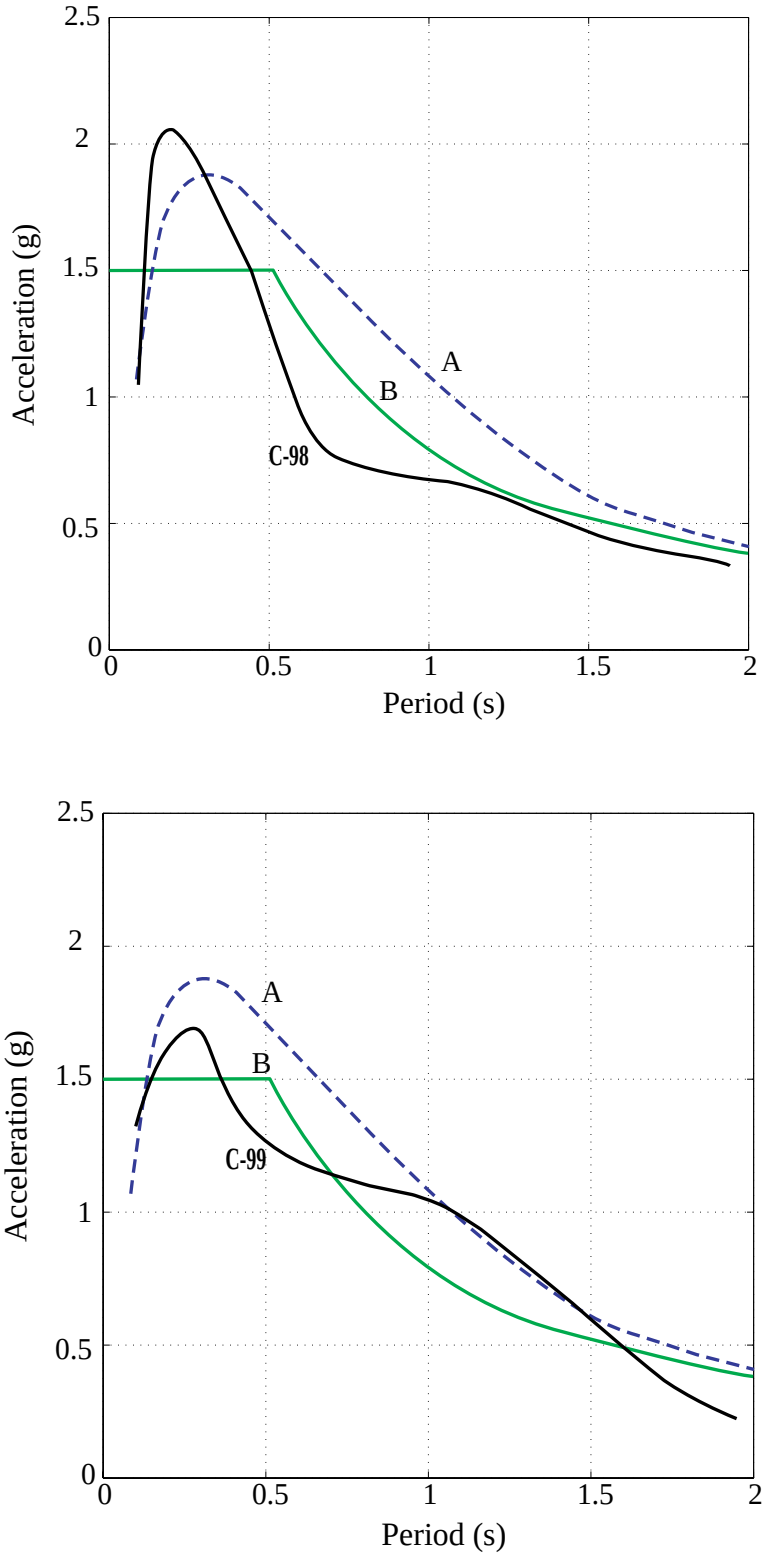

Figure 3.28 Comparison of various spectra in the IBC 2000 site-specific procedure for selecting the maximum earthquake motion to be considered, as applied to the UCSB campus.

4.0 STRUCTURAL DYNAMICS STUDIES OF ENGINEERING I

Engineering I is a 6-story concrete frame building with block shear walls. Its seismic retrofit was completed in 1998. The CEP structural studies performed for Engineering I thus were not for design. They demonstrate tools that can be applied to future building retrofits. These studies included a forced-vibration test of the building and new dynamic response analyses, under the Design-Basis Earthquake (DBE) and under the new CEP strong surface motions.

4.1 Forced Vibrations of Engineering I

4.1.1 The Forced-Vibration System

A shaker provided by U.C. San Diego was used for this test. It is of the counter-rotating-mass type, according to a design developed by Caltech in the 1960s (Hudson, 1962). It is capable of generating a maximum force of 5000 lbs at about 9 Hz. The force level may be varied by adjusting the rotating mass (inclusion or removal of modular weights installed within the rotating containers). Two available small masses can replace the rotating containers in order to extend the useable frequency range up to about 30 Hz (at which the force reaches 5,000 lbs). The electric motor controller allows for specification of the desired excitation frequency (by controlling the rotation rate), and can be conveniently used to conduct frequency-sweep tests. The shaker was employed earlier for testing the response of a reinforced concrete cantilever retaining wall along with the supported backfill ground (Elgamal et al., 1996).

4.1.2 The Forced-Vibration Test of November 23, 1998

An extensive array of seismometers was deployed in and around Engineering I, on November 23, 1998. The locations and types of the sensors are shown in Figure 4.1. A complete analysis or discussion of this experiment is beyond the scope of the present study, and the data were archived for potential future use. More information on the test results can be found at: http:// www-ccec.ece.ucsb.edu/people/smith/classnotes/130a/seismic.html. However, it is noteworthy that the shaker was successful in creating a strong transverse vibration of the building at a frequency measured at 2.47 Hz. This is quite close to the building's second vibration mode frequency of 2.34 Hz calculated with the structural model described in the next paragraph. Such shaker tests are reasonably quick to conduct (2 days or so). When performed before and after seismic retrofitting, they can help evaluate how retrofits actually modify the natural response of buildings.

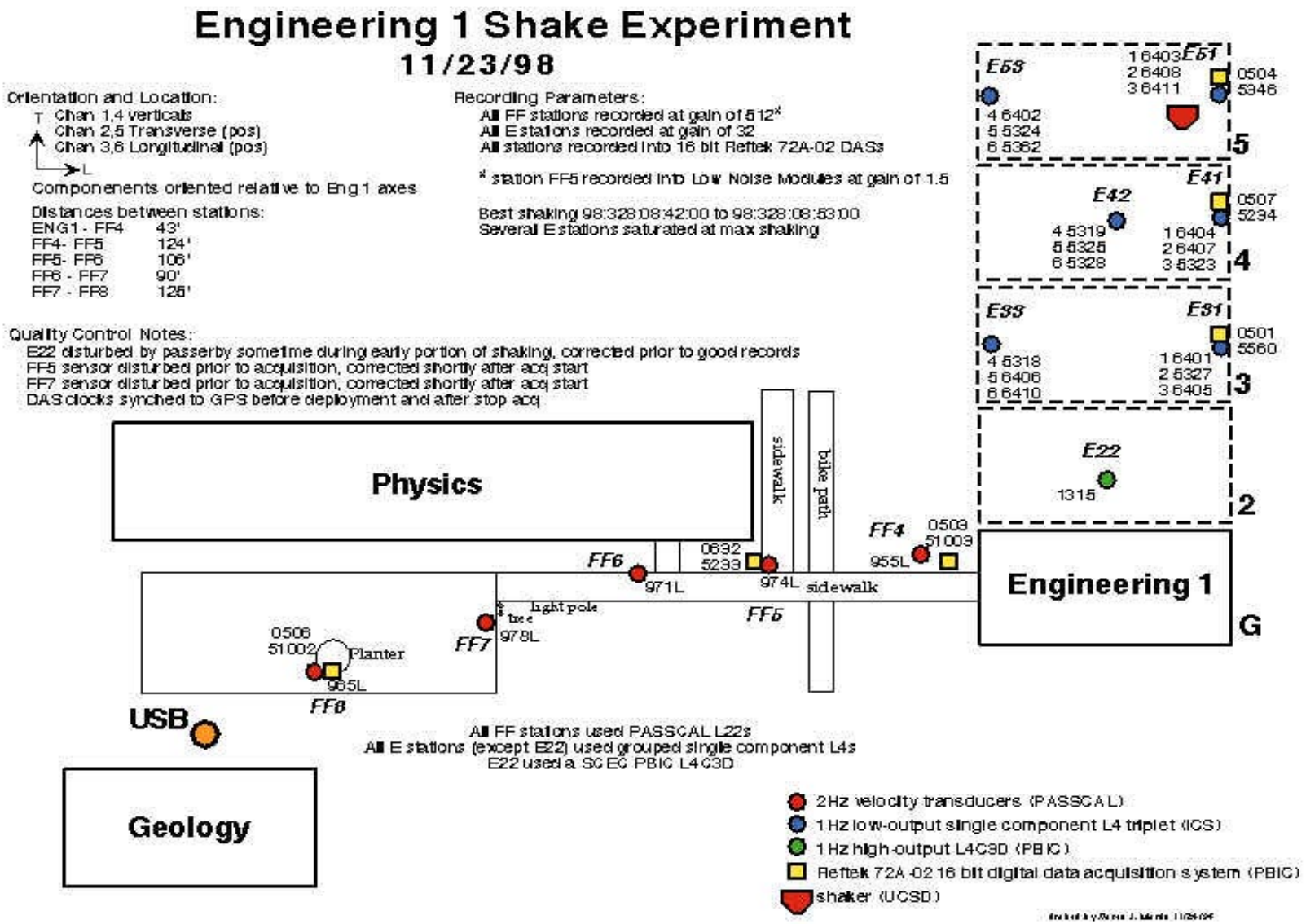

Figure 4.1 Schematic of instrumentation type and location for the forced-vibration test of Engineering 1

4.2 The Structural Dynamics Model of Engineering I

The seismic retrofit design of Enginering 1 had been performed by the firm of Hillman, Biddison, and Loevenguth (HBL), from Los Angeles. They built a model of the building with the ETABS computer program, which permits 3-dimensional dynamic analysis of structures (Figure 4.2). A copy of ETABS was purchased by the CEP from Computers and Structures Inc. in Berkeley, CA, and HBL graciously provided its model of Engineering I.

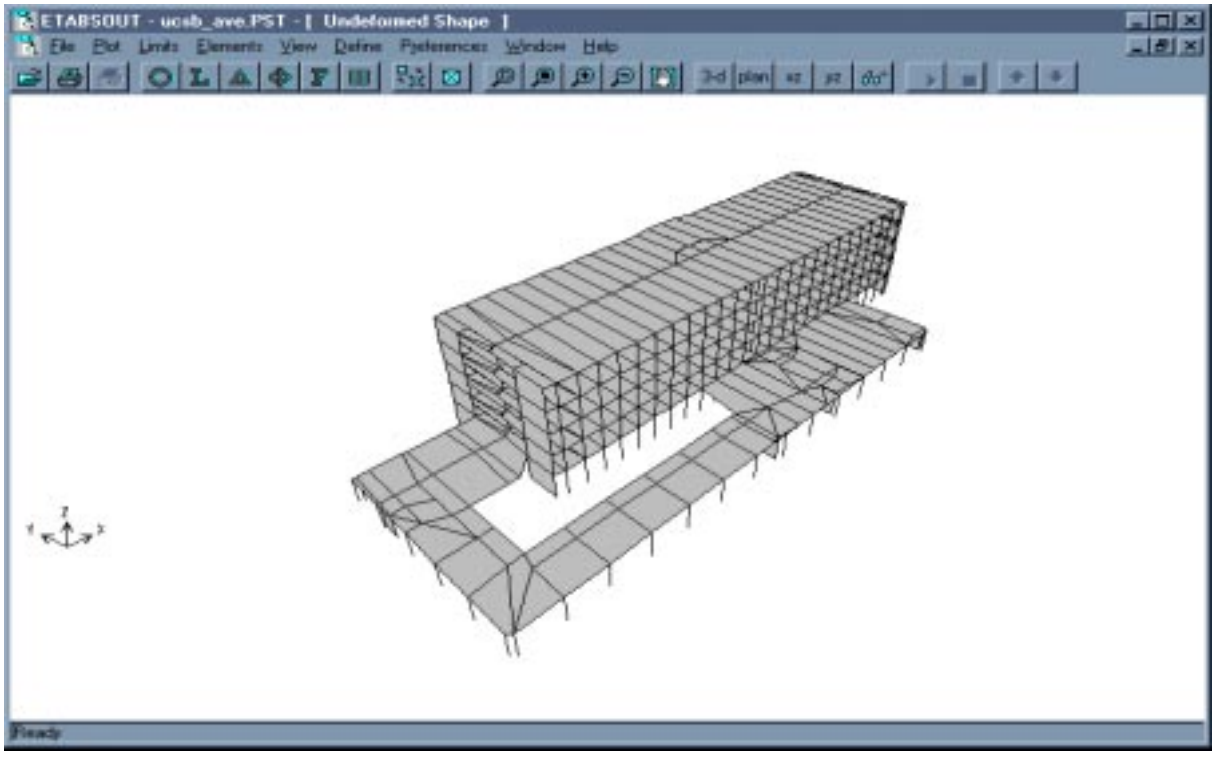

Figure 4.2: ETABS Finite Element model of UCSB's Engineering I building (courtesy of HBL).

4.3 Eigen Analysis of Engineering I

An eigen analysis of the structure was first performed. Results are summarized in Figure 4.3, and Table 4.1. It is shown that transverse (Y-direction) and longitudinal (X-direction) movements, occurring at periods of 0.43 seconds and 0.36 seconds respectively, dominate the dynamic response of the building. An integration time step of 0.01 seconds (~1/10th of the 10th mode period) was deemed acceptable for our transient time-history analyses. Assuming that the input time-history is sampled at a rate high enough to drive the building's 10th mode, our solution will mobilize more than 90% of the structure's mass participating in the primary response directions.

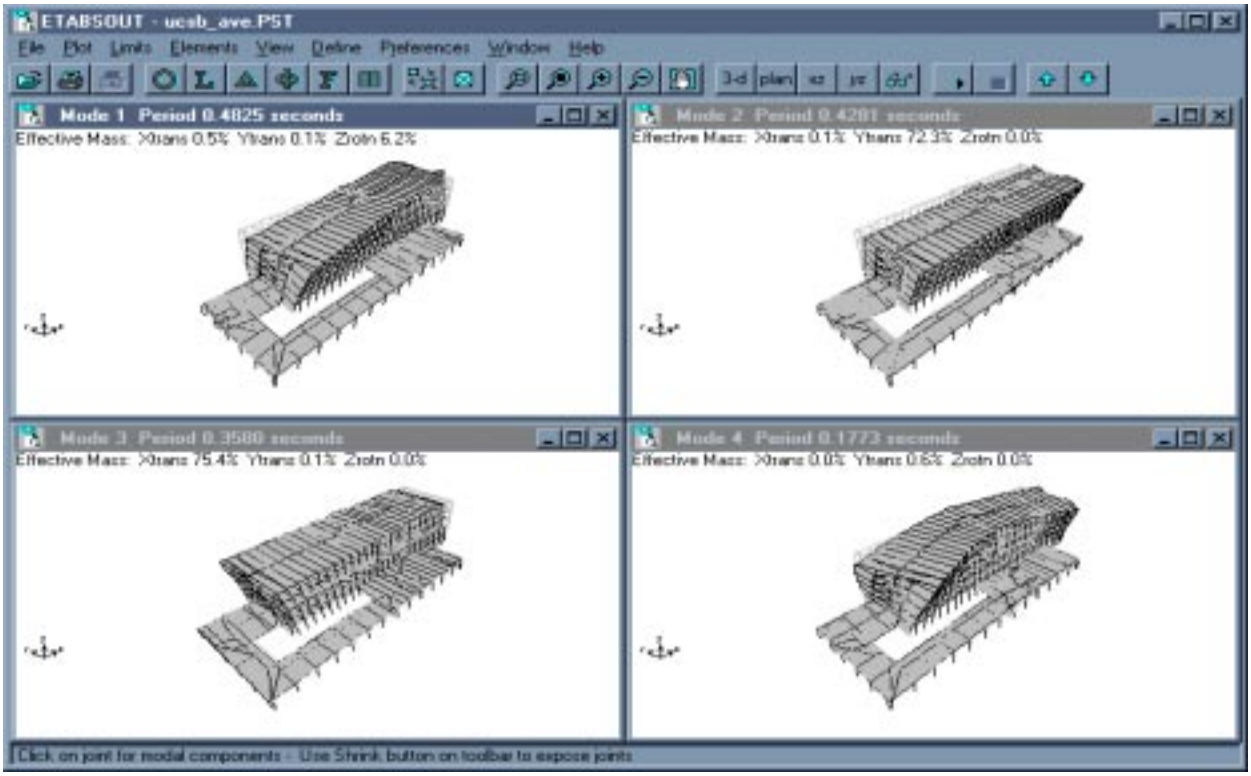

Figure 4.3 Modes shapes of modes 1 through 4 for the Engineering I building

Table 4.1: Summary of information from an eigen solution of the first 10 modes for Engineering I

Mode Number	Period (sec)	Frequency (Hz)	Effective Mass Participation		
			X Translation % mass [% sum]	Y Translation % mass [% sum]	Z Translation % mass [% sum]
1	0.48	2.07	0.54 [0.5]	0.13 [0.1]	6.20 [6.2]
2	0.43	2.34	0.07 [0.6]	72.34 [72.5]	0.00 [6.2]
3	0.36	2.79	75.42 [76.0]	0.06 [72.5]	0.02 [6.2]
4	0.18	5.64	0.00 [76.0]	0.61 [73.1]	0.00 [6.2]
5	0.14	6.94	15.16 [91.2]	0.07 [73.2]	0.38 [6.6]
6	0.13	7.45	0.39 [91.6]	14.12 [87.3]	0.15 [6.8]
7	0.13	7.95	0.71 [92.3]	2.17 [89.5]	1.15 [7.9]
8	0.10	10.26	0.22 [92.5]	1.91 [91.2]	1.47 [9.4]
9	0.09	10.64	2.49 [95.0]	0.04 [91.4]	3.19 [12.6]
10	0.09	10.88	0.59 [95.6]	0.10 [91.5]	5.46 [18.0]

4.4 Dynamic Response Analyses

4.4.1 Base-Motion Input for Dynamic Analyses of Engineering I

All the dynamic response analyses performed with ETABS by the CEP were linear, as were those performed earlier by HBL. The purpose of the CEP calculations was to illustrate the potential variations in building response due to different base input motions. The effects of three different inputs were compared: the acceleration spectrum corresponding to the 1994-DBE, used for the retrofit design, and two acceleration time-histories (mean and + 1 sigma) determined by the CEP, based on records of the1998 event on the NCPP Fault. The CEP accelerations were shown in Figure 3.14, and the DBE spectrum was presented in Figure 3.24.

A convenient way to understand the structure's response is by observing displacements at representative locations. Maximum relative displacements along selected columns and inter-story drift ratios were examined.

4.4.2 Roof-to-Base Relative Displacements of Selected Columns.

The ETABS code can provide the maximum relative displacement between the base of a structure and any user-selected joint. This feature is available for response spectra and time-history analyses. We selected three representative column lines, C5, C26, and C97, shown in Figure 4.4. Comparisons of roof-to-base relative displacements between 1994-DBE and CEP motions are shown in Table 4.2. The relative displacements under the CEP ground motion estimates are up to 5 times those corresponding to the 1994 DBE assumptions. This may have some design implications.

4.4.3 Inter-Story Drift Ratios

Inter-story drift ratios are calculated by dividing the difference in displacements on two adjacent stories by the story height. They can be calculated with ETABS for both response spectra and time-history analyses. ETABS reports ratios for the centers of mass of user-defined floor diaphragms. For response spectra analysis, the inter-story displacements are determined for each mode and then summed in an appropriate manner. For time-history analysis the global maximum and minimum story displacements are differenced to provide a worst case inter-story displacement. This manner of determining inter-story displacements for time-history analyses is too conservative and has no physical rationale. To obtain appropriate inter-story drift ratios for the

time-history analyses, it was necessary to record displacement time-histories at each node of interest and then difference the displacements at each time-step. This operation was performed with a simple C++ program written for this purpose. Thus, inter-story drift ratios from response spectra analyses are for the center of mass of diaphragms, whereas, drift ratios from time-history analyses are for joints along a column line.

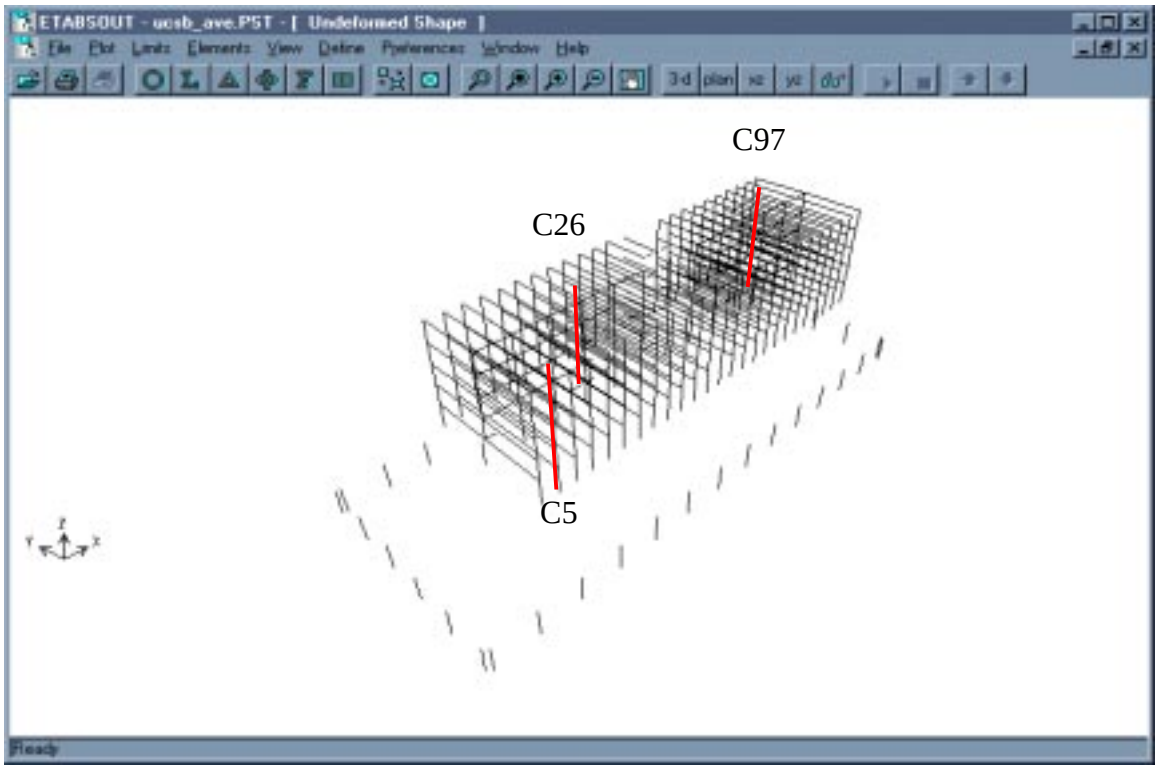

Figure 4.4: Locations of column lines selected for calculation of roof-to-base displacement.

Table 4.2: Displacement of structure at the roof level relative to base motion - 1994 DBE compared to CEP estimates based on the 1998 event.

Column Line	From 1994 DBE		From CEP 1998-EGF based Mean		From CEP 1998-EGF based +1 sigma	
	X-displacement (in)	Y-displacement (in)	X-displacement (in)	Y-displacement (in)	X-displacement (in)	Y-displacement (in)
C5	0.76	1.07	1.33	2.23	2.60	4.87
C26	0.76	0.98	1.30	1.99	2.76	4.61
C97	0.76	1.01	1.28	1.96	2.72	5.51

The drift ratios for the column lines of Figure 4.4, due to the CEP motions, are shown in Table 4.3 and 4.4.

Then, the locations of the center of mass for selected diaphragms used for comparing between 1994 DBE and CEP estimates are shown in Figure 4.5. For the reasons discussed above, a direct comparison of drift ratios for identical locations was not possible. Diaphragm centers of mass and column lines were, however, selected to provide the best possible comparison. The calculated comparisons are given in Tables 4.5. The drift ratios calculated based on the CEP estimates are up to 4 times higher than those corresponding to the 1994 Design-Basis Earthquake assumptions for retrofit.

Table 4.3: Inter-story drift ratios for selected column lines resulting from the CEP mean time-history of the 1998-based scenarios.

Story	Column Line 5		Column Line 26		Column Line 97	
	X Drift Ratio (%)	Y Drift Ratio (%)	X Drift Ratio (%)	Y Drift Ratio (%)	X Drift Ratio (%)	Y Drift Ratio (%)
1	0.10	0.18	0.13	0.21	0.11	0.14
2	0.15	0.30	0.14	0.30	0.19	0.30
3	0.14	0.33	0.14	0.30	0.19	0.30
4	0.25	0.34	0.24	0.30	0.18	0.29
5	0.19	0.32	0.16	0.25	0.14	0.26

Table 4.4: Inter-story drift ratios for selected column lines resulting from the CEP +1 sigma time-history of the 1998-based scenarios.

Story	Column Line 5		Column Line 26		Column Line 97	
	X Drift Ratio (%)	Y Drift Ratio (%)	X Drift Ratio (%)	Y Drift Ratio (%)	X Drift Ratio (%)	Y Drift Ratio (%)
1	0.27	0.33	0.28	0.40	0.25	0.32
2	0.33	0.62	0.31	0.67	0.40	0.79
3	0.28	0.72	0.29	0.70	0.39	0.87
4	0.51	0.73	0.53	0.63	0.40	0.81
5	0.36	0.67	0.37	0.51	0.32	0.71

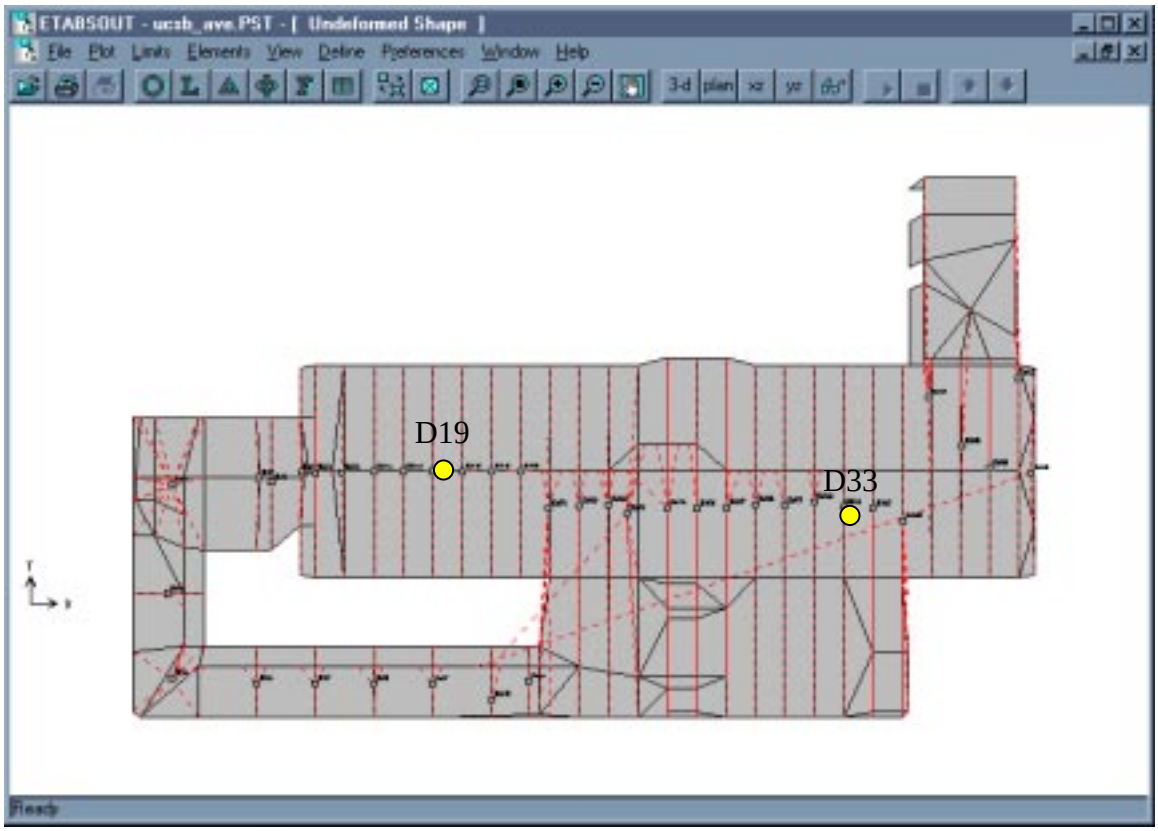

Figure 4.5: Locations of centers of mass for selected diaphragms.

Table 4.5: Building inter-story drift ratios: diaphragm center-of-mass drifts from response spectrum analysis under the 1994 DBE, and closest possible column-line drifts under the CEP time-histories of motion.

Diaphragm Number	From 1994 DBE		Column Line	From CEP 1998-EGF based Mean		From CEP 1998-EGF based +1 σ	
	X Drift Ratio (%)	Y Drift Ratio (%)		X Drift Ratio (%)	Y Drift Ratio (%)	X Drift Ratio (%)	Y Drift Ratio (%)
D19	0.14	0.19	C26	0.24	0.30	0.53	0.70
D33	0.10	0.19	C97	0.19	0.30	0.40	0.87

5. SUMMARY

This is the second report on the UC/CLC Campus Earthquake Program (CEP), concerning the estimation of exposure of the U.C. Santa Barbara campus to strong earthquake motions (Phase 2 study). The first report (Phase 1), dated December 1997, covered the following topics:

- seismotectonic study of the Santa Barbara region
- definition of causative faults threatening the UCSB campus
- geophysical and geotechnical characterization of the Engineering I site
- installation of the new CEP seismic station
- and, initial acquisition of earthquake data on campus.

The main results of Phase 1 are summarized in the current report.

This document describes the studies which resulted in site-specific strong motion estimates for the Engineering I site, and discusses the potential impact of these motions on the building. The main elements of Phase 2 are:

- determining that a M 6.8 earthquake on the North Channel-Pitas Point (NCPP) fault is the largest threat to the campus. Its recurrence interval is estimated at 350 to 525 years.
- recording earthquakes from that fault on March 23, 1998 (M 3.2) and May 14, 1999 (M 3.2) at the new UCSB seismic station.
- using these recordings as empirical Green's functions (EGF) in scenario earthquake simulations which provided strong motion estimates (seismic syntheses) at a depth of 74 m under the Engineering I site; 240 such simulations were performed, each with the same seismic moment, but giving a broad range of motions that were analyzed for their mean and standard deviation.
- laboratory testing, at U.C. Berkeley and U.C. Los Angeles, of soil samples obtained from drilling at the UCSB station site, to determine their response to earthquake-type loading.
- performing nonlinear soil dynamic calculations, using the soil properties determined in-situ and in the laboratory, to calculate the surface strong motions resulting from the seismic syntheses at depth.
- comparing these CEP-generated strong motion estimates to acceleration spectra based on the application of state-of-practice methods - the IBC 2000 code, UBC 97 code and Probabilistic Seismic Hazard Analysis (PSHA). This comparison will be used to formulate design-basis

spectra for future buildings and retrofits at UCSB.

- comparing the response of the Engineering I building to the CEP ground motion estimates and to the design-basis earthquake (DBE) motions used for its retrofit.

Because of the new, site-specific approach which the CEP studies represent, an extensive effort of validation is documented on several fronts:

- validation of the EGF methodology used in the seismic syntheses of strong motion at depth
- validation of the soil profile used for the Engineering I site
- validation of the 1-D vertical seismic wave propagation assumption at the UCSB site
- validation of the nonlinear soil models used to obtain strong motions at the surface

The ever-growing database of strong earthquake records clearly demonstrates the potential for great variability of ground motions from site to site in a given earthquake. These variations are only reflected in a coarse way in the state-of-the-practice Probabilistic Seismic Hazard Analyses, which are rather generic. They are not either described by the simplified design spectra of the Building codes (UBC 97, IBC 2000). These shortcomings provide a strong justification for augmenting the state-of-the-practice estimates with site-specific studies such as done by the Campus Earthquake Program.

At UCSB, the Phase 2 studies lead to the following important conclusions:

- the current (1999) design–basis earthquake (DBE) motions for the campus (10% in 50 years probability of occurrence, or 475-yr return period) are generally consistent with the mean of the CEP surface motion estimates. This means that 50% of the M 6.8 expected earthquakes on the NCPP fault would create ground motions exceeding the current DBE.
- ground motions in the 5% in 50-yr probabilistic event (950-yr return period) are generally compatible with the 84^{th} percentile of the CEP motions. The acceleration spectrum of that 950-yr event is very close to the new IBC 2000 spectrum for UCSB, and generally comparable to the UBC 97 spectrum. Only one in six M 6.8 NCPP earthquakes would be expected to exceed this level of motion.
- as to the Engineering I building retrofit, for which a 1994 DBE was used, the 50^{th} percentile CEP motions are about twice the retrofit design motions, and the 84^{th} percentile CEP motions are about 4 times the retrofit design motions. The CEP motions result in roof-to-base relative column displacements which are 2 to 5 times higher than those calculated with the1994 DBE.

6.0 REFERENCES

Abrahamson, N. and Becker, A. Eds. (1999) "Proceedings of the MCEER Workshop on Ground Motion Methodologies for the Eastern United States", Technical Report MCEER-99-0016, State University of New York at Buffalo, NY.

Aki, K. (1967) "Scaling Law of Seismic Spectrum", J. Geophys. Res., v. 72, pp. 1217-1231.

Aki, K., and Richards, P.G. (1980) "Quantitative Seismology, Theory and Methods", 2 volumes, (W.H. Freeman and Company, San Francisco, CA).

Archuleta, R., Nicholson, C., Steidl, J., Gurrola, L., Alex, C., Cochran, E., Ely, G., and Tyler, T. (1997) "Initial Source and Site Characterization Studies for the U.C. Santa Barbara Campus", U.C. Santa Barbara Institute for Crustal Studies report, UCRL-ID-129196, December.

Archuleta, R.J., Bonilla, L.F., and Lavallée, D. (1999), "Nonlinear Site Response Using Generalized Masing Rules Coupled with Pore Pressure", Proceedings OECD-NRC Workshop on Engineering Characterization of Seismic Input, Brookhaven National Laboratory, NY, 32 pp.

Archuleta, R.J., Bonilla, L.F. and Lavallee, D. (2000) "Nonlinearity in Observed and Computed Accelerograms", Proceedings 12th World Conference on Earthquake Engineering. Paper reference number 0338. (Aston Koedyk Ltd, 23b Westhaven Drive, Auckland, New Zealand).

Blake, T. (1999) "FRISKP 3.01b Brochure", 4568 Via Grande, Thousand Oaks, CA 91320-6712.

Bonilla, L.F., Lavallee, D. and Archuleta, R.J. (1998) "Nonlinear Site Response: Laboratory Modeling as a Constraint for Modeling Accelerograms", Proceedings Second International Symposium on the Effects of Surface Geology on Seismic Motion, Vol. 2, pp 793-800, K. Irikura et al. Eds. (A.A. Balkema, Brookfield, VT).

Brune, J.N. (1970). "Tectonic Stress and the Spectra of Seismic Shear Waves from Earthquakes", J. Geophys. Res., v. 75, pp. 4997-5009.

Brune, J.N. (1971). Correction, J. Geophys. Res., v. 76, p. 5002

Chen W-F, and Saleeb, A.F. (1982) "Constitutive Equations for Engineering Materials: Elasticity and Modeling", Volume 1, 580 pp., (John Wiley & Sons, New York).

Dan, K., Watanabe, T., Tanaka, T., and Sato, R. (1990) "Stability of Earthquake Ground Motions Synthesized by Using Different Small-Event Records as Empirical Green's Functions", Bulletin Seismological Soc. America, v. 80, pp. 1433-12455

Doroudian, M., and Vucetic, M., (1995) "A Direct Simple Shear Device for Measuring Small Strain Behavior", ASTM Geotechnical Testing Journal, v. 18, n. 1, pp. 69-85

Doroudian, M., and Vucetic, M., (1999) “Results of Geotechnical Laboratory Tests on Soil Samples from the U.C. Santa Barbara Campus”, Report ENG-99-203 from the Civil Engineering Department, University of California at Los Angeles, April.

Elgamal, A. W. (1991) "Shear Hysteretic Elasto-Plastic Earthquake Response of Soil Systems," Journal of Earthquake Engineering and Structural Dynamics, v. 20, n. 4, pp. 371-387.

Elgamal, A-W., Alampalli, S., and Van Laak, P., (1996) "Forced Vibration of Full-Scale Wall Backfill System," ASCE Journal of Geotechnical Engineering, v. 122, n. 10, pp. 849-858, Oct.

Elgamal, A. W. Parra, E., Yang, Z., Dobry, R., and Zeghal, M., (1999a) "Liquefaction Constitutive Model", Proceedings Intl. Workshop on The Physics and Mechanics of Soil Liquefaction, Lade, P., and Yamamuro, J. A. Eds., Sept. 10-11, Baltimore, MD, 1998, Physics and Mechanics of Soil Liquefaction, (A.A. Balkema,, Brookfield, VT), pp. 269-279.

Elgamal, A.W., Yang, Z., Parra, E., and Dobry, R., (1999b) "Modeling of Liquefaction-Induced Shear Deformations", Proceedings Second International Conference on Earthquake Geotechnical Engineering, Lisbon, Portugal, June 21-25, Earthquake Geotechnical Engineering, P. Seco e Pinto, Ed., (A.A. Balkema, Brookfield, VT) pp. 895-900,

Hardin, B. O., (1965) “The Nature of Damping in Sands”, ASCE J. Soil Mechanics and Foundations Division, v. 91, n. SM 1, pp. 63-97.

Hartzell, S. H. (1978). “Earthquake Aftershocks as Green's Functions”, Geophysics Research Letters, v. 5, pp. 1-4.

Hartzell, S. H., Liu, P.-C. and Mendoza, C. (1996) “The 1994 Northridge, California, Earthquake: Investigation of Rupture Velocity, Rise Time, and High-Frequency Radiation”, J. Geophys. Res., v. 101, pp. 20091-20108.

Haskell, N.A. (1966) “Total Energy and Energy Spectral Density of Elastic Wave Radiation from Propagating Faults”, Bulletin Seismological Soc. America, v. 56, pp. 125-140

Hornafius, J.S., Luyendyk, B.P., and Kamerling, M.J. (1995). “Seismic Images of the North Channel Fault Near Santa Barbara, CA”, SCEC Workshop on Thrust Ramps and Detachment Faults in the Western Transverse Ranges, Univ. Calif. Santa Barbara, Jan., p.11.

Hudson, D. E. (1962) “Synchronized Vibration Generators For Dynamic Tests of Full-Scale Structures”, EERL Report, California Institute of Technology, Nov.

Hutchings, L.J. (1991) “ ‘Prediction’ of Strong Ground Motion for the 1989 Loma Prieta Earthquake, Using Empirical Green’s Functions”, Bulletin Seismological Soc. America, v. 81, n. 5, pp 1813-1857.

Hutchings, L.J., Jarpe, S.P., Kasameyer, P.W., and Foxall, W. (1996) "Synthetic Strong Ground Motions for Engineering Design, Utilizing Empirical Green's Functions", Lawrence Livermore National Laboratory Report UCRL-JC-123762, April.

International Conference of Building Officials/ICBO (1998) "Maps of Known Active Fault Near-Source Zones in California and Adjacent Portions of Nevada", ISBN 1-58001-008-3 (ICBO, 5360 Workman Mill Road, Whittier, CA, 90601-2298).

International Conference of Building Officials/ICBO (2000) "International Building Code 2000", ISBN 1-892395-25-8, 756 pp., March (ICBO, 5360 Workman Mill Road, Whittier, CA, 90601-2298).

Ishihara, K., (1996)" Soil Behaviour in Earthquake Geotechnics", 350 pp. (Clarendon Press, Oxford, U.K.).

Jarpe, S.P., and Kasameyer, P.K. (1996) "Validation of a Procedure for Calculating Broadband Strong-Motion Time-Histories With Empirical Green's Functions", Bulletin Seismological Soc. America, v. 86, pp. 1116-1129.

Kamerling, M.J., and Sorlien, C.C. (1999) "Quaternary Slip and Geometry of the Red Mountain and Pitas Point-North Channel Faults, California", EOS Transactions American Geophysical Society, v. 80, n. 46, p. F1003

Kondner, R.L., and Zelasko, J.S. (1963) "A Hyperbolic Stress-Strain Formulation of Sands", Proceedings Second Pan-American Conference on Soil Mechanics and Foundation Engineering, Sao Paolo, Brazil, pp. 289-324.

Kramer, S. L., Von Laun, F-Y., and Sivaneswaran, N., (1992) "Strain-Controlled Variable-Frequency Cyclic Loading System for Soft Soils", ASTM Geotechnical Testing Journal, v. 15, pp. 264-270.

Kramer, S. L. (1996) "Geotechnical Earthquake Engineering", 653 pp. (Prentice Hall, Upper Saddle River, New Jersey).

Li, X.S., Wang, Z.L., and Chen, C.K. (1992) "SUMDES: A Nonlinear Procedure for Response Analysis of Horizontally-Layered Sites Subjected to Multi-Directional Earthquake Loading", Department of Civil Engineering, University of California, Davis, 86 p., March.

Masing, G. (1926) "Eigenspannungen und Verfestigung Beim Messing", Proc. 2nd Int. Congress Applied Mechanics, pp. 332-335.

McCall, K. R. (1994) "Theoretical Study of Nonlinear Elastic Wave", J. Geophys. Res., v. 99, pp. 2591-2600.

Muravskii, G., and Frydman, S. (1998) "Site Response Analysis Using a Nonlinear Hysteretic Model", Soil Dynamics and Earthquake Engineering, v. 17, pp. 227-238.

Pavic, R., Kollar, M.G., Bard, P-Y., and Lacave-Lachet, C. (2000) "Ground Motion Prediction with the Empirical Green's Function Technique: An Assessment of Uncertainties and Confidence Level", J. of Seismology, v. 4, pp. 59-77

Petersen, M. et al. (1996) "Probabilistic Seismic Hazard Assessment for the State of California", California Department of Conservation, Division of Mines and Geology, Open-File Report 96-08. Also available as U.S. Geological Survey Open-File Report 96-706.

Pitilakis, K.D. and Anastasiadis, A.J. (1998) "Soil and Site Characterization for Seismic Response Analysis", Proceedings Eleventh European Conference on Earthquake Engineering, Sept. 6-11, Paris, France, pp. 65-90 (A.A. Balkema, Brookfield, VT).

Pyke, R., (1979) "Nonlinear Soil Model for Irregular Cyclic Loadings", ASCE J. Geotechnical Engineering Div., v. 105, n. 6, pp. 715-726.

Riemer, M., and Abu-Safaqah, O., (1999) "Large Strain Triaxial Testing of Soil Samples from U.C. Santa Barbara", Report from the Civil Engineering Department, U.C. Berkeley, January.

Somerville, P.G. (2000) "Magnitude Scaling, Rupture Directivity, and Basin Response Issues at the Interface Between Earthquake Engineering and Seismology", Proceedings Annual Meeting Seismological Soc. of America, San Diego, CA, April.

Sorlien, C.C., Seeber, L., Pinter, N., and Geiser, P.A. (1995) "Listric Faults and Related Folds, Uplift, and Slip", Supplement to EOS., Transactions American Geophysical Union, v. 76, n, 46, p. F-625

Sorlien, C. C., Gratier, J. P., Luyendyk, B.P., Hornafius, J. S., and Hopps, T. E. (1999) "Map Restoration of Folded and Faulted Late Cenozoic Strata Across the Oak Ridge Fault, Onshore and Offshore Ventura Basin, California", Geological Society of America Bulletin, v.111.

Tumarkin, A.G., and Archuleta, R.J. (1994) "Empirical Ground Motion Prediction", Annali di Geofisica, v. 37, n. 6, pp. 1691-1720.

Vucetic, M. (1990) "Normalized Behavior of Clay Under Irregular Cyclic Loading", Canadian Geotechnical Journal, v. 27, pp. 29-46.

Wu, F. T. (1978) "Prediction of Strong Ground Motion Using Small Earthquakes", in Proceedings 2nd International Microzonation Conference, San Francisco, v. 2, pp. 701-704 (Nat. Science Foundation, Washington, D.C.).

Xu, H., Day, S.M., and Minster, J.B. (1998) "Model for Nonlinear Wave Propagation Derived from Rock Hysteresis Measurements", J. Geophys. Res., v. 103, pp. 29915-29929.

Yoshida, N. and Iai, S. (1998) “Nonlinear Site Response and its Evaluation and Prediction”, Proceeding Second International Symposium on the Effects of Surface Geology on Seismic Motion, v. 1, pp. 71-90 (A.A. Balkema, Brookfield, VT).

7.0 ACKNOWLEDGMENTS

These studies were funded from several sources: the University of California Senior Vice-President Business and Finance, Wayne Kennedy, the University of California Office of Research directed by Dr. Robert Shelton, the Office of the Vice-Chancellor Administrative Services at U.C. Santa Barbara, David Sheldon, and the University Relations Program at the Lawrence Livermore National Laboratory, previously headed by Dr. Claire Max and currently by Dr. Harry Radousky. We express our deep appreciation to all for their continued support.

We thank Steve Day at San Diego State University, and Jian-Chu Chen, Lawrence Hutchings, David McCallen, and Jeff Wagoner at LLNL, for their review comments. We acknowledge Bruce Kutter and Ari Balakrishnan at U.C. Davis for providing the SUMDES code. We are also very grateful to our colleagues Mark Petersen and Robert Sydnor of the California Department of Mines and Geology for their gracious contributions to the Campus Earthquake Program.